Study on plasmonic-photonic hybrid systems for efficient excitation of nonlinear phenomena

(非線形現象の高効率励起に向けたプラズモニックーフォトニックハイブリッドシステムの研究)

Graduate School of Information Science and Technology

Hokkaido University

REN, FANG

任 芳

A thesis submitted for the degree of

Doctor of Philosophy

2014

Abstract

Localized surface plasmons (LSPs) induced in metal nanostructures have been the subject of intensive research in recent years, because they have the ability to confine light into the nanoscale areas beyond the diffraction limit and to enhance the light-matter interaction. They have been used in various applications, such as optical sensing, surface enhanced Raman spectroscopy, two-photon excited fluorescence (TPF), and second harmonic generation (SHG). Specially, during the last decade, enhanced nonlinear phenomena induced by surface plasmon have been extensively studied as new light sources at the nanoscale. However, because of the huge scale mismatch between photons and metal nanostructures, it is difficult to couple light into single metal nanostructure efficiently, resulting in the use of a high intense pulsed laser excitation for nonlinear phenomena.

Therefore, to harness the merits of plasmonic nanostructures for nonlinear application, it is necessary to improve the coupling of light to single metal nanostructure. In this study, I propose two types of plasmonic-photonic hybrid systems to efficiently excite LSPs at the single metal nanostructure, and demonstrate the nonlinear phenomena (SHG and TPF) within these plasmonic-photonic hybrid systems under a weak continuous wave (CW) excitation.

Firstly, one plasmonic-photonic hybrid system composed of an Au-coated tip and a tapered-fiber-coupled microsphere resonator is proposed. From the results, it is found that a tapered-fiber-coupled microsphere resonator could focus the light into a nanoscale domain of the Au-coated tip with high coupling efficiency (~93%). This hybrid system is demonstrated to possess not only high Q factor (~10^6), but also small mode area (less than ~10^3 nm^2). In order to experimentally verify the efficient excitation of LSPs at the Au-coated tip, SHG from the top of Au-coated tip under a weak CW excitation is investigated. Furthermore, I also observe TPF from pseudoisocyanine (PIC) dye molecules attached on the Au-coated tip using the same plasmonic-photonic hybrid system. The results suggest that the synergetic effect of strong optical

confinement effect of a microsphere resonator and optical antenna effect of an Au-coated tip using this proposed system tremendously results in the strong light-matter interaction at the nanoscale.

Whereas the photonic microsphere resonator with the ultra-high *Q* factor facilitates the efficient coupling of light from the tapered fiber to the single plasmonic nanostructure, this hybrid system is complicated which result in difficult alignment in the experiment. Thus, I also demonstrate a simple tapered fiber based photonic-plasmonic hybrid nanostructure composed of a thin tapered fiber and an Au-coated tip. Using this simple hybrid nanostructure without photonic microresonator, a thin tapered fiber, which has small transverse dimensions, can also efficiently couple light into single metal nanostructure with small dimensions. I also succeed in observing TPF from the PIC dye molecules under a weak CW excitation condition, although it has weak field enhancement and low *Q* factor.

In brief, taking advantages of both plasmonic and photonic elements, the two types of plasmonic-photonic hybrid systems have been proposed to improve the efficient coupling of light into the nanoscale domain of single metal nanostructure, which tremendously result in the strong light-matter interaction at the nanoscale. Furthermore, nonlinear phenomena within these hybrid systems under a weak CW excitation condition (~kW/cm^2) are investigated. They are the promising tools for single photon sources, highly efficient plasmonic sensors, and integrated nonlinear plasmonic devices.

Contents

Abstract ..... **i**

Contents ..... **iii**

Chapter 1 Introduction **1**

1.1 Historical background 1

1.2 Motivation and objective 7

1.3 Organization of this thesis 8

Chapter 2 Basic theory **11**

2.1 Introduction 11

2.2 Propagation mode properties of tapered fibers 11

2.3 Whispering gallery mode microresonators 21

2.3.1 Whispering gallery modes 21

2.3.2 Quality factor 28

2.3.3 Mode spacing 32

2.3.4 Mode volume 33

2.3.5 Circulating power 34

2.4 General properties of localized surface plasmon resonance 35

2.5 Evanescent coupling theory 37

2.5.1 Coupling between tapered fiber and microsphere 37
2.5.2 Coupling between tapered-fiber-coupled microsphere and Au-coated tip 42
2.6 Summary 45
Chapter 3 Experimental preparation 47
3.1 Basic setup 47
3.2 Fabrication of tapered fibers 50
3.2.1 Transmittance properties of tapered fibers during the pulling process 50
3.2.2 Checking polarization state of incident light at the tapered region 55
3.3 Fabrication of silica microspheres 57
3.4 Fabrication of Au-coated tips 58
3.5 Preparation of PIC-attached Au-coated tip 61
3.6 Summary 63
Chapter 4 Second harmonic generation from the top of an Au-coated tip via a tapered-fiber-coupled microsphere resonator 65
4.1 Introduction 65
4.2 Experimental setup 66
4.3 Results and discussion 68
4.4 Summary 74
Chapter 5 Two-photon excited fluorescence from a PIC-attached Au-coated tip using a tapered-fiber-coupled microsphere resonator 75
5.1 Introduction 75
5.2 Experimental setup 76
5.3 Results and discussion 78

5.4 Summary 86

Chapter 6 Two-photon excited fluorescence from a PIC-attached Au-coated tip via a thin tapered fiber 89

6.1 Introduction 89

6.2 Experimental setup 90

6.3 Results and discussion 92

6.4 Summary 103

Chapter 7 Conclusions 105

References 109

Publication lists 119

Acknowledgements 121

Chapter 1 Introduction

1.1 Historical background

The ability to confine photons into the ultrasmall volumes has played a vital role for enhancing the light-matter interaction in the emerging fields of nanophotonics, quantum optics and quantum information science [1-3]. Localized surface plasmons (LSPs) induced in metallic nanostructures have been the subject of such intensive research owing to their ability to confine light into the nanoscale areas beyond the diffraction limit and to enhance the light-matter interaction [4-5], in recent years. Localized surface plasmon resonance is an optical phenomena generated by a light wave trapped within conductive nanoparticles smaller than the wavelength of light. The phenomenon is a result of the interactions between the incident light and surface electrons in a conduction band. This interaction produces coherent localized plasmon oscillations with a resonant frequency that strongly depends on the composition, size, geometry, dielectric environment and particle-particle separation distance of nanoparticles. Since the optical properties of LSPs are sensitively depending on the shapes and sizes of metal nanostructures, various metal nanostructures, such as tips, nanoparticles, nanorods, nanowires, and dimers, have been investigated. They have been widely used in various applications, such as optical sensing [6-7], surface enhanced Raman spectroscopy (SERS) [8-9], enhanced nonlinear fluorescence [10-18], and second harmonic generation (SHG) [18-23]. Specially, during the last decade, enhanced nonlinear phenomena induced by surface plasmon have been extensively studied as

new light sources at the nanoscale. Sanchez et al. [13] have demonstrated that two-photon excited fluorescence (TPF) from PIC dye molecules dispersed on a substrate was enhanced by an Au tip (Diameter (D) ~ 10 nm; Peak power: ~ 2 W), where the incident pulsed laser light was focused on the tip by an objective lens and the emission from PIC dye molecules were collected by the same objective. Grycaynski et al. [15] also have reported that TPF from rhodamine derivatives near silver islands formed quartz microscope slides was enhanced by the silver islands using the same excitation method (Peak power: ~ 70 kW). Meanwhile, Efficient SHG at the nanoscale also can be obtained by plasmon enhancement at the surface of an Au tip [19-20], at Ag nanoparticles coated on an optical fiber tip [22], or by a single dimer of Au nanoparticle [23] under a femtosecond optical pulsed laser excitation. Slablab et al. [23] also reported SHG from dimer Au nanospheres (D ~ 100 nm) under a femtosecond pulsed laser excitation in free space (Peak power: ~ 60 W). Although these nonlinear phenomena can be enhanced by different metal nanostructures, metal nanostructures are usually aggregated collectively either in a solution or immobilized on a surface. It has been shown that by using single plasmonic nanoparticles, the highly improving detection limits approaching the single molecule limit can be achieved [7]. In addition, the ability to excite and detect individual plasmonic nanostructures makes the study of resonance properties possible without the interference of collective effects of the ensemble of nanostructures. However, the excitation of single plasmonic nanostructure using free-space optics is not efficient. Therefore, to harness the merits of plasmonic nanostructures for nonlinear application, it is necessary to improve the focusing of light onto single metal nanostructure.

Achieving coupling of photons into LSPs must satisfy the phase match between the photon and surface plasmon wave vectors. Various methods have been proposed so far, such as prism coupling [22][24], objective lens (free-space excitation) [24], grating [25-27], silicon on insulator waveguides [28], and tapered fibers [29-30]. Free-space excitation efficiencies of LSPs induced metal nanostructures [20] are extremely low due to the huge scale mismatch between photons and nanostructures. Since the demonstration of efficient coupling via the overlap of evanescent fields [31] made a major breakthrough in light-coupling techniques, efficient excitation can be achieved using the evanescent coupling techniques, which use tunneling of evanescent field components with phase matched wave-vectors to achieve highly efficient coupling. A well-known implementation of this method is using a total internally reflected beam

within a prism. Prism coupling have become famous since the 1960's when the prism coupling was used to efficiently excite surface plasmon-polariton [32]. For far-field excitation of LSPs in metal nanostructures, Ropers et al. [25] has demonstrated an efficient nonlocal optical optical excitation of the apex of a nanostructured Au taper (D ~ 40 nm) by using grating-coupling of surface plasmon polaritons, as shown in Fig. 1.1(c). Bsudrion et al. [34] reported that coupling efficiency of light to surface palsmon polariton for single subwavelength holes in a gold film reached ~ 28%. Bouhelier et al. [20] and Takahashi et al. [19] also demonstrated the focusing of light onto the Au tips (D ~ 10 nm) via an objective lens and prism in order to measure SHG from the Au tips, as presented in Fig. 1.1(a) and (b). However, it is still a great challenge to focus a single propagating photon into a single plasmonic nanostructure efficiently due to the huge scale mismatch among photons, metallic nanostructures and molecules. It limits the level of possible field enhancement, which is of importance for efficient light-matter interaction at the nanoscale area. Therefore, to utilize the advantages of plasmonic nanostructure, we improve the focusing of propagating photons into a plasmonic nanostructure in this study.

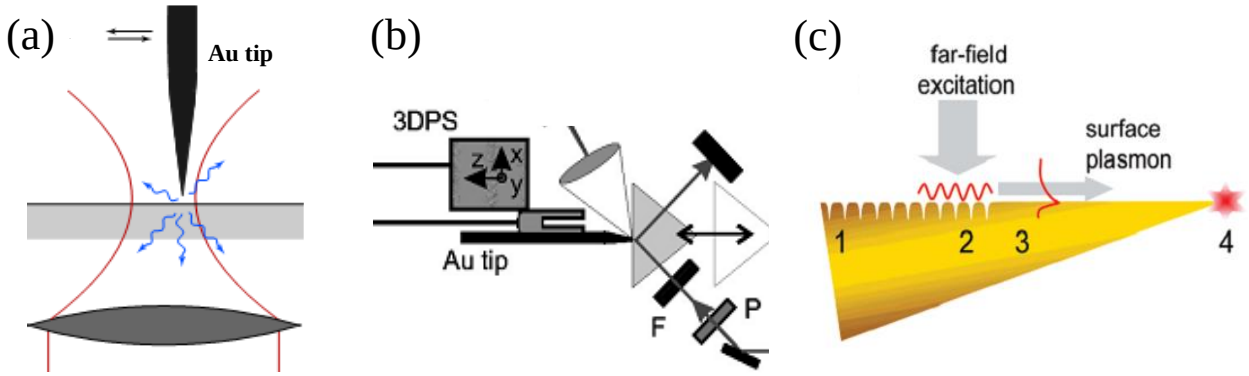

Fig. 1.1 Typical types of couplers for surface plasmon. (a) Objective lens [20]; (b) Prism [19]; (c) grating [25].

Microresonators have made a significant impact in practical systems and laboratory research due to high quality factor (Q) and strong buildup of optical energy. They are made from a wide variety of materials from polymers [35-37] to semiconductor [38-41]. One of the most common materials used is the silicon dioxide (SiO_2) due to the existing silica optical

telecommunications networks used all over the world. Of all geometries studied for confining light, it has been well-known that cavities, such as silica microspheres [42-44] and microtoroids [45-47], possess whispering gallery modes which can confine photons for a very long time through total internal reflection on the cavity interface. Vernooy et al. [44] has experimentally demonstrated a record *Q* factor as high as 9 billion for microsphere, limited only by the optical absortption of silica. Armani et al. [47] also has reported that on chip silica microtoroidal resonators provided high *Q* factor 4×10^8, owing to the minimized scattering losses from the smooth resonator surface created by surface tension during a laser reflow process. The small mode volume and long photon storage time can be used for nonlinear studies, because strong resonant buildup of energy in microscale volumes significantly reduces the threshold of nonlinear effects. This allowed the realization of low threshold of optical microcavity effects, such as lasing [48-50] and nonlinear phenomena [51-52]. Vahala et al. has experimentally realized stimulated Raman scattering [49], stimulated Brillouin scattering [50], etc. at very low input thresholds. Moreover, when the optical cavity loss and mode volume becomes small enough, an atom can coherently interact with the cavity for a substantial period of time. This ability is desirable for quantum optics [3, 53-55].

Besides these applications of microcavities, the microresonator modes also can provide the necessary momentum to excite the surface plasmon polariton (SPP) modes. Various types of these researches are proposed to efficiently couple light to metallic nanostructures, such as silver-coated microdisk [56], planar photonic crystal combined with a gold nanorod [1], microring resonator integrated with a plasmonic nanoresonator (theoretical) [59], and WGM microcavity with a metal nanoparticle (theoretical) [60], have been reported. Min et al. [56] have shown that by coating a silica microdisk with a layer of silver, whispering gallery–surface plasmon polariton (SPP) hybrid modes can by supported at the interface of silica and silver, which can achieve *Q* factor of ~ 1800. White et al. [57] have also shown that the Raman emission of Rhodamine 6G molecules attached to silver nanoparticles can be enhanced, when a silica microsphere is immersed in a solution consisting of mixture of silver nanoparticles and Rhodamine 6G molecules. In this experiment, it has been demonstrated that the whispering gallery modes of a microsphere can excite the localized surface plasmon resonance of the silver nanoparticles which are attached to the surface of the microspheres randomly and from clusters.

It was shown that field enhancement is possible by combining silica microspheres and silver nanoparticles for surface enhanced Raman emission. Angelis et al. [58] have demonstrated that a plasmonic nanoantenna with an ogival-shape tip combined with a planar photonic crystal cavity. The photonic crystal cavity, and this nanoantenna placed at the planar photonic crystal cavity center supports SPP modes and acts as a nanoscale waveguide, able to propagate and focus the SPP toward the tip. And the nanoantenna focues the incident light into a nanoscale region to interact with molecules. This hybrid system is excited in free space. Barth et al. [1] also have proposed a nanoassembled plasmonic-photonic hybrid cavity that consists of a planar photonic crystal cavity and the Au nanorods (50 nm × 20 nm), as shown in Fig. 1.2(a). These plasmonic structures are placed inside the cavity by using an AFM tip. This hybrid system has low *Q* factor of ~ 900. However, this method of hybridization cannot be easily used for making practice devices. In the last two examples, a planar photonic crystal cavity is used as the photonic structure that is excited in free space, which results in low coupling of light into a plasmonic structure. And the lack of an efficient on-chip excitation mechanism has limited their application. Recently, Chamanzar et al. [59] have also numerically demonstrated a hybrid nanoplasmonic-photonic resonators composing of a photonic microring resonantor strongly coupled to a single Au nanorod (100 nm × 56 nm × 30 nm), as shown in Fig. 1.2(b). According to simulation, it is shown that more than 73% of the incident light in the waveguide can be coupled to the localized surface plamson resonance mode of the plamonc nanostructures. Xiao et al. [60] have shown a hybrid photonic-plasmonic resonant structure consisting of a metal nanoparticle (D ~ 60 nm) and a whispering-gallery-mode microcavity in Fig. 1.2(c). It is found theoretically that the hybrid mode enables strong interaction between light and metal nanostructure. In these methods, the synergetic effect of strong optical confinement effect of microcavity structures and optical antenna effect of metallic nanostructures makes it possible to efficiently couple light to metallic nanostructures. Moreover, high coupling of light into a single metal nanostructure would be achieved by tuning the coupling conditions between the metal nanostructure and mcirocavity. However, the metallic nanostructures were placed directly on the cavity surface and their cavity parameters were controlled only by the size and shape of the structure, resulting in the experimental difficulty in coupling conditions between the incident photons and LSPs. Thus, for studying the underlying physics and achieving the high coupling efficiency flexibly, the

adjustability of the cavity parameters such as photon-cavity and cavity-LSP coupling constants is indispensable. In this study, one new plasmonic-photonic hybrid system composed of an Au-coated tip and a tapered-fiber-couple microsphere resonator is proposed to efficiently excite LSP of metal nanostructures, which strongly enhance the light-matter interaction.

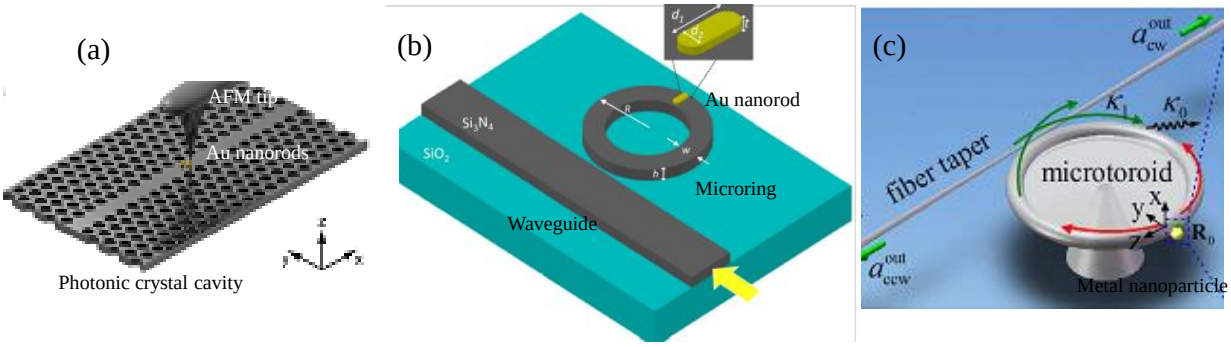

Fig. 1.2 Several types of plamonic-photonic hybrid systems using microresonators. (a) photonic crystal cavity and Au nanorods [1]; (b) microring and Au nanorod [59]; (c) a tapered-fiber-coupled microtoroid and metal nanoparticle [60].

On the other hand, the tapered fibers have been a very powerful tool for various optical studies such as biological sensing, optical power delivery systems, quantum optics and quantum information science, owing to their low loss, single mode guidance, and their intense evanescent field outside the optical thin tapered fiber [61-63]. It has been demonstrated that fluorescence photons from light nanoemitters, such as atoms, quantum dots, and nanodiamonds can be channeled into the guided modes of the thin tapered fibers [64-66]. Furthermore, trapping atoms around the optical nanofibers using the strong evanescent tail of the guided field has been proposed [67-68] and the spontaneous emission of atoms can be strongly modified around the nanofiber [69]. The tapered fiber is also a promising tool to efficiently and controllably couple light into or out of a microresonator and a metal nanostructure. For microresonators, free-space excitation efficiencies of whispering gallery modes (WGM) [70] are extremely low due to the huge scale mismatch between photons different phase velocities in air and silica. The prism coupling also has been used to excite WGM of microspheres [71]. However, the prism coupling is difficult to control and alignment during the experiment. Alternative types of evanescent couplers have been proposed, such as angle polished fiber tips [64], planar waveguides [72], and

tapered optical fibers [73-75]. A particularly suitable method of tapered optical fibers has been proposed by [74-76], in which a fiber is drawn into a thin filament, and the evanescent field of the fiber is brought to overlap with the microspheres, to achieving almost perfect coupling (99.99%) using an adiabatically tapered optical fiber. As for metal nanostructures, to realize the excitation of LSPs, so far alternative methods had included silicon on insulator waveguides [77], and tapered fibers [78-79]. By bringing the evanescent field region in close proximity to the metal nanostructures, the evanescent coupling can be achieved. Among these methods, optical tapered fibers with sub-wavelength diameter are particularly promising in view of their highly efficient LSPs excitation. The special advantages of this method in which tapered optical fiber are used to couple light into microspheres and metal nanostructures as follow. First, the tapered fibers can be fabricated with low loss. Secondly, the tapered fibers allow highly efficient excitation of LSP or WGM. Moreover, they allow not only excitation but also extraction of cavity fields or enhance nonlinear fields through the same tapered fiber. Thirdly, the tapered fibers have small transverse dimensions, making them unique tools to excite WGM-microcavities or LSP induced metal nanostructures with small dimensions.

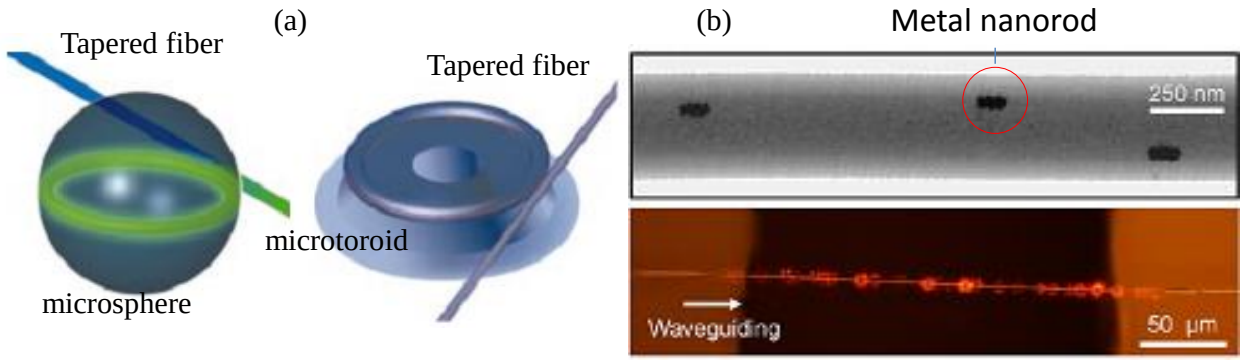

Fig. 1.3 Tapered fibers' application as couplers. (a) Tapered fibers couple light into and out of microresonators [66-68]; (b) Tapered fiber couples light into metal nanorods [79].

1.2 Motivation and objective

Localized surface plasmons (LSPs) induced in metal nanostructures have the ability to confine light into the nanoscale areas beyond the diffraction limit and to enhance the light-matter

interaction. They have been used in various applications, such as optical sensing, surface enhanced Raman spectroscopy, two-photon excited fluorescence (TPF), and second harmonic generation (SHG). Specially, during the last decade, enhanced nonlinear phenomena induced by surface plasmon have been extensively studied as new light sources at the nanoscale. However, because of the huge scale mismatch between photons and metal nanostructures, it is difficult to focus light onto single metal nanostructure efficiently, resulting in the use of a high intense pulsed laser excitation for nonlinear phenomena.

Therefore, in order to harness the merits of plasmonic nanostructures for nonlinear application, the objective of this thesis is to improve the focusing of light to single metal nanostructure at the nanoscale area. In this study, I propose two types of plasmonic-photonic hybrid systems to efficiently excite LSPs at the single metal nanostructure, and demonstrate the nonlinear phenomena (SHG and TPF) within these plasmonic-photonic hybrid systems under a weak continuous wave (CW) excitation.

1.3 Organization of this thesis

This thesis is divided into 6 chapters including the current chapter 1.

Chapter 2 theoretically describes propagation modes of tapered fibers, optical properties of microresonators, general properties of localized surface plasmon resonance. The optical properties of microresonators include optical modes, mode volume, *Q* factor, mode spacing. Regarding general properties of localized surface plasmon resonance, we present absorption cross section, scattering cross section and field enhancement. Then, coupling theory among tapered fibers, microspheres, and Au-coated tips are briefly discussed.

Chapter 3 presents the basic experiment setup. The experimental setup for fabrications of tapered fibers, silica microspheres, Au-coated tips, as well as measurements of transmittance of tapered fiber during pulling process and scattering spectrum of Au-coated tip are described.

Chapter 4 investigates the efficient coupling of light from a tapered-fiber-coupled microsphere resonator to localized surface plasmon modes of an Au-coated tip. To verify efficient localized surface plasmon excitation at the metal tip via a tapered-fiber-coupled

microsphere resonator, we measured second harmonic generation (SHG) from the top of Au-coated tip. From the results, in spite of a weak CW excitation (~ 28 μW), we succeeded in repeatedly observing SHG from the top of the Au-coated tip via a tapered fiber coupled microsphere resonator system, which could focus the light with the coupling efficiency of about 63.2 % into the nanoscale domain of the metal tip with the effective cross section (σ_{ext}) of 358.2 nm^2 with the diameter (D_{ext}) of ~ 21 nm.

Chapter 5 reports a plasmonic-photonic hybrid system composed of a tapered-fiber-coupled microsphere resonator and a pseudoisocyanine (PIC)-attached Au-coated tip to focus the incident light into a nanoscale domain (σ_{ext} ~728.8 nm^2; D_{ext} ~ 30 nm) with high coupling efficiency of ~80.3 % and the Q factor of ~1.9×10^6. In order to experimentally verify the strong interaction between light and matter owing to efficient excitation of localized surface plasmon at the Au-coated tip, we demonstrated to observe two-photon excited fluorescence (TPF) from PIC dye molecules attached on the Au-coated tip even under a weak CW excitation condition (~ 3 μW) via a tapered-fiber-coupled microsphere resonator.

Chapter 6 demonstrates a simple tapered fiber based photonic-plasmonic hybrid nanostructure composed of a thin tapered fiber and a PIC-attached Au-coated tip. We succeeded in observing TPF from the PIC dye molecules under a weak continuous wave excitation condition (~ 120 μW) using this simple hybrid nanostructure, which could focus the light with the coupling efficiency of about 95 % into the nanoscale domain of the metal tip with the effective cross section (σ_{ext}) of ~ 8×10^4 nm^2 (D_{ext} ~ 320 nm). From the results of the tip-fiber distance dependence and excitation polarization dependence, we found that using a thin tapered fiber and an Au-coated tip realized efficient coupling of the incident light and LSP excitation at the Au-coated tip, suggesting the possibility of efficiently inducing two-photon excited fluorescence from the PIC dye molecules attached on the Au-coated tip.

Chapter 7, the final chapter, draws on the general conclusions of the previous chapters.

Chapter 2 Basic theory

2.1 Introduction

In this section, the propagation mode properties of tapered fibers are described. In addition, optical properties of microresonators (e.g. optical modes, *Q* factor, mode volume…), general properties of localized surface plasmon, such as absorption cross section and scattering cross section, and evanescent couplings to microsphere using a tapered fiber and to an Au-coated tip using a tapered-fiber-coupled microsphere resonator are introduced.

2.2 Propagation mode properties of tapered fibers

According to refs. [61][62], to numerically analyze the propagation mode properties of a thin tapered fiber, we consider a thin tapered fiber that has a cylindrical silica core of diameter (D), refractive index (n_1), an infinite air clad of refractive index (n_2=1.0), and a step-index profile. The tapered fiber is fabricated from a fused-silica single-mode optical fiber heated by a ceramic heater at the temperature of ~1400 ^{0}C and meanwhile stretched at both ends of the fiber in this study, as shown in Fig. 2.1(a). Owing to the adiabatic pulling process, the original core is almost vanishing. Therefore, the refractive indices that determine the guiding properties of the tapered fiber are the refractive index of the original silica clad and the refractive index of the surrounding

air. We assume that the tapered region is very uniform in diameter and smooth in sidewall. The model of an air-clad dielectric tapered fiber is shown in Fig. 2.1(b). It has the following index profile, where *a* denotes the radius of the tapered fiber.

$$n(r)=\begin{cases} n_1 & (0<r<a) \\ n_2 & (a\le r<\infty) \end{cases} \tag{2.1}$$

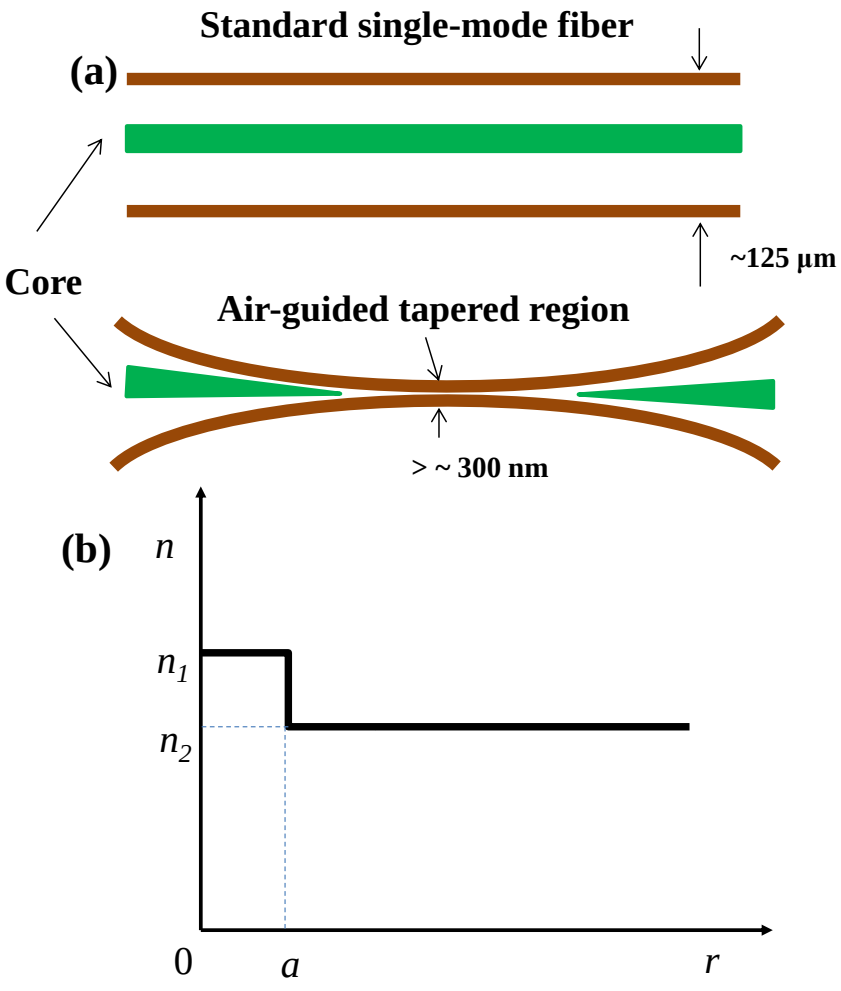

Fig. 2.1 (a) An illustration of the before and after the pulling process; (b) A model of an air-clad cylindrical dielectric tapered fiber.

A taper is considered to be approximately adiabatic, which enusure that there is negligible loss of power from the fundamental mode as it propagates along the tapered region [80]. The fields and propagation constant within an approximately adiabatic tapered region of a single mode fiber can be described accurately by those of the local fundamental mode, which conserves power as it propagates and is the solution to the wave equation with the geometry of the local cross section. The wave equation of light propagation in such a fiber is described by,

$$\nabla^2 E - \mu_0 \varepsilon(r) \frac{\partial^2 E}{\partial t^2} = -\nabla\left(\frac{E}{\varepsilon(r)} \cdot \nabla \varepsilon(r) \right). \tag{2.2}$$

It can be derived from Maxwell's equations:

$$\nabla \times H = \varepsilon(r) \frac{\partial E}{\partial t}, \tag{2.3a}$$

$$\nabla \cdot H = 0, \tag{2.3b}$$

$$\nabla \times E = -\mu_0 \frac{\partial H}{\partial t}, \tag{2.3c}$$

$$\nabla \cdot \left(\varepsilon(r) E \right) = 0, \tag{2.3d}$$

where E denotes the electric field vector, μ_0 is the vacuum permeability, and $\varepsilon\left(=n^2\right)$ presents the electric permittivity of the medium. The wave equation for the magnetic field H takes the same form as Eq. (2.2). Assuming that the model of the tapered fiber is non-dissipative and source free, which is true for most of the dielectric materials within their transparent ranges, one can reduce Maxwell's equations to the following Helmholtz equations.

$$(\nabla^2 + n^2k^2 - \beta^2)E = 0, \tag{2.4a}$$

$$\left(\nabla^2 + n^2k^2 - \beta^2\right)H = 0, \tag{2.4b}$$

where $k = 2\pi/\lambda$, and β is the propagation constant. The eigenvalue equations [62] of Eq. (2.4) for various modes describe below.

For $HE_{\upsilon m}$ and $EH_{\upsilon m}$ modes:

$$\left\{\frac{J_\upsilon'(U)}{UJ_\upsilon(U)} + \frac{K_\upsilon'(W)}{WK_\upsilon(W)}\right\}\left\{\frac{J_\upsilon'(U)}{UJ_\upsilon(U)} + \frac{n_2^2K_\upsilon'(W)}{n_1^2WK_\upsilon(W)}\right\} = \left(\frac{\upsilon\beta}{kn_1}\right)^2\left(\frac{V}{UW}\right)^4. \tag{2.5}$$

Here J_υ is the Bessel function of the first kind, and K_υ is the modified Bessel function of the second kind. Each set of modes, labeled as $HE_{\upsilon m}$ and $EH_{\upsilon m}$, exhibits different solutions depending on the value υ. And m denotes the different solutions of Eq. 2.5 for a fixed υ. $U = a\left(k_0^2n_1^2 - \beta^2\right)^{1/2}$, $W = a\left(\beta^2 - k_0^2n_2^2\right)^{1/2}$, $V = k_0 \cdot a\left(n_1^2 - n_2^2\right)^{1/2}$.

All modes (apart from HE_{11}) have a cut-off value in V. Each propagation constant takes the value of β, where $n_{eff} = \beta/k_o$ is the effective refractive index of the corresponding mode. As a mode approaches cut-off, the fields penetrate deeply into the cladding medium. Thus, the mode is poorly confined and poorly guided, and most of the energy propagates in medium 2, leading to $n_2 = 1$ in the tapered fiber. Below the cut-off value of $V = 2.405$, only the fundamental mode (HE_{11}) can propagate. The diameter (D) dependence of effective refractive index of the guided mode (n_{eff}) is obtained numerically, as shown in Fig. 2.2 where refractive index of tapered region (n_1), that of surrounding medium (n_2), and the incident light wavelength (λ) are assumed to be 1.45, 1.0, 780 nm. It is found that, when the diameter of the tapered fiber (D) is reduced to 565 nm ($V = 2.405$) (red dashed line in Fig. 2.2), the tapered fiber only supports the fundamental mode HE_{11} with quasi-linear polarization.

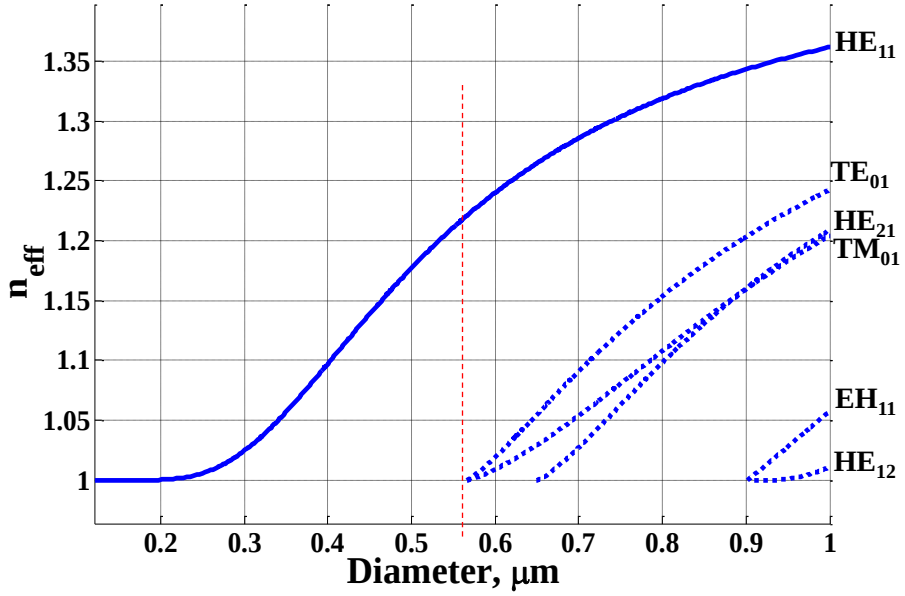

Fig. 2.2 Numerical results of diameter dependence of effective refractive index n_{eff} of the guided mode at 780-nm wavelength. Solid line: fundamental mode. Dot lines: higher order modes; Red line: cut off condition for the fundamental mode HE_{11}.

As for fundamental mode (HE_{11} mode; υ=1), Eq. (2.5) becomes

$$\left\{\frac{J_1'(U)}{UJ_1(U)}+\frac{K_1'(W)}{WK_1(W)}\right\}\left\{\frac{J_1'(U)}{UJ_1(U)}+\frac{n_2^2K_1'(W)}{n_1^2WK_1(W)}\right\}=\left(\frac{\beta}{kn_1}\right)^2\left(\frac{V}{UW}\right)^4. \tag{2.6}$$

$$J_{\upsilon-1}(x)+J_{\upsilon+1}(x)=\frac{2\upsilon}{x}J_\upsilon(x), \tag{2.7a}$$

$$J_{\upsilon-1}(x)-J_{\upsilon+1}(x)=-2J_\upsilon'(x). \tag{2.7b}$$

$$K_{\upsilon-1}(x)-K_{\upsilon+1}(x)=-\frac{2\upsilon}{x}K_\upsilon(x), \tag{2.8a}$$

$$K_{\upsilon-1}(x)+K_{\upsilon+1}(x)=-2K_\upsilon'(x). \tag{2.8b}$$

After considering the spherical Bessel function recursion relation of Eqs. (2.7) and (2.8), Eq. (2.6) can be simplified:

$$\frac{J_0(U)}{UJ_1(U)} = -\frac{n_1^2+n_2^2}{2n_1^2}\left(\frac{K_0(W)}{WK_1(W)}+\frac{1}{W^2}\right)+\frac{1}{U^2}-\left\{\left[\frac{n_1^2-n_2^2}{2n_1^2}\left(\frac{K_0(W)}{WK_1(W)}+\frac{1}{W^2}\right)\right]^2+\frac{\beta^2}{n_1^2k^2}\left(\frac{V}{WU}\right)^4\right\}^{1/2} \tag{2.9}$$

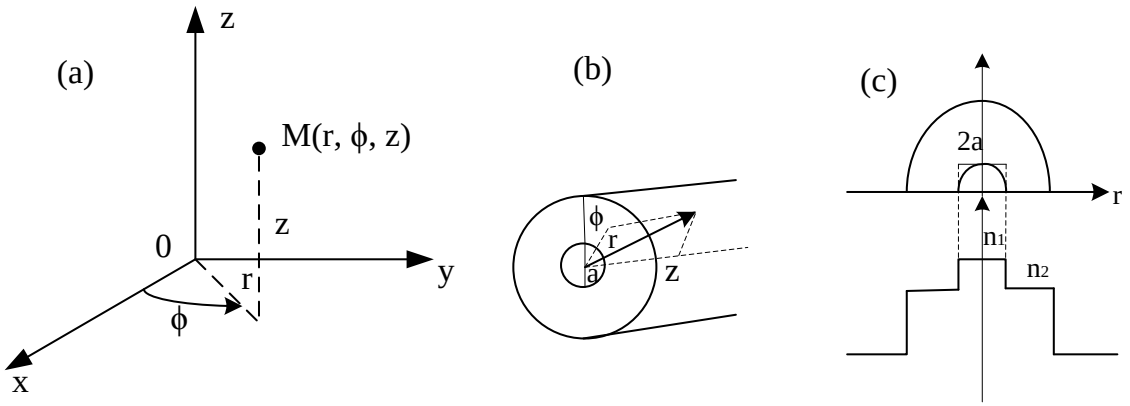

Fig. 2.3 (a) Cylindrical coordinate; (b) Geometry of a standard glass fiber; (c) The profile of its refractive index as a function of *r*.

We study a fundamental mode with quasi-linear polarization. In the cylindrical coordinates (*r*, ϕ ,*z*), as shown in Fig. 2.3, the electromagnetic fields are expressed as

$$\begin{cases} \vec{E}(r,\phi,z) = \left(E_r\vec{r}+E_\phi\vec{\phi}+E_z\vec{z}\right)e^{i\beta z}e^{-i\omega t}, \\ \vec{H}(r,\phi,z) = \left(H_r\vec{r}+H_\phi\vec{\phi}+H_z\vec{z}\right)e^{i\beta z}e^{-i\omega t}. \end{cases} \tag{2.10}$$

The solutions of Maxwell equations for Cartesian components of the electric field $\vec{E}$ of the fundamental mode are given by [61-62]

Inside the core ($0 < r \le a$):

$$E_x = -iA\frac{\beta}{2u}\left[(1-s)J_0(ur)\cos\varphi_0 - (1+s)J_2(ur)\cos(2\phi-\varphi_0)\right]e^{i\beta z}e^{-i\omega t},$$

(2.11a)

$$E_y = -iA\frac{\beta}{2u}\left[(1-s)J_0(ur)\sin\varphi_0 - (1+s)J_2(ur)\sin(2\phi-\varphi_0)\right]e^{i\beta z}e^{-i\omega t},$$

(2.11b)

$$E_z = AJ_1(ur)\cos(\phi-\varphi_0)e^{i\beta z}e^{-i\omega t}.$$

(2.11c)

Outside the core ($a < r < \infty$):

$$E_x = -iA\frac{\beta}{2w}\frac{J_1(U)}{K_1(W)}\left[(1-s)K_0(wr)\cos\varphi_0 + (1+s)K_2(wr)\cos(2\phi-\varphi_0)\right]e^{i\beta z}e^{-i\omega t},$$

(2.12a)

$$E_y = -iA\frac{\beta}{2w}\frac{J_1(U)}{K_1(W)}\left[(1-s)K_0(wr)\sin\varphi_0 + (1+s)K_2(wr)\sin(2\phi-\varphi_0)\right]e^{i\beta z}e^{-i\omega t},$$

(2.12b)

$$E_z = A\frac{J_1(U)}{K_1(W)}K_1(wr)\cos(\phi-\varphi_0)e^{i\beta z}e^{-i\omega t},$$

(2.12c)

where $s = \left(U^{-2}+W^{-2}\right)\Big/\left[J_1'(U)/UJ_1(U) + K_1'(W)/WK_1(W)\right]$, $u = \left(n_1^2k^2-\beta^2\right)^{1/2}$ and $w = \left(\beta^2-n_2^2k^2\right)^{1/2}$. The coefficient *A* is determined by the normalization condition. The angle φ_0

describes the orientation of the transverse $\vec{E}_{\perp} = \left(E_x, E_y\right)$ field, which determines the orientation axis of the field's polarization [61]. $\varphi_0 = 0$ leads to polarization in the *x*-direction and $\varphi_0 = \pi/2$ corresponds to polarization in the *y*-direction. The designation quasi-linear polarization refers to the non-vanishing longitudinal component E_z of the HE_{11}. Because E_z is out of phase by π/2 with respect to the perpendicular components E_x and E_y, this phase difference causes an elliptical rotation of the $\vec{E}$ field in a plane parallel to the fiber axis *z*.

In practical applications such as evanescent wave based optical sensing [81] and evanescent coupling [64-66] [82-83], it is necessary to know the profile of the power distribution around the waveguide. For the model of tapered fibers considered here, according to Eqs. (2.11) and (2.12), expressions for the total intensity $|E|^2$ can be obtain as [61-62]

Inside the core ($0 < r \le a$):

$$|E|^2 = g_{in}\left\{J_0^2(ur) + bJ_1^2\left(ur\right) + fJ_2^2\left(ur\right) + \left[bJ_1^2\left(ur\right) - f_pJ_0\left(ur\right)J_2\left(ur\right)\right]\cos 2\left(\phi - \varphi_0\right)\right\}, \quad (2.13)$$

Outside the core ($a < r < \infty$):

$$|E|^2 = g_{out}\left\{K_0^2\left(wr\right) + cK_1^2\left(wr\right) + fK_2^2\left(wr\right) + \left[cK_1^2\left(wr\right) + f_pK_0\left(wr\right)K_2\left(wr\right)\right]\cos 2\left(\phi - \varphi_0\right)\right\}, \quad (2.14)$$

where $b = 2u^2/\beta^2\left(1-s\right)^2$, $c = 2w^2/\beta^2\left(1-s\right)^2$, $f = \left(1+s\right)^2/\left(1-s\right)^2$, $f_p = 2\left(1+s\right)/\left(1-s\right)$, $g_{in} = |A|^2/2b$, and $g_{out} = |A|^2 J_1^2\left(U\right)/2cK_1^2\left(W\right)$.

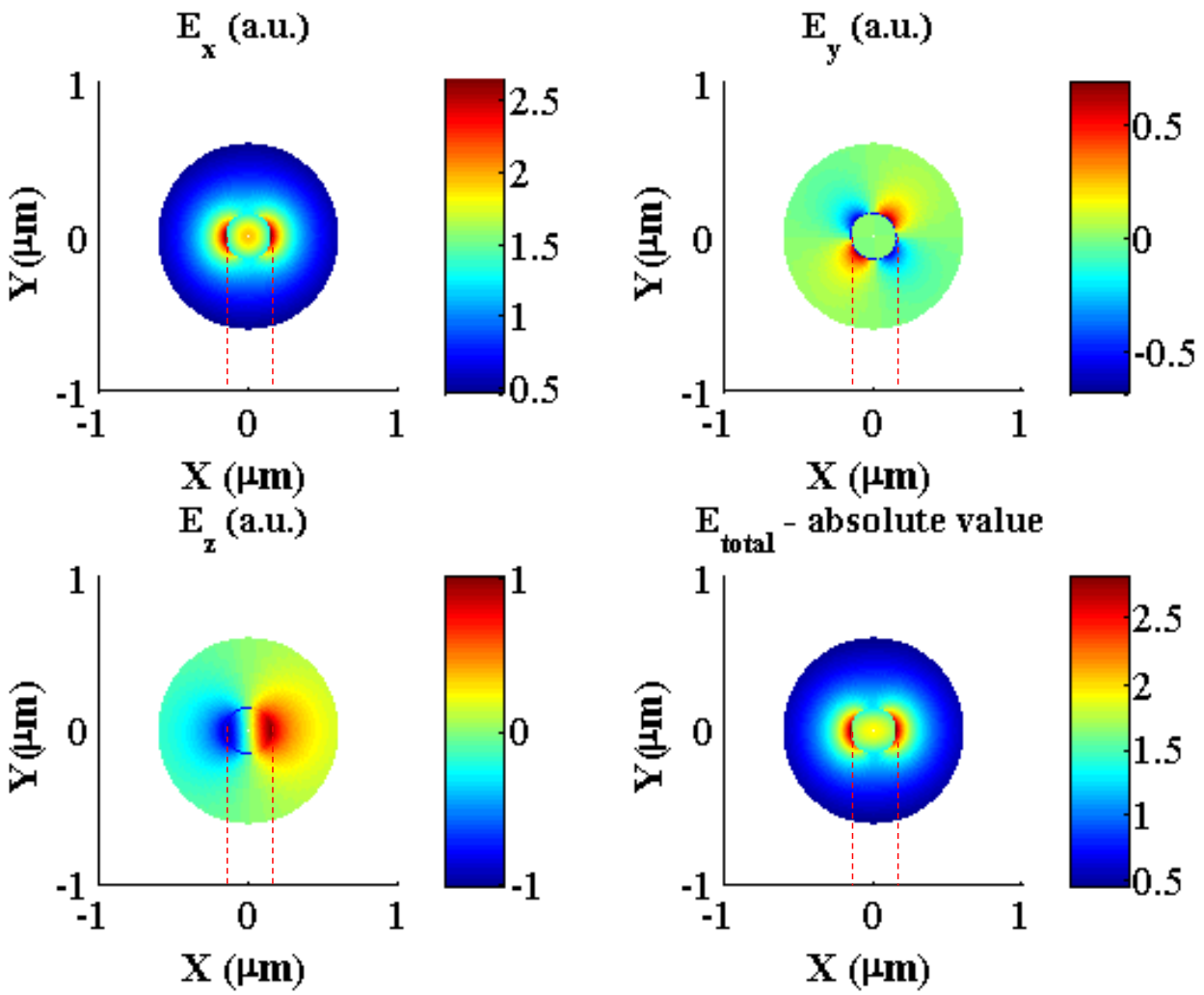

Fig. 2.3 Field profile of HE_{11} in a thin tapered fiber with the diameter of 300 nm at the wavelength of 780 nm. Red dashed lines: diameter size of tapered fiber.

To further understand the field components of the fundamental mode, we numerically calculate the field profile of E_x, E_y, and E_z of the Cartesian-coordinate components of the electric field at a thin tapered fiber with the diameter of 300 nm at the wavelength of 780 nm, as shown in Fig. 2.3. Comparing with the scales of the vertical axes of E_x, E_y, and E_z in Fig. 2.3, it is found that the field of the minor transverse component E_y and the field of the longitudinal component E_z are weaker than the field of the major transverse component E_x. However, the field E_y of the minor transverse component and the field E_z of the longitudinal component are not negligible at all.

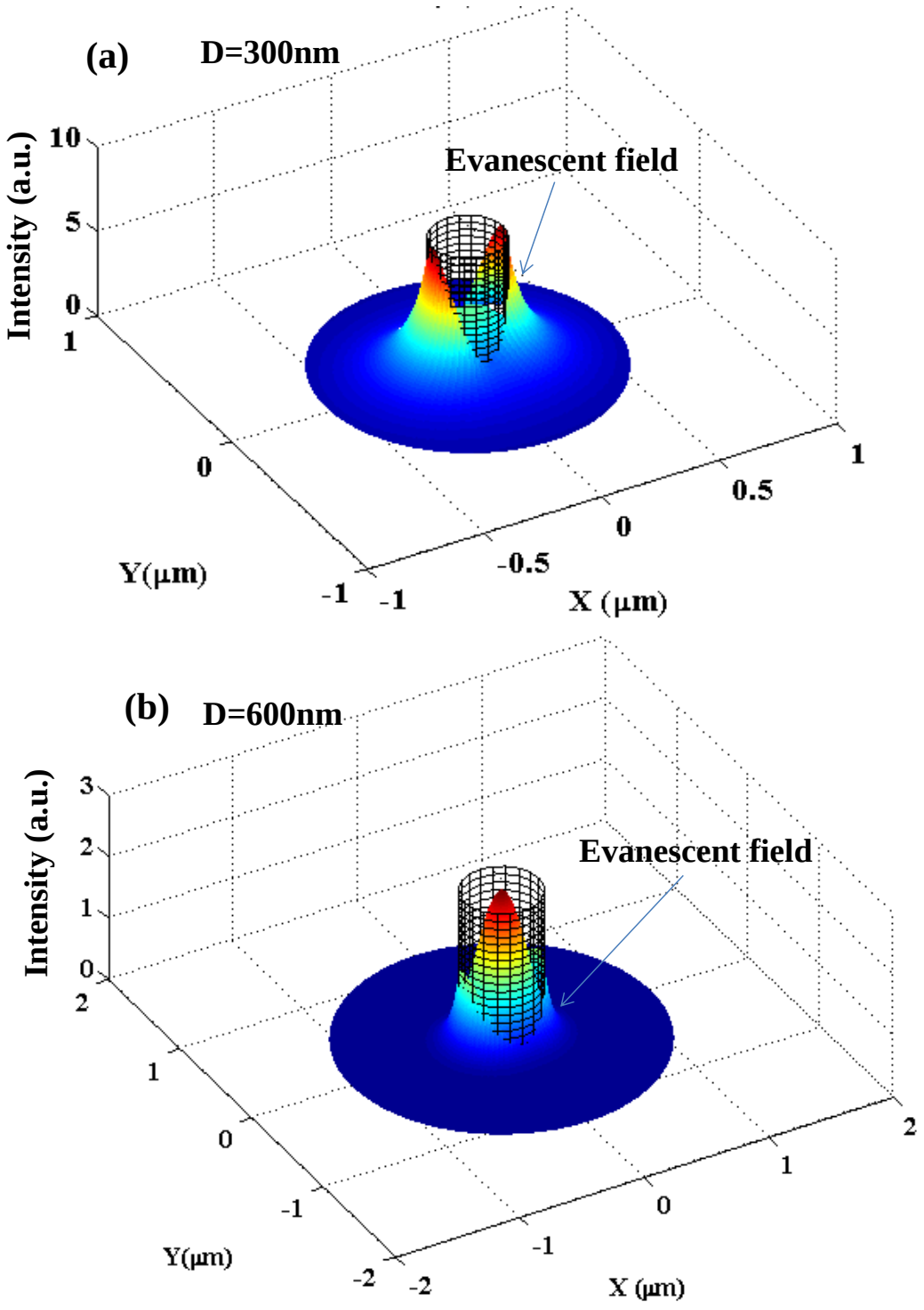

Fig. 2.4 Cross section profiles of the electric field intensity in a fundamental mode HE_{11} of a tapered fiber with the diameters of 300nm (a) and 600 nm (b) at 780-nm wavelength. Cylindrical mesh indicates the tapered fiber as a reference.

Then we also numerically calculate the fundamental mode intensity distributions of a thin tapered fiber with the diameters of 300 nm and 600 nm, as shown in Figs. 2.4(a) and 2.4(b). From the results, the thick tapered fiber with the diameter of 600 nm confines major power inside the tapered fiber, while a large amount of light as an evanescent field is in the outside of the thin tapered fiber with the 300-nm diameter. These results correspond to the previous reports [61-62] that an intense evanescent field is generated in the vicinity of a thin tapered fiber.

2.3 Whispering gallery mode microresonators

2.3.1 Whispering gallery modes

Whispering gallery modes (WGMs) are optical resonances (or modes) of a wave field that are confined inside a given resonator (cavity) with smooth edges due to continuous total internal reflection. In order to investigate the optical modes in a microsphere resonator, we study the Maxwell's equation in time-free form for the electric and magnetic fields *E* and *B* both outside and inside the sphere with constant scalar permittivity (ε) and permeability (μ), and free of charge and current.

$$\nabla \cdot D = 0, \tag{2.15a}$$

$$\nabla \cdot B = 0, \tag{2.15b}$$

$$\nabla \times E = -\mu \frac{\partial H}{\partial t}, \tag{2.15c}$$

$$\nabla \times H = -\varepsilon \frac{\partial E}{\partial t}. \tag{2.15d}$$

According to Maxwell Eqs. 2.15 (a-d), the wave equation can be obtained,

$$\nabla^2 E - \mu\varepsilon \frac{\partial^2 E}{\partial t^2} = 0. \tag{2.16}$$

Assuming the field quantities to vary as $E(\vec{r},t) = E(\vec{r})e^{i\omega t}$. Helmholtz equation can be described, where $k = \omega\sqrt{\varepsilon\mu}$.

$$\nabla^2 E + k^2 E = 0, \tag{2.17}$$

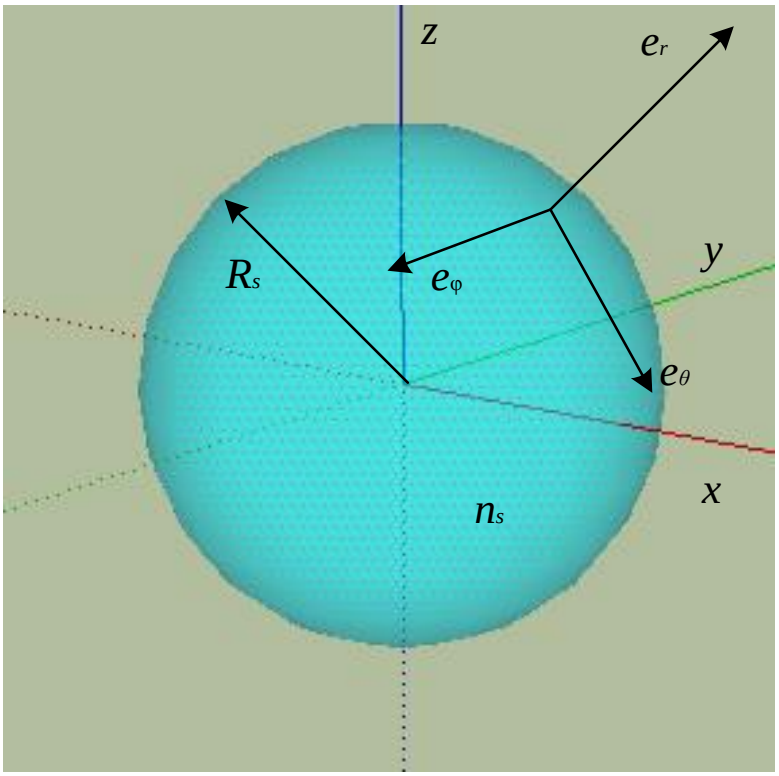

Fig. 2.5 Coordinate system with the unit vectors e_r, e_φ and e_θ, coupled with the sphere surface.

Figure 2.5 shows the spherical coordinate system (r,θ,ϕ). The solution of Maxwell's equations for space with a dielectric sphere can be reduced to the solution of a scalar equation for the Debye potentials [84]. Assuming that the polarization direction of the electromagnetic field of a sphere can be approximated constant along the same spherical coordinate axes at all points in space, which has been verified numerically, the either *E* or *H* component of the electromagnetic field is separable, $E=\psi_r(r)\cdot\psi_\theta(\theta)\cdot\psi_\phi(\phi)$ or $H=\psi_r(r)\cdot\psi_\theta(\theta)\cdot\psi_\phi(\phi)$. There are two kinds of optical WGM modes in microsphere resonator-transverse magnetic (TM) and transverse electric (TE). In the case of TM modes, the magnetic field is tangent to the surface of the sphere and perpendicular to the direction of propagation. In the case of TE modes, these properties are reversed. Here, we consider TE modes. The Helmholtz equation (2.17) in spherical coordinate system can be followed,

$$\frac{1}{r^2}\frac{\partial}{\partial r}\left(r^2\frac{\partial E}{\partial r}\right)+\frac{1}{r^2\sin\theta}\frac{\partial}{\partial\theta}\left(\sin\theta\frac{\partial E}{\partial\theta}\right)+\frac{1}{r^2\sin^2\theta}\frac{\partial^2 E}{\partial\phi^2}+k^2E=0 \tag{2.18}$$

After solving Eq. (2.18) by separation of variables (ψ_r, ψ_θ and ψ_ϕ), there are three ordinary differential equation ($\psi_r(r)$, $\psi_\theta(\theta)$ and $\psi_\phi(\phi)$).

1. The radial dependence

$$\frac{d^2\psi_r}{dr^2}+\frac{2}{r}\frac{d\psi_r}{dr}+\left(k^2-\frac{l(l+1)}{r^2}\right)\psi_r=0. \tag{2.19}$$

The solutions of this spherical Bessel differential equation (2.19) are spherical Bessel functions of the order *l*.

$$\psi_r=c_1 j_l(kn_s r)+c_2 n_l(kr). \tag{2.20}$$

After the approximated solution of Eq. (2.20), the full radial dependence follows [85]:

$$\psi_r(r) = \begin{cases} Aj_l(kn_s r) & r \le R_s \\ B\exp\left(-\alpha \cdot (r - R_s)\right) & r > R_s \end{cases} \tag{2.21}$$

Here, A and B are constants, which are determined by boundary condition at surface and normalization condition. R_s and n_s are the radius of the sphere and refractive index of microsphere. $\alpha = \sqrt{l(l+1)/R_s^2 - k^2}$. The radius dependence of the fields is related to mode numbers l and n. $l = 2\pi n_s R_s / \lambda$. Furthermore, the number of field maximum along the radial direction is determined by n. n is the root number of zeroes of the function (Eq. (2.21) (Bessel function) located inside the sphere. Figure 2.6 shows an example of the field profile in the radial direction for a microsphere with the radius (R_s) of 35 μm.

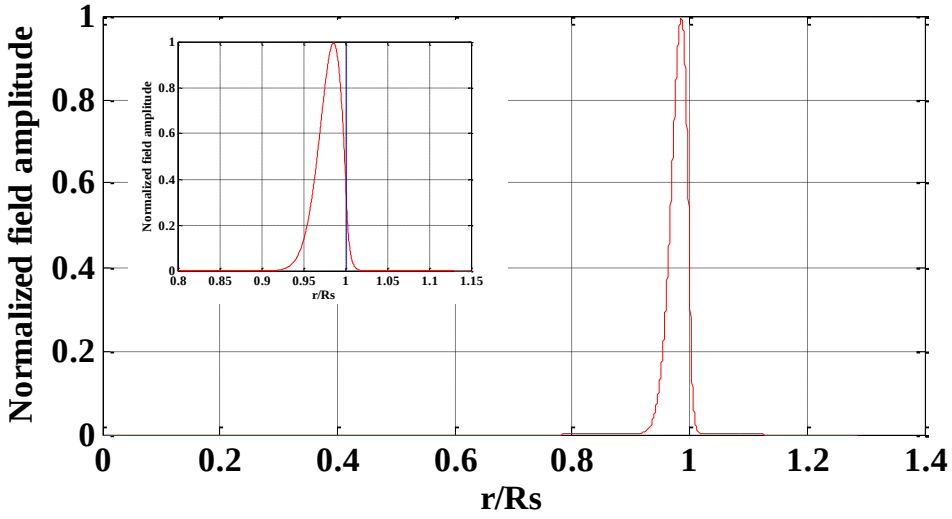

Fig. 2.6 The field profile of a TE mode in the radial direction for a microsphere with the radius (R_s) of 35 μm at the wavelength of 0.78μm. n=1, and l=397. Inset enlarges field profile.

2. The azimuthal dependence

$$\frac{d^2\psi_\phi}{d\phi^2} + m^2\psi_\phi = 0. \tag{2.22}$$

As the field in the azimuthal direction has a periodicity of 2π, the azimuthal dependence of the field represents [85]:

$$\psi_\phi = N_\phi \exp\left(\pm im\phi\right), \tag{2.23}$$

where m is an integer and N_ϕ is the normalization constant to be chosen so that after one revolution the integral of $\left|\psi_\phi\right|^2$ is unity.

3. The polar dependence

$$\frac{1}{\sin\theta}\frac{d}{d\theta}\left(\sin\theta\frac{d\psi_\theta}{d\theta}\right) + \left[l\left(l+1-\frac{m^2}{\sin^2\theta}\right)\right]\psi_\theta = 0. \tag{2.24}$$

The solution of the polar dependent part of a spherical harmonic differential equation is associated Legendre polynomials. The polar solution of the field shows:

$$\psi_\theta = N_\theta P_l^m\left(\cos\theta\right), \tag{2.25}$$

where $P_l^m\left(\cos\theta\right)$ is an associated Legendre polynomial and $m = -l, -(l-1), ..., l-1, l$. N_θ is the normalization constant to be chosen so that the integral of $\left|\psi_\theta\right|^2$ over θ is unity. Figure 2.7 shows the field intensity profile of a TE mode in the azimuthal direction for a microsphere. The polar

contribution ψ_θ is expressed in terms of the exact solutions of the associated Legendre polynomials $P_l^m(\cos\theta)$. We are mainly interested in large m and l values, and the polar angles near $\theta \approx 0$. In this case, according to the ref. [85], the polynomials are well represented by the Hermite-Gauss functions, with Hermite polynomials H_N of the order $N = l - m$.

$$\psi_\theta(\theta) = \exp\left[-\frac{m}{2}\theta^2\right] H_N\left(\sqrt{m}\theta\right), m \geq 1 \geq \theta \tag{2.26}$$

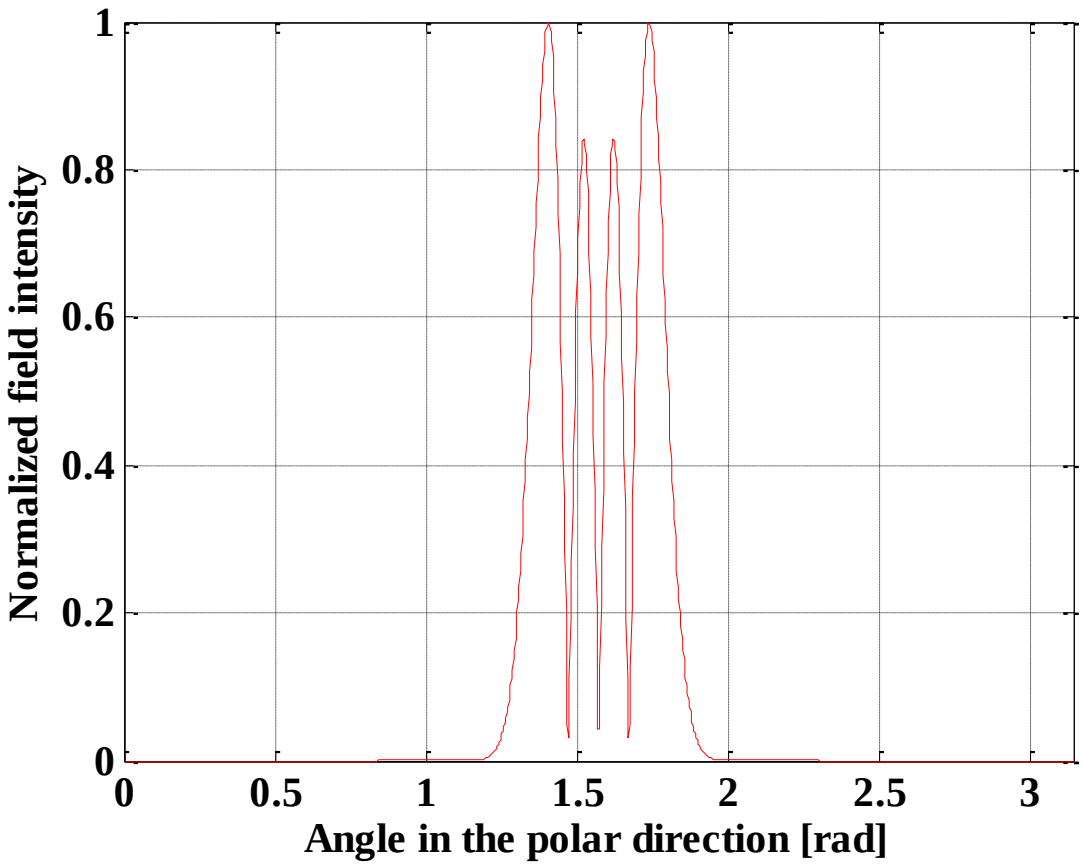

Fig. 2.7 The field intensity profile of a TE mode in the azimuthal direction for a microsphere. $n = 1, l = 150, m = l - 2$.

Characteristic equations

The characteristic equation which describes the relationship between the wave vector *k* and the eigenvalues *l* and *n*, is determined by matching tangential electric and magnetic fields across the surface $r = R_s$. Two independent cases are identified as a consequence of separable solutions [84-85]: (1) transverse electric (TE) modes, where the electric field is parallel to the surface. The vector components are $\vec{E} = \hat{\theta}E_\theta \equiv \hat{\theta}\psi_{n,l,m}, E_\phi = E_r = 0$. (2) transverse magnetic (TM) modes, where the magnetic field is parallel to the surface. The vector components are $\vec{H} = \hat{\theta}H_\theta \equiv \hat{\theta}\psi_{n,l,m}, H_\phi = H_r = 0$. The remaining $\vec{H}$ fields of TE modes, or $\vec{E}$ fields of TM modes, are determined by Maxwell equations. (3) Matching tangential fields leads to the simple characteristic equations.

For TE modes

$$\frac{\frac{j_l\left(k_0 n_s R_s\right)}{R_s} + k_0 n_s j_l'\left(k_0 n_s R_s\right)}{j_l\left(k_0 n_s R_s\right)} = \frac{1}{R_s} - \alpha_s, \tag{2.27}$$

For TM modes

$$\frac{j_l\left(k_0 n_s R_s\right)\Big/ R_s + k_0 n_s j_l'\left(k_0 n_s R_s\right)}{j_l\left(k_0 n_s R_s\right)} = \left(\frac{1}{R_s} - \alpha_s\right)\frac{n_s^2}{n_0^2}. \tag{2.28}$$

We use the following spherical Bessel function recursion relation,

$$j_0\left(x\right) = \frac{\sin x}{x}, \tag{2.29a}$$

$$j_1(x)=\frac{\sin(x)}{x^2}-\frac{\cos(x)}{x}, \tag{2.29b}$$

$$j_{l+1}(x)=\frac{2l+1}{x}\,j_l(x)-j_{l-1}(x). \tag{2.29c}$$

The characteristic equations are expressed by using Eq. (2.29) [85].

TE modes:

$$\left(\frac{l}{R_s}+\alpha_s\right)j_l(k_0 n_s R_s)=k_0 n_s\, j_{l+1}(k_0 n_s R_s), \tag{2.30}$$

TM modes:

$$\left(\left(l+1-\frac{n_s^2}{n_0^2}\right)\frac{1}{R_s}+\frac{n_s^2}{n_0^2}\alpha_s\right)j_l(k_0 n_s R_s)=k_0 n_s\, j_{l+1}(k_0 n_s R_s). \tag{2.31}$$

2.3.2 Quality factor

Quality (Q) factor is an important parameter of a microresonator which quantifies its ability to store light. It is a measure of energy losses and defined as 2π times the ratio of the total energy stored in the cavity divided by the energy lost in a single cycle [82-84]:

$$Q=2\pi\times\frac{Stored\quad energy}{Energy\quad loss\quad per\quad cycle}=\frac{\omega_0 U}{W}. \tag{2.32}$$

Here, ω_0 denotes the angular resonant frequency, U is the energy stored in the mode, and W is the energy loss rate of the mode. Therefore, the behavior of stored energy U in the cavity is described by a differential equation.

$$W = \frac{dU}{dt} = -\frac{\omega_0}{Q}U. \tag{2.33}$$

The solution of the Eq. (2.33) can be obtained as

$$U(t) = U_0 e^{-\frac{\omega_0}{Q}t}. \tag{2.34}$$

Therefore, the optical field in the cavity can be expressed as

$$E(t) = E_0 e^{i\omega t} e^{-\frac{\omega_0}{2Q}t}. \tag{2.35}$$

After Fourier analysis, the optical field in the frequency domain is described as

$$\left|E(\omega)\right|^2 = \frac{E_0^2}{(\omega-\omega_0)^2 + (\omega_0/2Q)^2}. \tag{2.36}$$

From the Eq. (2.36), we find that the WGM resonance has a Lorentzian shape with a linewidth (FWHM) equal ω_0/Q. Thus the Q factor can also be expressed as related both to the linewidth $\Delta\upsilon$ of the resonance located at υ_0, and to the cavity photon lifetime τ through the equation,

$$Q = \frac{\omega_0}{\Delta\omega} = \frac{\upsilon_0}{\Delta\upsilon} = \frac{\lambda}{\Delta\lambda} = \omega_0\tau$$

(2.37)

In the experiment, a WGM is represented by a dip in the fiber throughput. So according to the transmittance spectrum in the fiber throughput and Eq. (2.37), the *Q* factor is obtained, as show in Fig. 2.8.

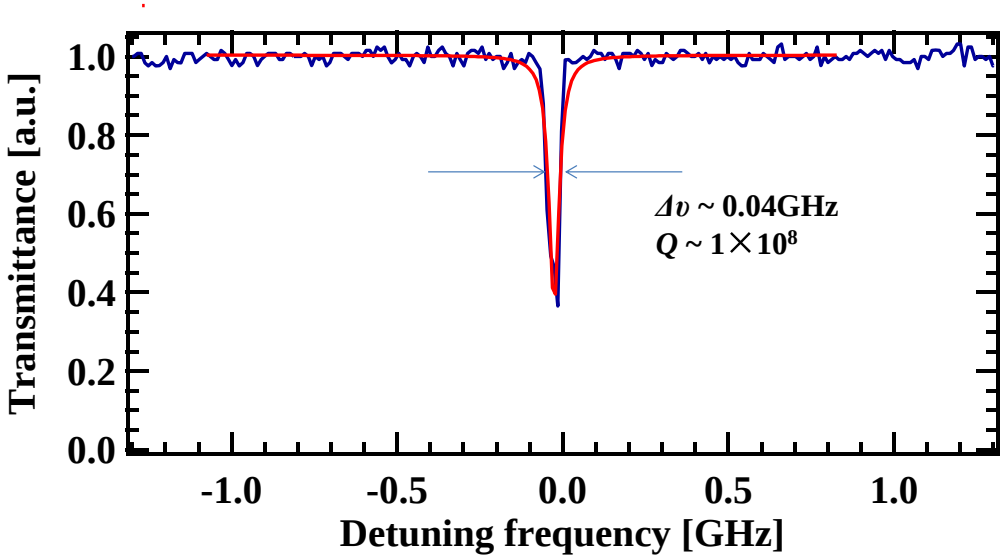

Fig. 2.8 Transmittance spectrum with a WGM mode. *Q* factor is 1×10^8 at 780-nm wavelength. Red curve: Lorentzian fitting curve.

Loss mechanisms in microspheres include scattering loss from surface contaminants, absorption loss due to molecular resonances, Rayleigh scattering, and radiative loss. Radiative loss is the tunneling loss due to the curvature of the waveguiding boundaries in the direction of propagation. Absorption and Rayleigh scattering are the predominant effects limiting the magnitude of the *Q* for air clad microspheres. The total *Q* factor of a WGM spherical cavity is made up of all the loss contribution, which can be decomposed into the following equation:

$$\frac{1}{Q_{total}} = \frac{1}{Q_{mat}} + \frac{1}{Q_{rad}} + \frac{1}{Q_{ss}} + \frac{1}{Q_{coupling}} + \ldots \tag{2.38}$$

Here, Q_{total} denotes the total cavity quality factor, Q_{mat} denotes the material absorption loss, Q_{rad} accounts for radiation loss, Q_{ss} presents scattering loss from surface imperfections, and $Q_{coupling}$ represents the energy loss due to input and output coupling.

The Q_{mat} factor associated with materials absorption is determined by [43]:

$$Q_{mat} = \frac{2\pi n}{\lambda \alpha}, \tag{2.39}$$

where λ is the light wavelength, n is the refractive index of the materials at the light wavelength, and α is the linear attenuation in the cavity caused by materials absorption.

The Q_{ss} factor owing to scattering loss by the surface homogeneity can be estimated by [43]:

$$Q_{ss} = \frac{\lambda^2 R_s}{\pi^2 \sigma^2 B}, \tag{2.40}$$

where σ and B are the rms size and the correlation length of surface inhomogeneities, respectively.

The Q_{rad} factor due to radiative loss is shown to be [85]:

$$Q_{rad} = \frac{l^2 n_s}{k^3 c\varepsilon_0 n_s^2 n_0^2 R_s^5 Z_0}\left[n_0 \left(\frac{\pi}{\gamma_1}\right)^{1/4} j_l\left(kn_0 R_s\right) j_{l+1}\left(kn_0 R_s\right) - n_s \left(\frac{\pi}{\gamma_2}\right)^{1/4} j_{l-1}\left(kn_s R_s\right) j_l\left(kn_0 R_s\right)\right]^{-2} \tag{2.41a}$$

$$\gamma_1 = l - \frac{1}{2} - kn_0 R_s \frac{j_l\left(kn_0 R_s\right)}{j_{l-1}\left(kn_0 R_s\right)} + \frac{\left(kn_0 R_s\right)^2}{l} \tag{2.41b}$$

$$\gamma_2 = l + \frac{1}{2} - kn_0 R_s \frac{j_{l+1}\left(kn_0 R_s\right)}{j_l\left(kn_0 R_s\right)} + \frac{\left(kn_0 R_s\right)^2}{l} \tag{2.41c}$$

where c is the speed of light, ε_0 is the permittivity of free space, and $Z_0 \approx 377$ is the impedance of free space. R_s and n_s are the radius and refractive index of microsphere, respectively.

2.3.3 Mode spacing

The free spectral range (FSR) of a cavity represents the frequency (wavelength) spacing between consecutive longitudinal modes. This definition, commonly used for Fabry-Perot (FP) cavities, is somewhat ambiguous for the cavities in this work, as the mode spectrum is highly complex. However, by using the most direct analogy to a FP, a microresonator can be considered as a FP cavity wrapped around onto itself, such that the periphery of the resonator corresponds to the FP mirror spacing. The distance between adjacent resonances has consecutive mode number such that FSR can be defined as

$$\Delta\lambda_{FSR} = \frac{\lambda^2}{2\pi n_s R_s}. \tag{2.42}$$

As for WGM microresonators, the mode spacing is defined as the wavelength difference between two consecutive mode numbers *l* in the same order mode *n*:

$$\Delta\lambda_{n,l} = \lambda_{n,l+1} - \lambda_{n,l} = \frac{\lambda^2}{2\pi R_s} \frac{\tan^{-1}\left(\sqrt{m^2-1}\right)}{\sqrt{m^2-1}}. \tag{2.43}$$

Here, *m* is the relative refractive index. The mode spacing is defined for TE and TM modes. Comparing with Eq. (2.42) and Eq. (2.43), the effective refractive index of a microsphere resonator can be defined as

$$n_{eff} = \frac{\sqrt{m^2-1}}{\tan^{-1}\sqrt{m^2-1}} \tag{2.44}$$

2.3.4 Mode volume

The volume that each cavity mode occupies is dependent on the cavity resonant field distribution, which in turn depends on the particular cavity geometry. Modal volume plays a fundamental role in many applications of microcavities, resulting in optical energy that is tightly confined to physical volumes on the order of hundreds to a couple thousand cubic microns. This coupled with the low loss possible in high-*Q* microcavities results in a very large energy density in the cavity. These large energy densities are of use for areas ranging from nonlinear optical

wave generation to quantum optics, where the large electric field per photon can allow a strong interaction with an atomic system. The mode volume is defined as [82-84],

$$V_m = \frac{\int_{V_Q} \varepsilon(\vec{r}) \left|\vec{E}\right|^2 d^3\vec{r}}{\left|\vec{E}_{\max}\right|^2}, \tag{2.45}$$

where $\left|\vec{E}\right|$ represents the cavity electric field, $\varepsilon(\vec{r}) = n^2(\vec{r})$ is the refractive index at $\vec{r}$ squared, and V_Q denotes the integration volume. According to refs. [82][86], the mode volume for a spherical WG resonator can also be estimated as,

$$V_m = 3.4\pi^{3/2} \left(\frac{\lambda}{2\pi n}\right)^3 l^{11/6} \sqrt{l-m+1}. \tag{2.46}$$

2.3.5 Circulating power

The combination of high *Q* factor and tight mode confinement in a WGM microresonator significantly enhances the light field, leading to an extraordinarily high light intensity inside the cavity with a modest input power. This enables strong interactions between the light field and objects placed in the cavity mode volume. For a microlaser configuration, it is the reason that higher *Q* devices with smaller size have lower lasing thresholds. One of the benefits of the long photon storage time in high-*Q* microcavities is that they can build up a significant internal circulating power with low pump powers. The power enhancement (η) in a WGM microresonator can be expressed by [87-88]

$$\eta = \frac{P_{circ}}{P_{in}} = \frac{1}{\tau_r} \frac{4\kappa_{ex}}{4\Delta\omega^2 + \left(\kappa_0 + \kappa_{ex}\right)^2}, \tag{2.47}$$

where P_{in} and P_{circ} denote the input power and the intracavity circulating power, respectively. τ_r is the photon round trip time, $\Delta\omega$ represents the detuning between the input light frequency and the resonant mode frequency ω_c. $\kappa_0 = \omega_c / Q_0$ is the intrinsic cavity loss and $\kappa_{ex} = \omega_c / Q_{ex}$ expresses the coupling loss. Q_0 and Q_{ex} are the intrinsic and coupling quality factors. When the incident light frequency is on resonance with a WGM in the cavity ($\Delta\omega$=0), at the critical coupling point ($\kappa_0 = \kappa_{ex}$), the power enhancement η is maximized.

$$\eta = \frac{P_{circ}}{P_{in}} = \frac{Q_0}{\tau_r \omega_c}. \tag{2.48}$$

This formula indicates that the cavity buildup factor is proportional to Q_0, explaining why ultra-high quality factor cavities can result in a substantial amplification of the input resonant field energy. For mW input power and mode volumes of 1000 μm^3, it is possible to achieve the power in the cavity of the order of GW/cm^2. WGM resonators are especially suitable as laser cavities for ultra-low threshold lasing.

2.4 General properties of localized surface plasmon resonance

Surface plasmon resonance (SPR) is the collective oscillation of electrons that are confined to the interface of a metal and a dielectric stimulated by incident light. The resonance condition is established when frequency of light photons matches the natural frequency of surface electrons oscillating against the restoring force of positive nuclei and the phase match between photons and surface plasmon wave-vectors is satisfied. SPR in nanometer-sized structures is called localized surface plasmon resonance. The fully three-dimensional solution of the electrodynamics response of a particle excited by an electromagnetic wave turns out to be important in general. But, the underlying phenomena and physics can be analyzed and understood by means of the much simpler quasi-electrostatic model. For particles being smaller

than the incident wavelength λ, the exciting field E_{in} is nearly uniform across the whole particle and the retardation arising owing to the finite speed of light is negligible. Figure 2.9 shows schematic diagram illustrating localized surface plasmon of metal sphere. Assuming a metal sphere in a uniform dielectric medium, the dipole moment for a metal sphere is given by the polarizability α [89-92].

$$\vec{p} = 4\pi R^3 \varepsilon_0 \frac{\varepsilon_p - \varepsilon_m}{\varepsilon_p + 2\varepsilon_m} \varepsilon_m \vec{E} = \alpha \varepsilon_m \vec{E}, \tag{2.49}$$

where R is the radius of metal sphere. ε_p and ε_m are the dielectric constants of the material of sphere and of the surrounding medium, respectively. According to Eq. (2.49), the polarizability α of the metal sphere is expressed by [89-92],

$$\alpha = 4\pi\varepsilon_0 R^3 \frac{\varepsilon_p - \varepsilon_m}{\varepsilon_p + 2\varepsilon_m}. \tag{2.50}$$

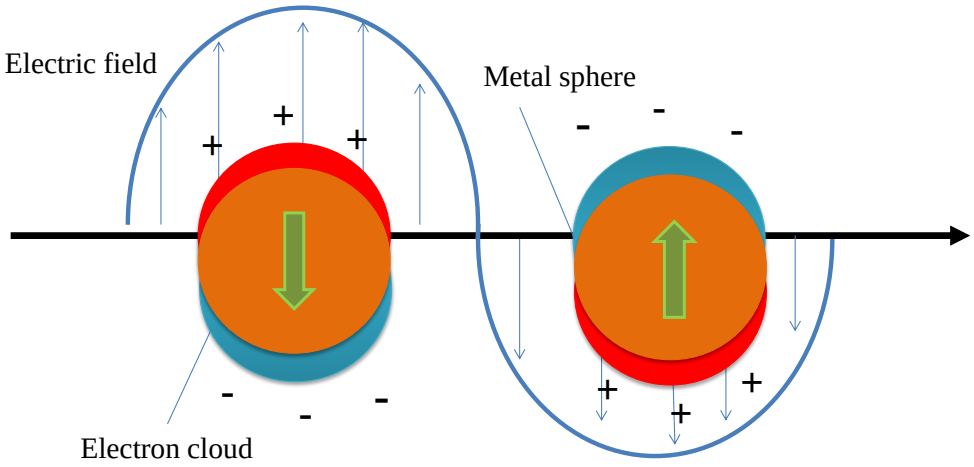

Fig. 2.9 Schematic diagram illustrating a localized surface plasmon.

Thus, the polarization of the metal sphere is driven by the oscillating incident field. The oscillating charges on the sphere cause a scattering into the far field as well as absorption of

electromagnetic radiation. Within the framework of the quasi-electrostatic model the absorption cross section is simply represented by[92],

$$C_{abs} = k\,\mathrm{Im}\left[\alpha / \varepsilon_0\right] = k\,\frac{\varepsilon_p''}{\varepsilon_m}\,\frac{4\pi R^3}{3}\left|\frac{3\varepsilon_m}{\varepsilon_p + 2\varepsilon_m}\right|^2, \tag{2.51}$$

where $k = 2\pi/\lambda$. And ε_p'' is the imaginary component of the metal dielectric function. Furthermore, the internal losses are proportional to the particle volume, whereas the scattering cross section is given by [92],

$$C_{sca} = \frac{k^4}{6\pi}\left|\alpha / \varepsilon_0\right|^2 = \frac{8\pi}{3}k^4 R^6\left|\frac{\varepsilon_p - \varepsilon_m}{\varepsilon_p + 2\varepsilon_m}\right|^2. \tag{2.52}$$

From the Eq. (2.52), the scattering cross section is proportional to the square of the volume, resulting in a rapidly vanishing scattering for very small spheres. The polarization inside the sphere is directly related to the local electric field enhancement (FE). FE is shown by [92],

$$\frac{\left|E_{loc}\right|}{\left|E_{in}\right|} = \left|\frac{\varepsilon_p}{\varepsilon_p + 2\varepsilon_m}\right|. \tag{2.53}$$

2.5 Evanescent coupling theory

2.5.1 Coupling between tapered fiber and microsphere

A tapered fiber is used to coupling light in and out of microsphere resonator by evanescent coupling. The waveguide/resonator system, H. A. Haus [93] has proposed a simple model based on the assumption of weak coupling between the resonator and waveguide, and low

intrinsic resonator loss. This model is also valid for the tapered-fiber-coupled microsphere resonator (Fig. 2.10), which has been demonstrated by K. J. Vahala [94-95]. On resonance the internal field can be described by the following equation [95].

$$\frac{d\alpha}{dt} = -\frac{1}{2}\left(\kappa_0 + \kappa_{ex}\right)\alpha + i\sqrt{\kappa_{ex}}s. \tag{2.54}$$

Here, α is the internal resonator field and s denotes the power normalized waveguide field. κ_0 is the intrinsic resonator loss rate. κ_{ex} represents the fiber-sphere coupling rate. According to Eq. (2.54), the internal resonator field α is determined by considering both excitation by the fundamental waveguide mode, and decay due to the intrinsic cavity loss and input-ouput coupling loss.

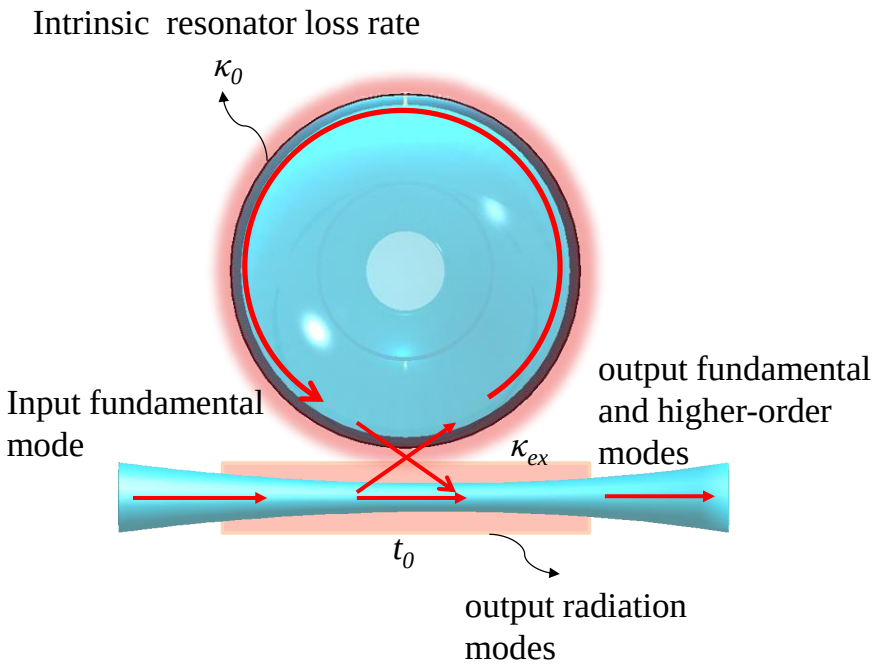

Fig. 2.10 Coupling and loss parameters in a tapered-fiber-coupled microsphere resonator system.

Assuming that the power coupled into higher-order modes are radiated or coupled to cladding modes upon the transition to single-mode fiber, the transmittance through the waveguide consists of an interference of the partially transmitted input field with the field

coupled from the resonator back into the fundamental mode (HE_{11}) of tapered fiber. It is expressed by,

$$T_a = \left| \frac{t_0}{s} + i \frac{\sqrt{\kappa_{ex}}\alpha}{s} \right|^2, \tag{2.55}$$

where t_0 is the transmitted amplitude which is not coupled into the microsphere resonator. In steady state, the transmittance can be described by,

$$T_a = \left(\frac{1 - K_a}{1 + K_a} \right)^2. \tag{2.56}$$

Here, K_a is the coupling parameter, which is defined as,

$$K_a = \frac{\kappa_{ex}}{\kappa_0}. \tag{2.57}$$

Figure 2.11 shows coupling regimes for a tapered-fiber-coupled microsphere resonator system. The transmittance and linewidth properties dependent on the distance between tapered fiber and microsphere resonator are characterized by under coupling, critical coupling and over coupling regimes.

According to Eq. (2.37), the loss rate κ (intrinsic loss rate or coupling rate) is presented by,

$$\kappa = \frac{1}{\tau} = \frac{\omega}{Q} = \omega = 2\pi\Delta\upsilon, \tag{2.58}$$

where Q is the total quality factor of microsphere, τ and ω denote the photon round trip time and resonant mode frequency. $\Delta\upsilon$ represents the linewidth of resonant mode.

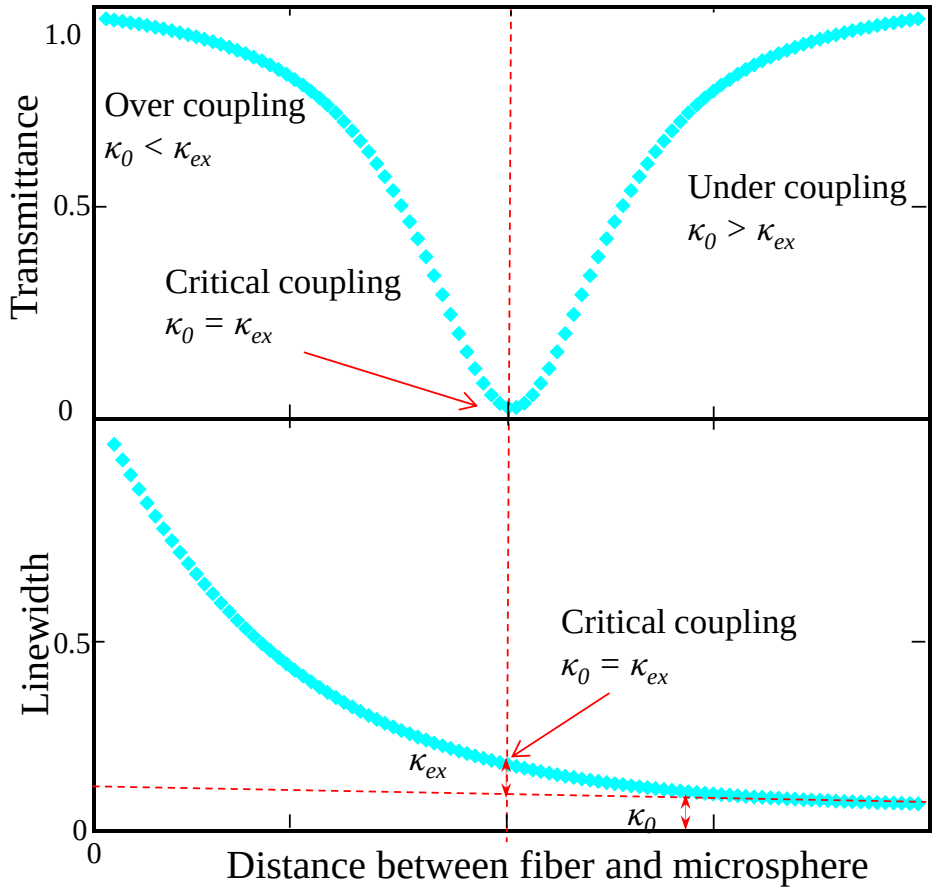

Fig. 2.11 Coupling regimes for a tapered-fiber-coupled microsphere resonator system. It shows the transmittance and linewidth (Δυ) on resonance versus the distance. The zero point corresponds to the tapered fiber in contact with the surface of microresonator. $\kappa = 2\pi\Delta\upsilon$.

Under coupling regime:

When the tapered fiber is far away from the microsphere resonator, the coupling is weak and the intrinsic resonator loss rate (κ_0) exceeds the fiber-sphere coupling rate (κ_{ex}), $\kappa_0 > \kappa_{ex}$ according to Eq. (2.58) and Fig. 2.11 (b). In this case, the amplitude of the cavity field is much less than the amplitude of the transmitted waveguide field and the resonant peak with narrow linewidth $\Delta\upsilon$ appears. The linewidth $\Delta\upsilon$ on resonance gradually increases by approaching the tapered fiber to the surface of microsphere resonator. Because the fiber is far away from the surface of microsphere that the fiber-sphere coupling rate κ_{ex} is considered to be very small, the

linewidth of the resonant peak $\Delta\upsilon$ is almost regard as the linewidth due to the intrinsic cavity loss rate κ_0 ($\kappa_0 = 2\pi\Delta\upsilon$), corresponding to the Q factor of microsphere resonator. According to Eq. (2.56), the transmittance from the end of tapered fiber T_a is smaller than unity ($0<T_a<1$).

Critical coupling regime:

When the tapered fiber is continuously approached to the microsphere resonator at a distance, the coupling is increased to the point where fiber-sphere coupling rate (κ_{ex}) balances the intrinsic resonator loss rate (κ_0), $\kappa_0 = \kappa_{ex}$, (Fig. 2.11(b)). The transmittance from the end of tapered fiber vanishes ($T_a = 0$, in Fig. 2.11 (a)) due to the destructive interference of the resonator field and the transmitted pump field. At this critical coupling point, there is no waveguide transmittance, all the incident power is coupled into the microresonator, indicating a maximum of the circulating power inside the resonator.

Over coupling regime:

Further approaching the tapered fiber to the surface of microsphere resonator, the linewidth $\Delta\upsilon$ on resonance continues to increase. Accordingly, the fiber-sphere coupling rate (κ_{ex}) gradually increased, which is larger than the intrinsic resonator loss rate (κ_0), $\kappa_0 < \kappa_{ex}$ (Fig. 2.11(b)). The transmittance for the end of tapered fiber is smaller than 1, $0<T_a<1$ (Fig. 2.11(a)). Specially, in the case of completely over coupling regime ($\kappa_{ex} \gg \kappa_0$), the transmittance reaches unity, which is important for the critical propagating photon to localized surface plasmon (PP-LSP) coupling condition between the Au-coated tip and the tapered-fiber-coupled microsphere resonator for the purpose of obtaining highly efficient coupling light into the metal tip. Because, as for the coupling between the metal tip and the tapered-fiber-coupled microsphere resonator, at the critical PP-LSP coupling regime, the intrinsic cavity loss is negligibly small and fiber-sphere coupling rate is equal to the tip-sphere coupling rate, the waveguide transmission vanishes, and all incident light power is coupled to the metal tip, implying that the coupling efficiency reaches nearly 100%, discussed in section 2.5.2.

2.5.2 Coupling between tapered-fiber-coupled microsphere and Au-coated tip

In order to achieve highly efficient coupling of light into Au-coated tip, a tapered-fiber-coupled microsphere resonator was proposed to efficiently couple light into Au-coated tip in this paper, as shown in Fig. 2.12. According to refs. [95-96], we consider the coupling conditions among a tapered fiber, a microsphere resonator and an Au-coated AFM tip. The coupling from a tapered fiber to an Au-coated AFM tip are basically described by three parameters, the fiber-sphere coupling rate (κ_{ex}), the intrinsic cavity loss rate (κ_0), and the tip-sphere coupling rate (κ_{tip}). The internal cavity field (α) in the tapered-fiber-microsphere coupled Au-coated tip on resonance can be described by,

$$\frac{d\alpha}{dt} = -\frac{1}{2}\left(\kappa_0 + \kappa_{ex} + \kappa_{tip}\right)\alpha + \mathrm{i}\sqrt{\kappa_{ex}}\,s, \tag{2.59}$$

where s is the power normalized waveguide field. The first term is the total energy loss rate from the cavity because of the fiber-sphere coupling loss, the intrinsic cavity loss and the tip-sphere coupling loss. And the second term gives the excitation of the microsphere cavity via the tapered fiber. The transmittance past the resonator consists of the transmitted optical field and the field coupled out of the resonator into the tapered fiber, and is expressed in the form,

$$T_b = \left| t_0 / s + i\sqrt{\kappa_{ex}}\,\alpha / s \right|^2, \tag{2.60}$$

where t_0 is the transmitted amplitude which is not coupled into the microsphere cavity. In the steady state, the waveguide transmission under the resonant condition can be given by,

$$T_b = \left(\frac{1-K_b}{1+K_b}\right)^2. \tag{2.61}$$

In this expression, the coupling parameter K_b is introduced, defined as the ratio of coupling loss rate between the tapered fiber and microsphere resonator to intrinsic resonator loss rate and the tip-sphere coupling loss rate.

$$K_b = \frac{\kappa_{ex}}{\kappa_0 + \kappa_{tip}}. \tag{2.62}$$

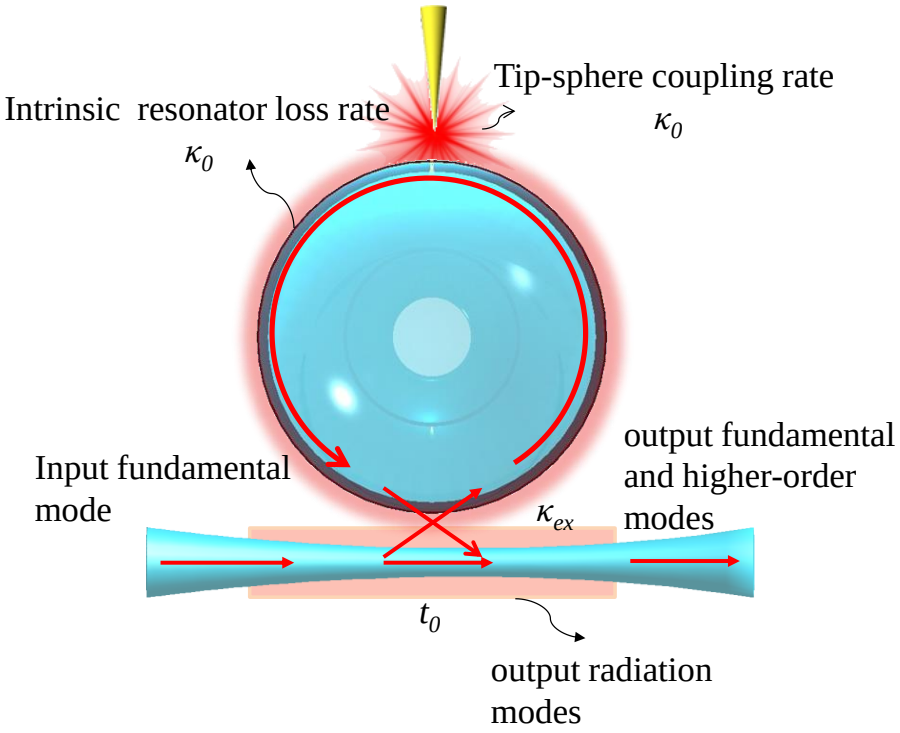

Fig. 2.12 Illustration of coupling and loss parameters between a tapered-fiber-coupled microsphere resonator and Au-coated tip system.

This coupling parameter K_b allows a simple way to study the coupling regimes and properties of this system. In this plasmonic-photonic hybrid cavity system, the intrinsic cavity loss of microsphere resonator is considered to be negligibly small, and the tip-sphere coupling rate is larger than the intrinsic loss rate of microsphere resonator ($\kappa_{tip} \gg \kappa_0$) owing to the existence of LSP at the Au-coated tip (D < 100 nm). Therefore, to obtain highly efficient

coupling of light into the metal tip ($\kappa_{ex} = \kappa_{tip} \gg \kappa_0$), the tapered-fiber-coupled microsphere resonator should be under over coupling regime ($\kappa_{ex} \gg \kappa_0$). In the experiment, before approaching an Au-coated AFM tip to the surface of microsphere resonator, the tapered-fiber-coupled microsphere resonator must be in the completely over coupling regime ($\kappa_{ex} \gg \kappa_0$), in which the high *Q* and about unity of transmittance are required. In practice, considering the experiment conditions (e.g. vibration of air conditioner…), usually, the tapered fiber is contacted to the surface of the microsphere resonator under over coupling condition. Figure 2.13 shows coupling regimes between a tapered-fiber-coupled microsphere and Au-coated tip system. When approaching an Au-coated tip to the surface of microsphere, the coupling conditions are from over coupling, critical propagating photon (PP) to Localized surface plasmon (LSP) coupling to under coupling regime. In brief, K_b=1 is the critical PP-LSP coupling regime, K_b<1(>1) is the under (over) coupling regime. At the critical PP-LSP coupling regime, if we can assume that the intrinsic cavity loss is negligibly small and fiber-sphere coupling rate is equal to the tip-sphere coupling rate ($\kappa_{ex} = \kappa_{tip} \gg \kappa_0$), the waveguide transmission vanishes, and all incident light power is coupled to the metal tip, implying that the coupling efficiency reaches nearly 100%. In addition, if these coupling rates are smaller than the cavity round trip time κ_{ex}, κ_0, $\kappa_{tip} \ll c/l_c$, where *c* and l_c denote the light velocity and the effective cavity length, κ_{tip} can be given by,

$$\kappa_{tip} = \frac{c}{l_c} \times \frac{\sigma}{A} \tag{2.63}$$

Here *A* and σ are the cross-section of the WGMs and the effective extinction cross-section of the metal tip.

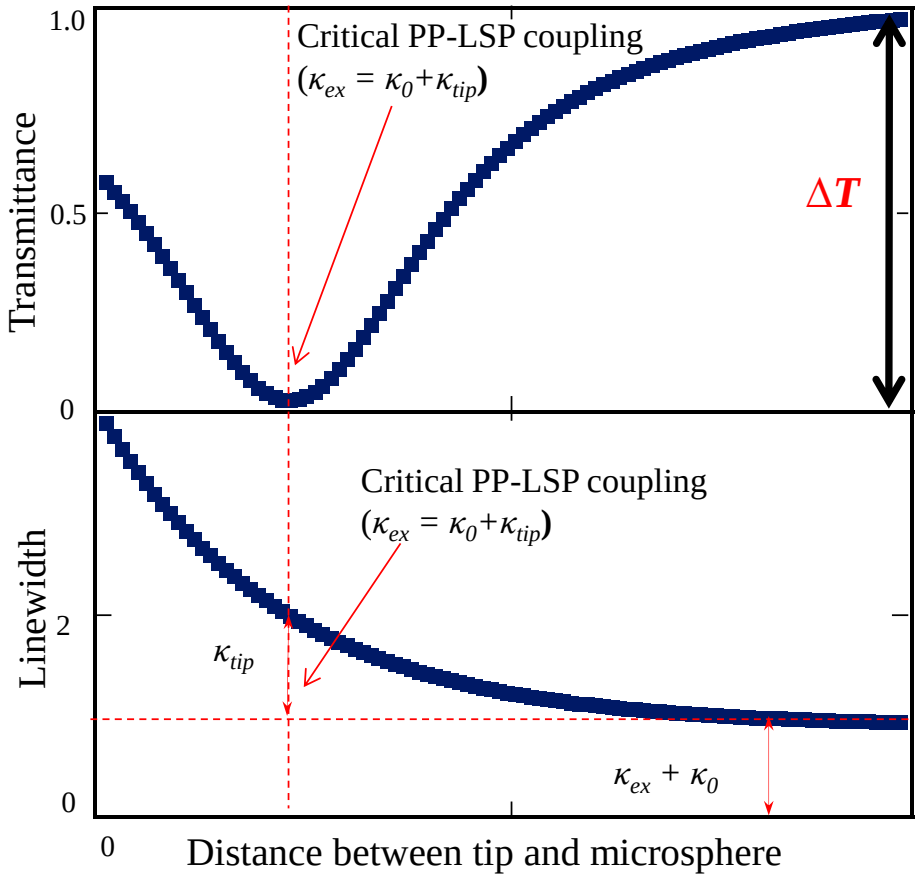

Fig. 2.13 Coupling regimes for a tapered-fiber microsphere coupled Au-coated tip system. It shows the transmittance on resonance versus the distance. The zero point corresponds to Au-coated tip in contact with the surface of microsphere. ΔT: Evaluation of PP-LSP coupling efficiency into metal nanostructures.

2.6 Summary

In this chapter, the properties of the field in the fundamental mode HE_{11} of a tapered fiber using the exact solutions of Maxwell equations are studied. The simple analytical expressions for the total intensity of the electric field are obtained. We find that an intense evanescent field was generated in the vicinity of a thin tapered fiber, indicating the possibility of the efficient interaction of the propagating photons in the tapered fiber with the metal tip. In addition, basic properties of dielectric WGM microresonators, such as *Q*-factor, mode volume and TE/TM

modes are discussed. General properties of localized surface plasmon, such as absorption cross section and scattering cross section are introduced.

And coupling conditions among tapered fiber, microsphere resonators and Au-coated tip is also investigated analytically. Highly efficient coupling of light into a metal tip is theoretically demonstrated using a tapered-fiber-coupled microsphere resonator. Controlling the distance between the tapered fiber and microsphere resonator changes the coupling conditions of the tapered-fiber-coupled microsphere resonator. The coupling conditions are from the under coupling regime to the completely over coupling regime. Under the completely over coupling regime, by approaching the Au-coated tip to the surface of microsphere resonator at the opposite direction, the coupling conditions between the Au-coated tip and microsphere are discussed. When under the critical PP-LSP coupling condition between the Au-coated and microsphere resonantor, the coupling efficiency of light from the tapered fiber to the Au-coated tip can reach 100%.

Chapter 3 Experimental preparation

3.1 Basic setup

The basic setup in this study is shown in Fig. 3.1. A tunable external cavity diode laser (New Focus, TLB-6312, Linewidth~300 kHz, Wavelength~780 nm), whose frequency was controlled by a triangle wave from a function generator (FG: NF, DF1906), was introduced into the tapered fiber as a probe and excitation light. The pair components of half wave plates (HWP1, λ/2) and polarization beam splitters (PBS) controlled the power of the incident light coupled into the tapered fiber. Two quarter wave plates (QWP1, 2, λ/4) and a half wave plate (HWP2) were used to adjust the polarization state of the excitation light to selectively excite transverse magnetic modes (TM) parallel to the tip axis in order to efficiently induce TPF and SHG [11][19-20]. The power of the incident light was monitored using an optical power meter (Newport, 2935-C) connected to the output of a fused fiber coupler (95:5, 50:50). In order to control the coupling conditions, the separation distances between the tapered fiber and microsphere, between the tapered fiber and Au-coated tip, and also between the Au-coated tip and microsphere were controlled by three-dimensional piezo manipulators (PI-Polytec, P-620.ZCL, P-621.1CD, P-621.ZCD). These components were placed in a plastic box, which was kept at a stable condition, in order to suppress the environmental disturbances for the

stabilization of the tip position. The Transmitted light from the end of the tapered fiber was measured using a high sensitive photodiode (Thorlabs, DET36A) and a digital oscilloscope (Tektronix, TDS5034). The SHG and TPF intensity emitted from the Au-coated tip and PIC-attached Au-coated tip was measured by a microscopy system set on the top of the samples. The emission signal was collected by an objective lens with 0.42 NA (Mitutoyo Corp.; M Plan Apo SL 50×) and 0.28 NA (Mitutoyo Corp.; M Plan Apo 20×) and then passed through a dichroic mirror and shortpass filters to eliminate the excitation light, and was incident into the multimode fiber bundle connected to a spectrometer (JASCO Corporation; iDus; Andor).

In this study, an AFM silicon tip is one of main elements for coating Au film on the surface of this silicon tip. The Au-coated tip was set on a piezo stage with the maximum resolution of 1 nm and we did not use any feedback program for controlling the Au-coated tip position. In order to measure the tip-fiber distance and tip-microsphere distance, I first confirmed the zero-distance where the Au-coated tip was contacted to the surface of the tapered fiber and microsphere, and then we determined the distance between the tip and tapered fiber and the distance between the tip and the microsphere from the displacement of the piezo-stage to the zero-distance. For the stabilization of the tip, the tapered fiber and microsphere positions, all samples were placed in a plastic box placed on an optical table and performed the experiments in it, in order to suppress the environmental disturbances. And all electric instruments (e.g. air conditionor, electric supplies), which did not used in the experiments and would generate vibration, were turned off during the measurements for suppressing the air turbulences. From the transmittance measurements, we confirmed that these could lead to a stable condition for at least 30 min.

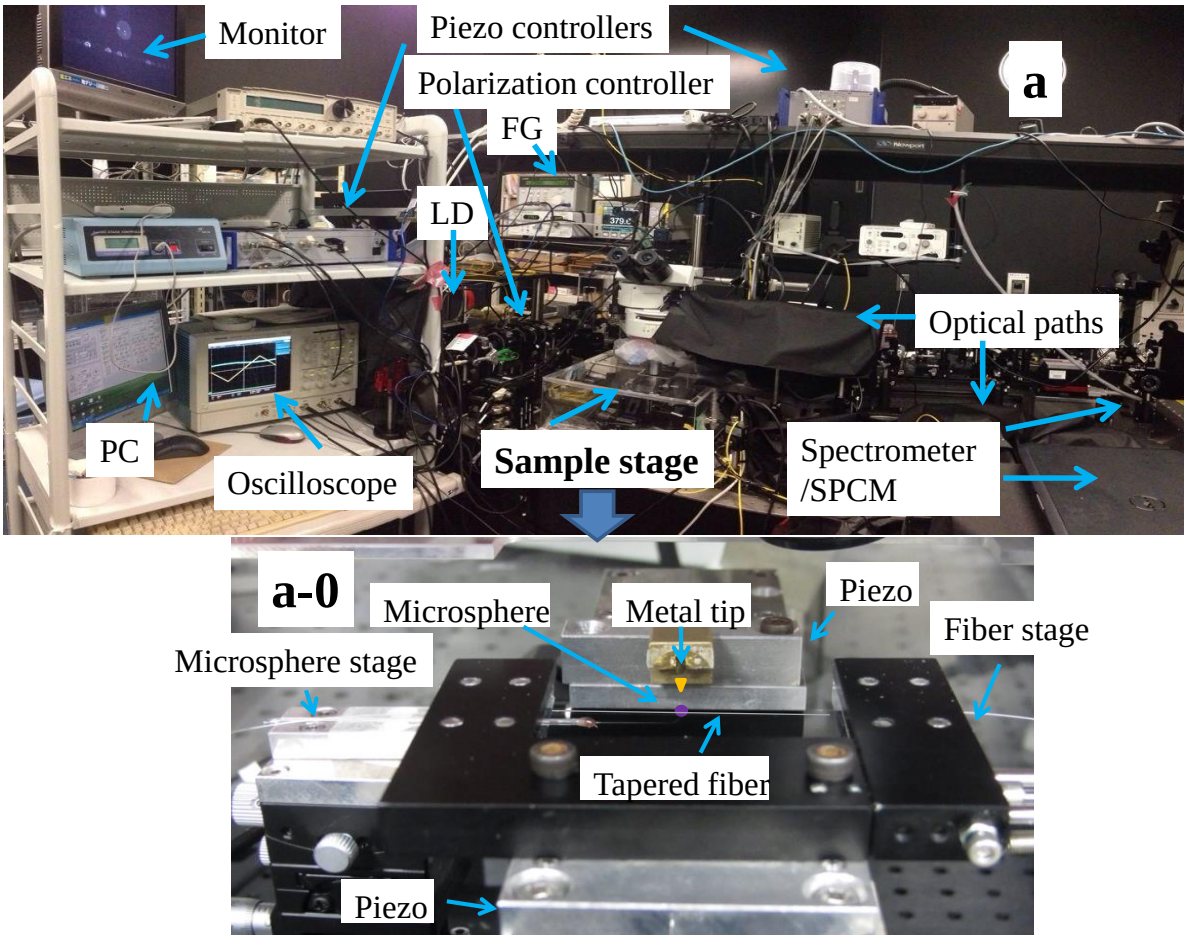

Fig. 3.1 (a) The image of basic experimental setup; (a-0) Image of sample stage; (b) Schematic diagram of experimental setup.

3.2 Fabrication of tapered fibers

3.2.1 Transmittance properties of tapered fibers during the pulling process

A tapered fiber was fabricated from a fused-silica single-mode optical fiber (Thorlabs, 780HP). Figure 3.2 (a) and (b) show a schematic of the tapered fiber fabrication setup. Figure 3.2 (c) shows the fabrication flow of the tapered fiber. After removing the polymer coating of the fiber, the fiber was heated by a ceramic heater and simultaneously stretched at both ends of the fiber [49-50][96-98], which was controlled by a computer-controlled system equipped with a ceramic heater and a motorized stage. The parameters, such as pulling current, pulling speed, and pulling time can be controlled using the computer-controlled system. The tapered fiber is held with fiber clamps which are located on two linear translation stages. During the fabrication process, the fiber is pulled by two linear translation stages moving in opposite directions. The diameter of tapered fibers depended on pulling current, pulling speed, the total pulling time, humidity of environment, and heater's temperature. Keeping the pulling current, humidity and heater's temperature constant, we measured pulling time and pulling speed dependence of diameters of tapered fibers, as shown in Figs. 3.3 (c) and (d). For the pulling time dependence measurement (Fig. 3.3 (c)), it was found that the diameter of the tapered fiber decreased as the pulling time increased under the same conditions. From the Fig. 3.3 (d), when the pulling time was fixed to 125 s and the pulling speed increased, the diameters of the tapered fiber decreased. The diameters of the tapered fibers were inversely proportional to the puling time and pulling speed. In the experiments, the speed of pulling the fiber was optimized to be 340 μm/s at a heater temperature of ~1400 ^{0}C. Thus, the diameter of the tapered fibers was mainly determined by the total puling time. In addition, in the experiments, the taper fabrication was separated from the coupling setup, and the minimum waist of tapered fiber can reach about 200 nm, which was easily broken. Tapered fiber consists of the two ends of an un-tapered fiber of a standard optical fiber and a region reduced in size such that the optical field in the fiber extends into the external environment, where it can interact with matter, such as molecules, plasmonic nanostructures and microcavities. In this study, the tapered fiber was used to couple light into and out of a silica

microsphere resonator and a single metal nanostructure, which largely enhance the light-matter interaction.

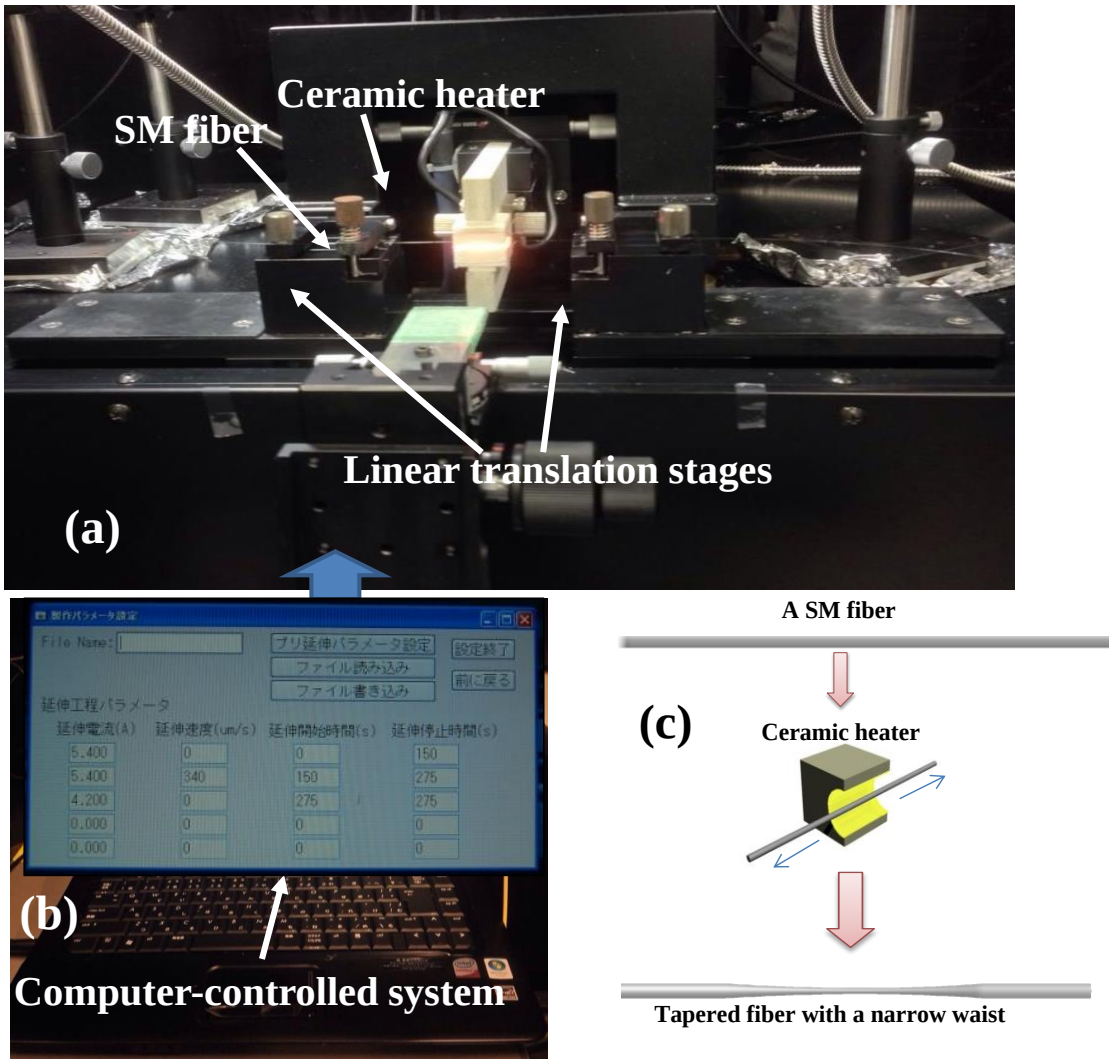

Fig. 3.2 (a) and (b) A schematic of the tapered fiber fabrication setup and computer-controlled system. (c) The fabrication flow of the tapered fiber.

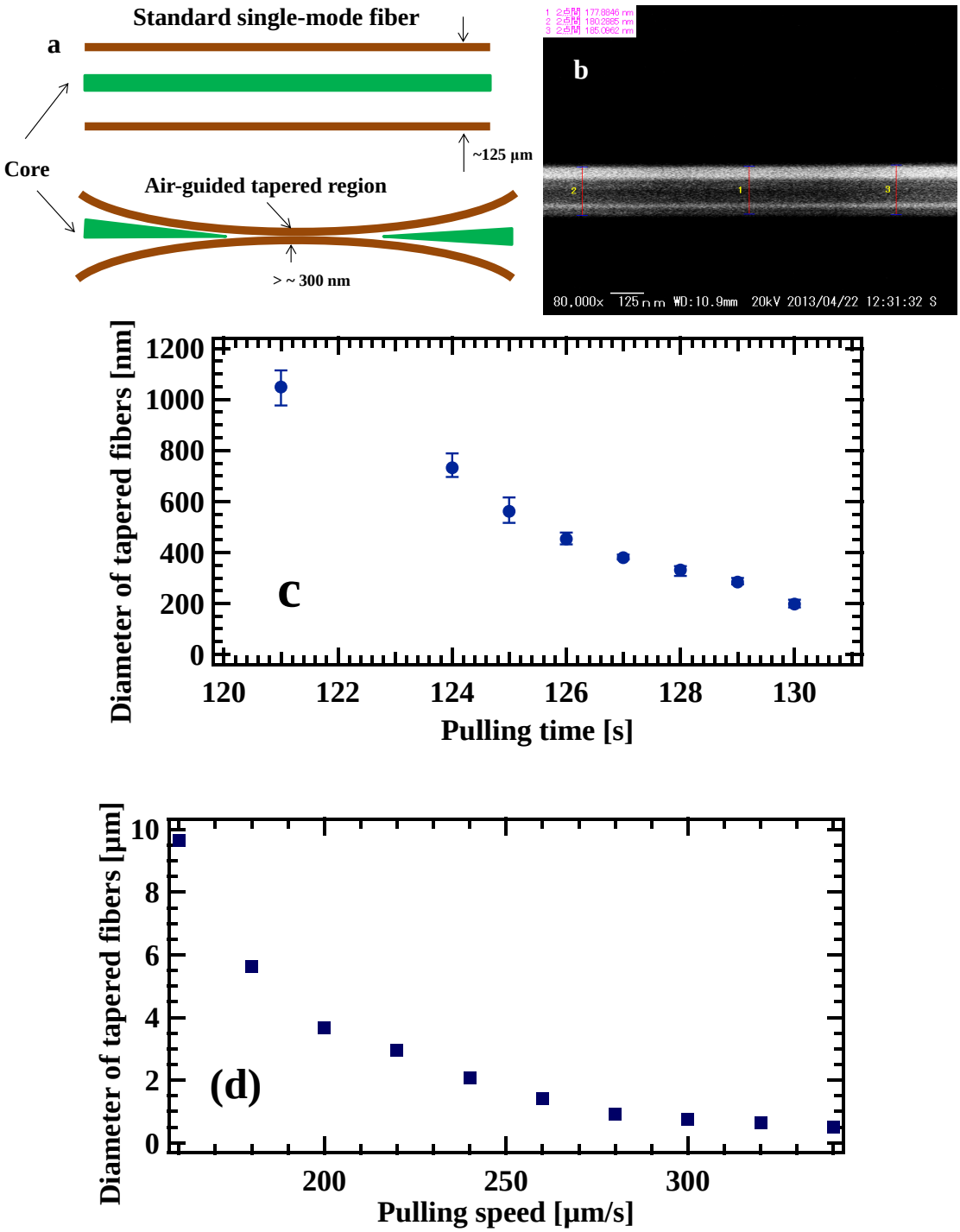

Fig. 3.3 (a) An illustration of the before and after the pulling process; (b) SEM image of tapered fiber with the diameter of ~ 300 nm; Pulling time (c) and pulling speed (d) dependence of diameters of tapered fibers at the temperature of ~ 1400 ^{0}C.

According to refs. [80][99], the variation of the transmitted intensity during the pulling process gave an insight into the mode guiding and coupling properties of tapered fibers. The coupling strength of modes can be affected by the slope of the transition regions. The coupling effects of waveguide modes are expected to be negligible for slowly varying adiabatic tapers. If the changes in slope of the tapered transitions are strong, higher order modes of equal symmetry or even leaky modes are accessible due to mode coupling, and transmittance observed will then be reduced.

Figure 3.4(a) shows the schematic of transmittance measurement for a tapered fiber during the fabrication. The tunable laser light at the wavelength of ~780 nm was incident into the fiber, and then the transmittance in a tapered fiber at a wavelength of 780 nm was detected using a photodiode (Thorlabs, DET36A). After that, through the digital multimeter (Agilent, 34401A), transmittance of tapered fiber can be recorded by the computer. During the fiber pulling process, the transmittance of the tapered fiber was measured, as shown in Fig. 3.4(b).The initial transmittance was defined as the ratio of the transmitted intensity before and after the pulling process. At the beginning of the pulling process, only the fundamental mode HE_{11} of the standard single-mode fiber exists in the fiber core, and nearly no change in transmittance was observed. While the cross section of fiber was reduced, the fundamental mode was guided by the silica-air interface as the higher order modes with strong evanescent field around the tapered region. At this time, the variations of different modes' propagation constants lead to the phase difference, in which interference of multiple modes happened. Continuing reduction and elongation, the single-mode diameter condition of the tapered region reached, which resulted in mainly single mode propagating in tapered region (see also Fig. 2.2 of chapter 2). However, as demonstrated in ref. [100], to keep constant transmittance (~ 1) (keep hybrid propagation mode), there is the critical diameter of tapered fiber, which can be estimated to be ~0.25 λ (λ: light wavelength). If the diameter of tapered fiber were smaller than ~0.25 λ (~ 200 nm in our experimental condition), the transmittance would decrease obviously.

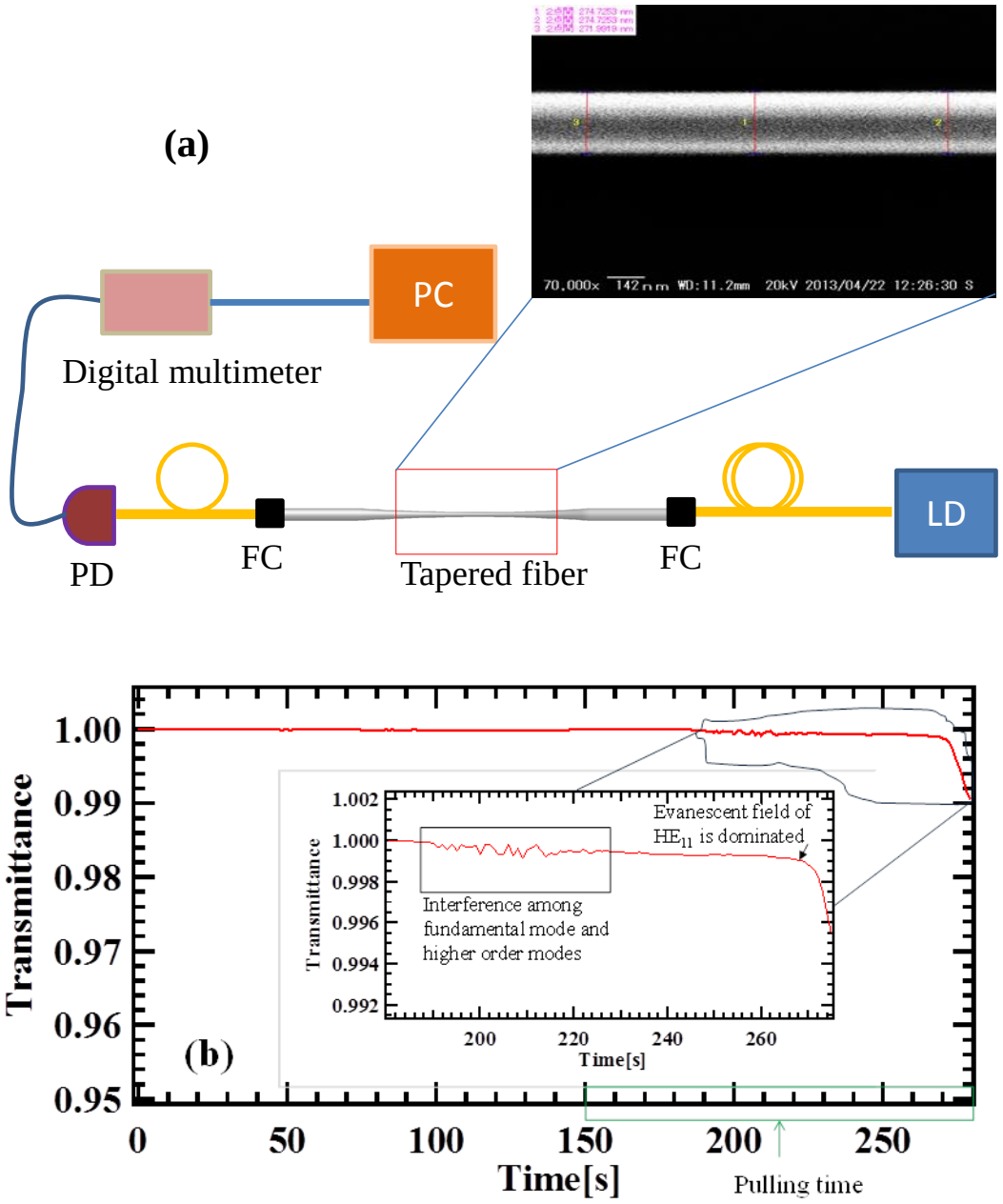

Fig. 3.4 (a) Transmittance in a tapered fiber at a wavelength of ~780 nm; (b) Schematic of transmittance measurement for tapered fiber. PD: photodiode; FC: fiber coupler. Inset of (b): SEM image of the tapered fiber.

3.2.2 Checking polarization state of incident light at the tapered region

In this study, linearly polarized excitation light is important not only for LSPs at the metal tip but also for the coupling conditions between the tapered fiber and the microsphere resonator and between the metal tip and microsphere resonator. There are TM and TE modes in the microsphere resonator (see section 2.3 of chapter 2). The polarization state of the incident light propagating in the tapered fiber is adjusted by the polarization controller to selectively excite TM modes parallel to the tip axis. In addition, for the coupling system (see chapter 2), critical coupling regime (T = 0), which is important for the experiments, require the linearly polarized excitation light. In the experiments, the incident light first propagates in the tapered fiber, and then is coupled directly or via a microsphere to the Au-coated tip. Therefore, it is prerequisite to ascertain and control the polarization state of incident light at the tapered region. The polarization controller was adjusted to obtain a linearly polarized light in the tapered fiber, in which the polarization state at the tapered region was determined by the use of the same method of Konishi et al. [97]. The initial polarization state of the incident light in the tapered region is confirmed by monitoring the polarization state of the scattered light through Rayleigh scattering process. The dim scattering light of tapered fiber is observed through a polarizing filter using a microscope equipped with a highly sensitive charge-coupled device camera (EMCCD, Roper Scientific, Cascade512B), as shown in Fig. 3.5(a). The small dim light spots at the tapered region were focused. When the intensity of the same dim scattering points at the tapered region can reach maximum and almost 0 by adjusting the polarization controller, the light beam with the intensity of maximum or almost 0 at the tapered region was considered as the linearly polarized light [97]. According to the polarization axis of the polarizer, polarization direction of the linearly polarized light can be confirmed. For example, figures 3.5(b) and 3.5(c) show the scattering images of the tapered fiber, when the polarization axis of the polarizer perpendicular to the light propagation direction in the tapered fiber. It was found that, by adjusting the polarization controller (see Fig. 3.1) when the polarization axis of the polarizer is perpendicular to the light propagation direction in the tapered fiber, the polarization state of the light beam with the maximum dim scattering intensity is perpendicular to the light propagation direction in the

tapered fiber, and polarization state of the light beam with almost zero dim scattering intensity is parallel to the light propagation direction in the tapered fiber.

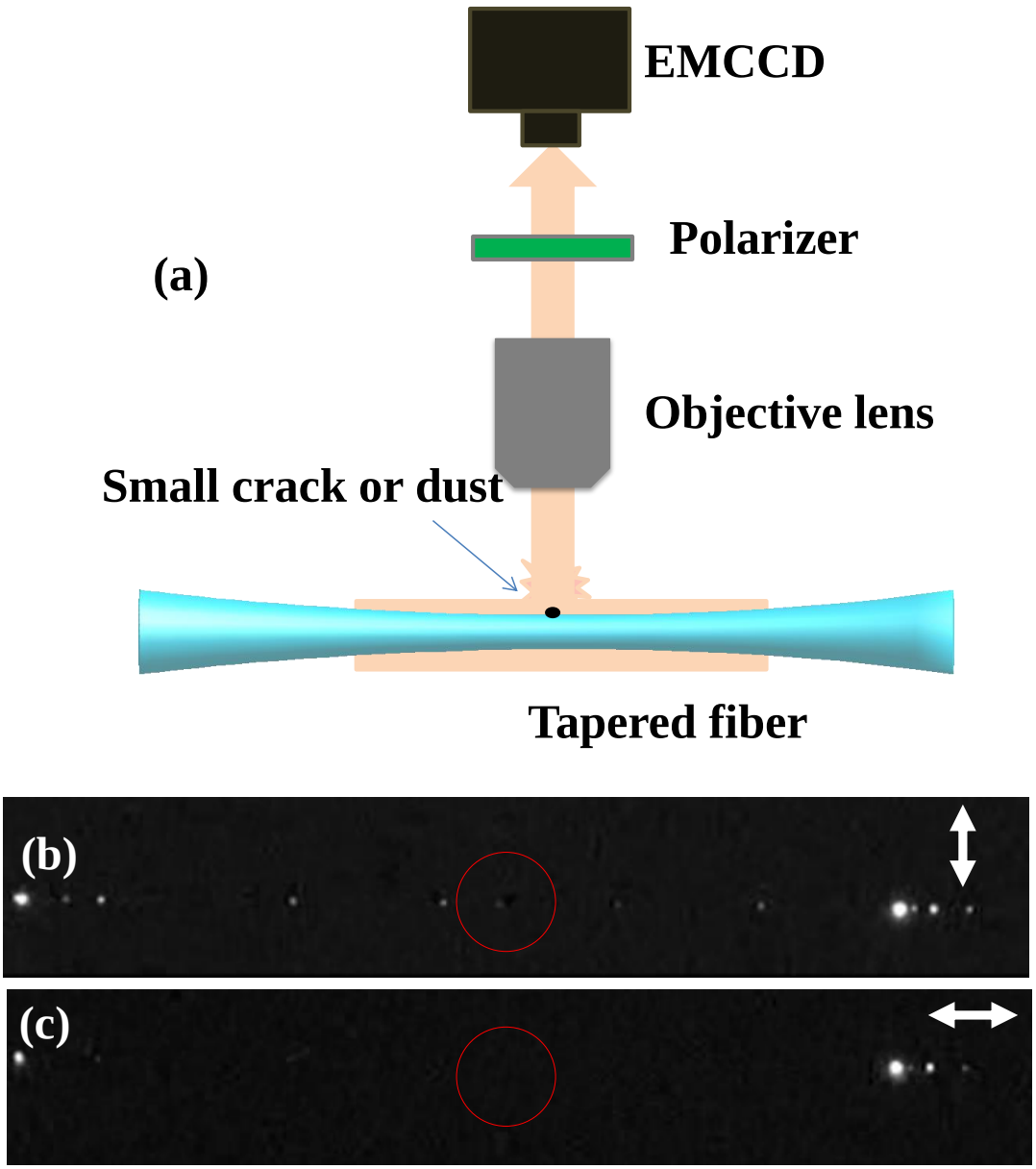

Fig. 3.5 (a) Schematic illustration of setup for checking polarization state of incident light at the tapered region. (b) and (c) Scattering images of scattering light in the tapered fiber with different polarization states of incident light when the polarization axis of the polarizer perpendicular to the light propagation direction in the tapered fiber. Arrows: polarization state of incident light at the tapered region.

3.3 Fabrication of silica microspheres

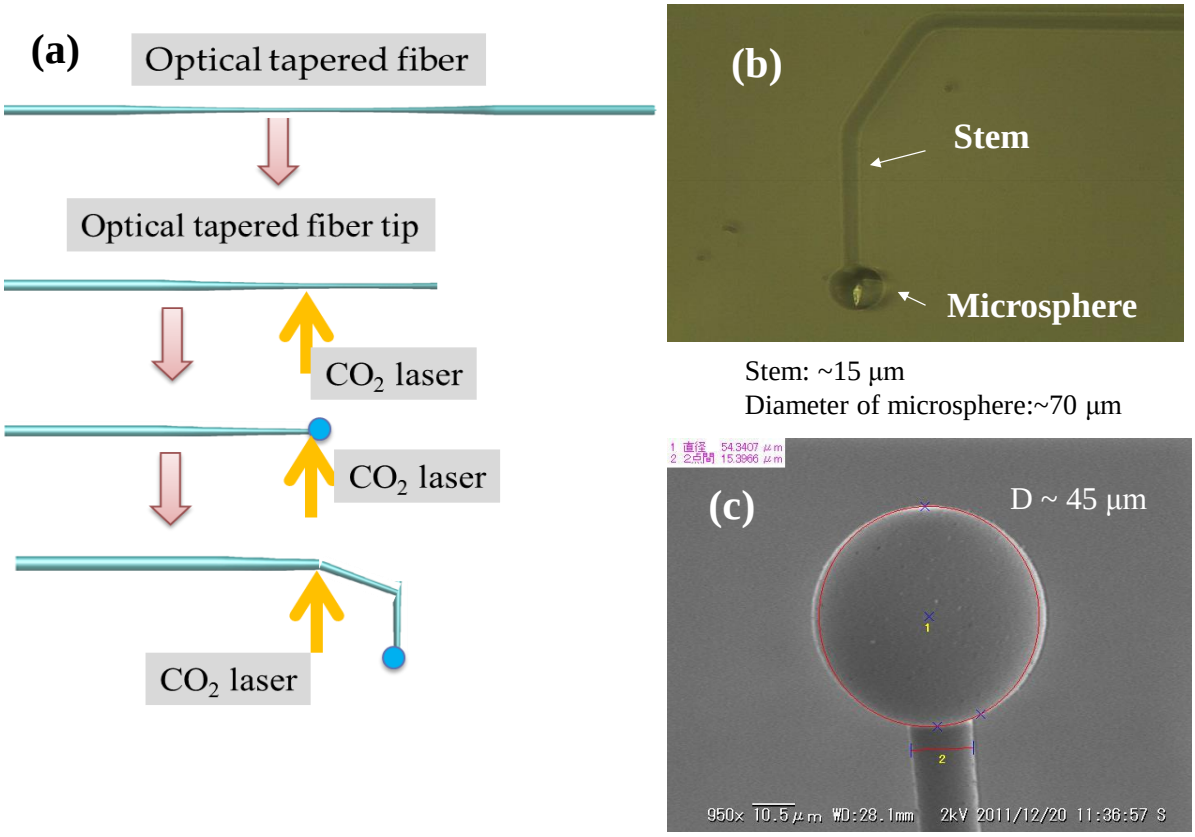

Fig. 3.6 (a) The fabrication procedures of silica microspheres; (b) An optical micrograph of a silica microsphere; (c) A SEM image of a silica microsphere.

Silica microspheres are very easily fabricated in a laboratory setting. One standard technique for producing a single pure, undoped, silica microsphere is by heating the tip of a tapered optical fiber in a flame [74], electric arc [101], and the focused beam of a carbon dioxide laser (CO_2) [94-98]. In this thesis, a silica microsphere with a stem was formed by melting the edge of a tapered fiber tip with the irradiation of a carbon dioxide laser (CO_2 laser; wavelength: 10.64μm). Figure 3.6(a) shows the fabrication procedures of silica microspheres. Surface tension pulls the melted glass tip into a spherical volume, thereby creating a microspherical WGM resonator. Due to the high viscosity of silica, the reflowed structure is not only highly spherical but also extremely uniform. The spherical surface has very low intrinsic roughness, and thus has

a very small surface scattering loss. The remaining part of the fiber acts as a stem so that the microsphere can be held and manipulated in space. The diameter of the microsphere can be controlled by the laser intensity and irradiation time. Typical sizes of microspheres produced in this way are 30~200 μm in diameter. Figures 3.6(b) and 3.6(c) show an optical micrograph and a SEM image of silica microspheres. The presence of the fiber stem can usually be ignored, as the excited optical modes typically propagate in the equatorial plane and thus have negligible overlap with this perturbed region.

3.4 Fabrication of Au-coated tips

A silicon atomic force microscope (AFM) probe tip (Olympus, OMCL-AC160TS-C3), as a metal nanostructure, was coated by Au thin film with the thickness of about 50 nm using a helicon sputter (MPS-4000C1/HC1) or an ion coater (EIKO, iB-3) (in Figs. 3.7(a) and 3.7(b)). The curvature diameters of the Au-coated tips are smaller than 100 nm. The surface of the Au-coated tip using the ion coater is rougher than that using the helicon sputter, as shown in Figs. 3.7(c) and 3.7(d), which is observed by field emission-scanning electron microscopy (FE-SEM, JSM-6700FT). Not only the effect of the uniformly coated tip but also those contributions from a rough (not uniformly) coated tip which may result in small Au nanostructure contribute to the emission enhancement. In order to obtain the reproducibility of the results using different Au-coated tips in the experiments, Au-coated tips using the helicon sputter are employed. However, from the Fig. 3.7(d), it is still difficult to clarify the existence of the roughness under the present resolution, such that we could not discuss on the enhancement caused by the surface roughness.

To confirm the localized surface plasmon resonance property of the Au-coated tip, we measured the scattering spectrum from the apex of the Au-coated tip, when a white light was incident into the tapered fiber and the Au-coated tip was contacted to the surface of the tapered fiber. Figure 3.8(b) shows the result, which was obtained from the scattered intensity spectrum at the apex of the Au-coated tip collected by the objective lens divided by the transmitted intensity spectrum from the end of the tapered fiber without the Au-coated tip. Figure 3.8(a) shows the experimental setup for this measurement. From the result, because we found that the wavelength

of the excitation light (~780 nm) was close to the LSP resonance peak wavelength, which could be expected the efficient excitation of the LSPs at the tip apex in the experiment.

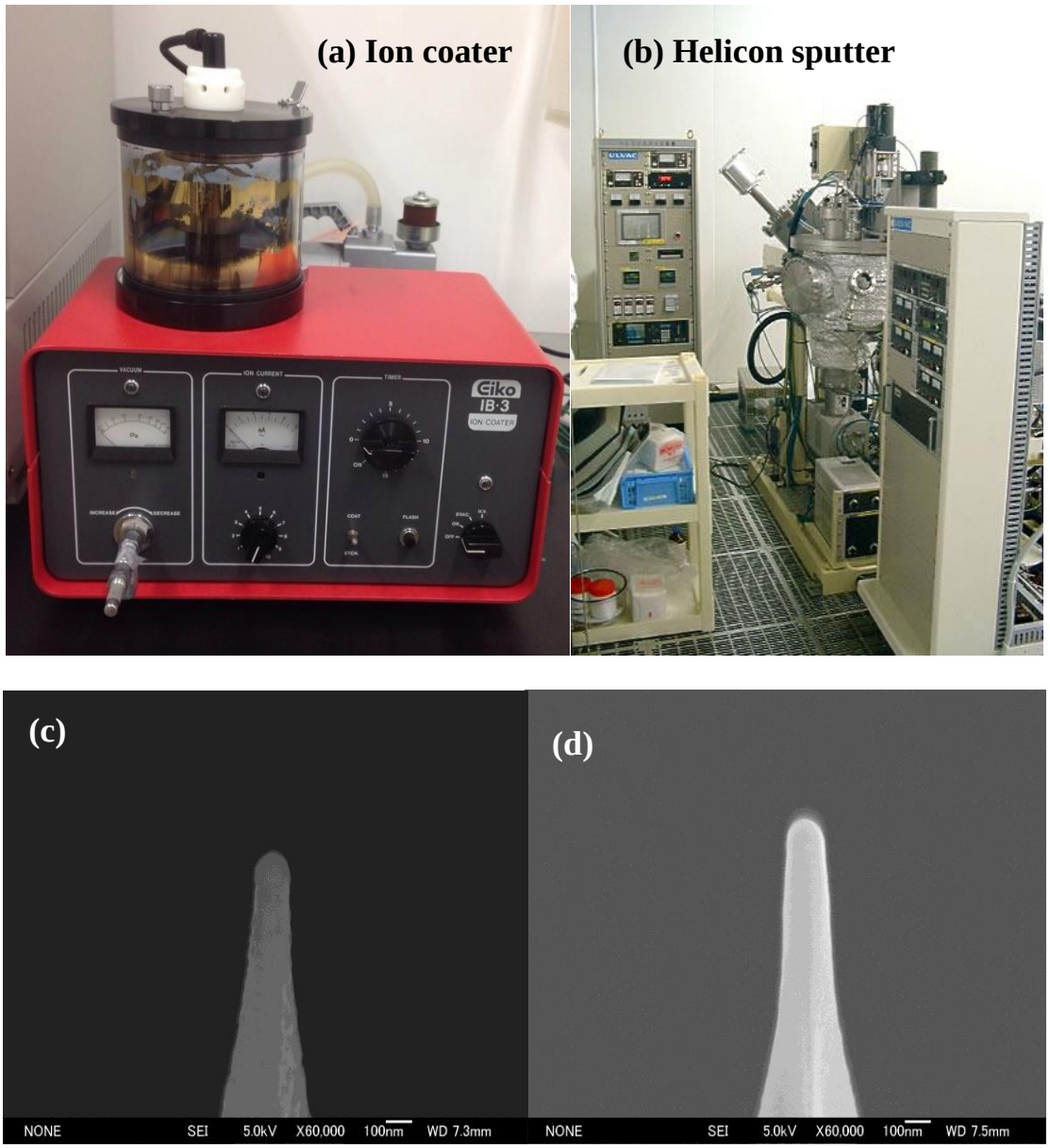

Fig. 3.7 Photograph of ion coater (a) and helicon sputter (b), which coat Au film to the surface of silicon AFM tip; SEM images of Au-coated tips using ion coater (c) and using helicon sputter (d). The thickness of Au film: ~ 50 nm.

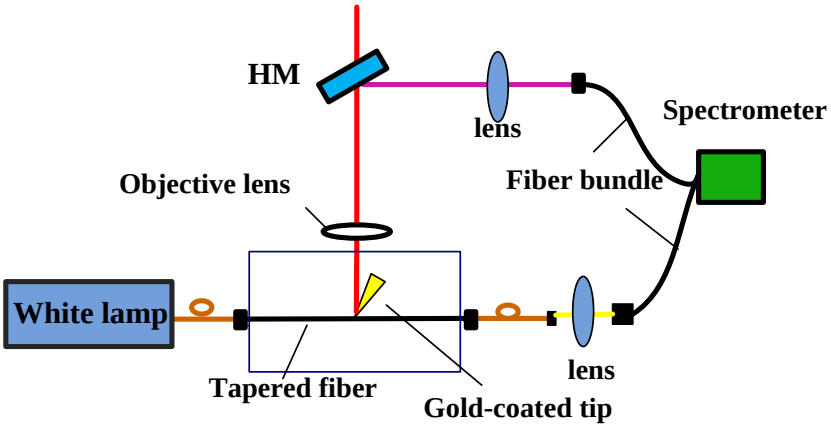

(a)

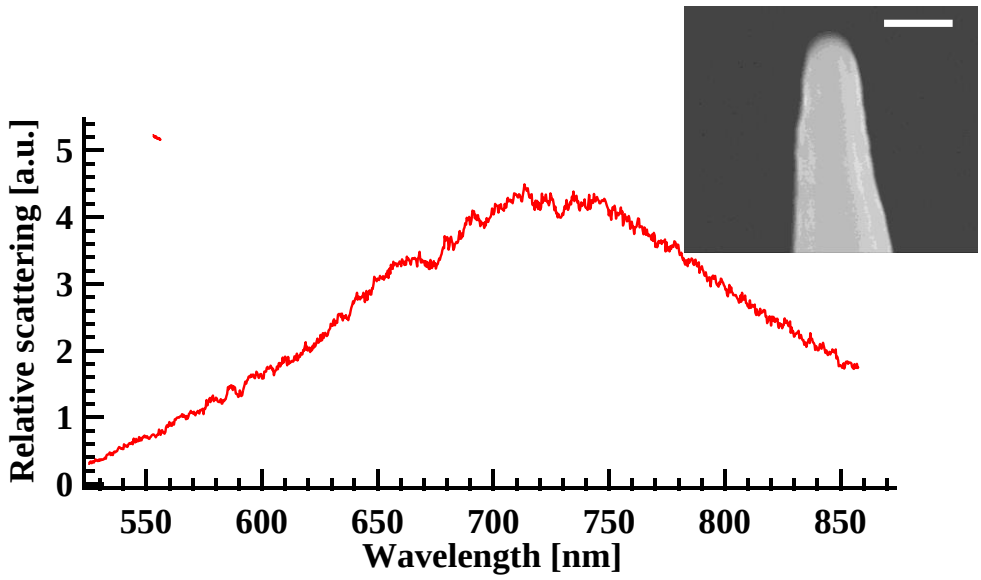

(b)

Fig. 3.8 (a) Schematic of experimental setup for scattering spectrum at an Au-coated tip. (b) Localized surface plasmon resonance scattering spectrum of an Au-coated tip; Inset: SEM image of an Au-coated tip by FE-SEM. Scale bar: 100 nm.

3.5 Preparation of PIC-attached Au-coated tip

For the preparation of the PIC-attached Au-coated tip, Pseudoisocyanine (PIC) dye molecules, which have been well known as dye molecules with a large two-photon absorption cross section (~ 200GM) at the excitation wavelength ~ 780 nm [102-104], as shown in Fig. 3.9(a), could be attached on the surface of the Au-coated tip using a self-assembly technique [105]. From the absorption spectrum of PIC dye molecules in Fig. 3.9(b), there is no absorption at the excitation wavelength of ~ 780 nm. This kind of fluorescence molecules has low fluorescence quantum yield (< 2.5%). Its fluorescence peak [103] is around ~ 700 nm, as presented in Fig. 3.9 (c). Figure 3.10 shows the flow of preparation of PIC-attached Au-coated tip using the self-assembly technique. In this method, firstly the Au-coated tip was slowly immersed into 1 mM ethanol solution of 3-mercaptopropionic acid (MPA) at room temperature for approximately 20 min, followed by rinsing it with ethanol solution to remove excess thiol MPA molecules. The MPA was chemically bonded to the surface of the Au-coated tip, because the thiol function groups presented in MPA facilitate the attachment of the Au-coated tip. Then we dipped the Au-coated tip into 0.1 mM aqueous solution of $AgNO_3$ at room temperature for about 20 min in order to activate the reactive chemical group of the MPA able to bind to PIC dye molecules. After rinsing it by pure water to remove excess $AgNO_3$ molecules, we immersed the Au-coated tip into 0.01 mM ethanol solution of PIC dye molecules at room temperature for nearly 1 h. PIC dye molecules were attached on the surface of the Au-coated tip after rinsing it using pure water to remove unbound PIC dye molecules.

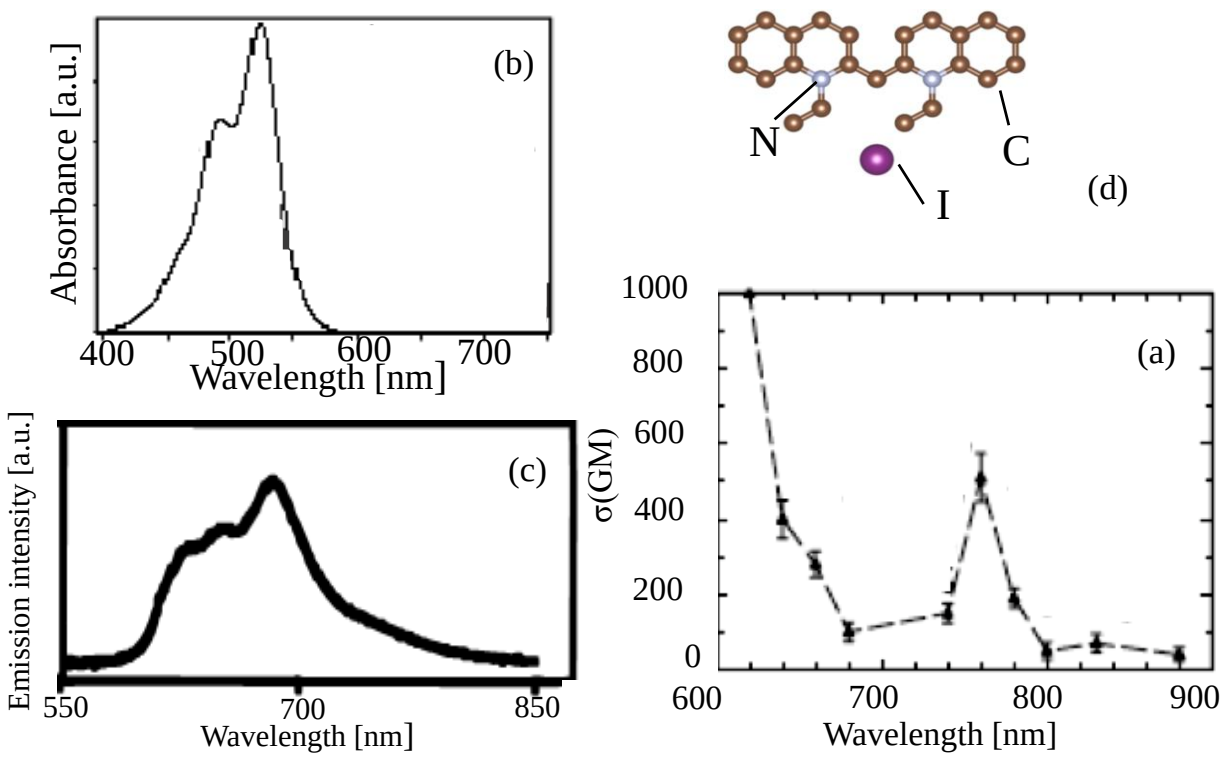

Fig. 3.9 (a) Two-photon absorption cross section spectrum of PIC molecules; (b) Absorption spectrum of PIC molecules; (c) Fluorescence spectrum of PIC molecules; (d) molecule structure of PIC

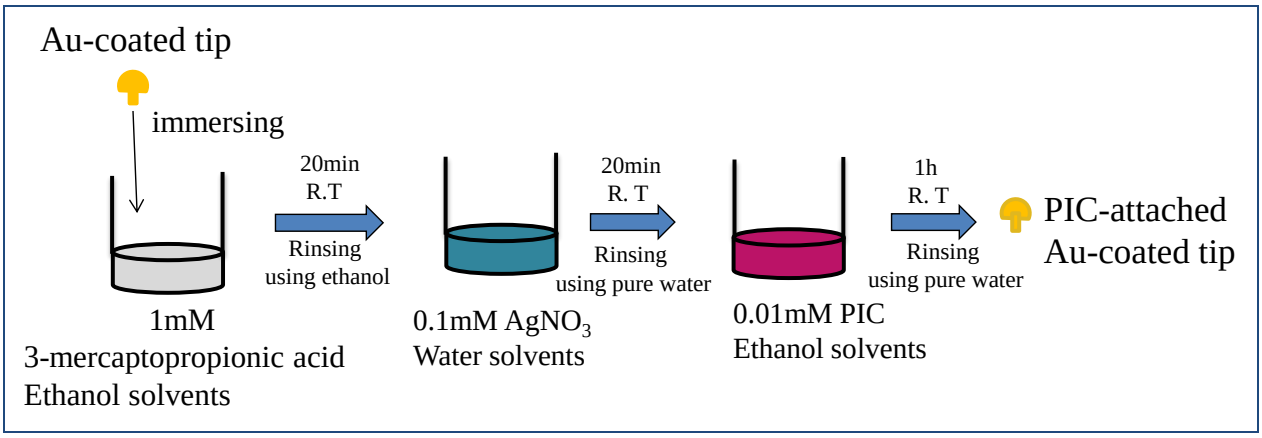

Fig. 3.10 Flow of preparation of PIC-attached Au-coated tip using the self-assembly technique.

3.6 Summary

In this chapter, the basic setup for experiments and fabrication of experimental samples (tapered fibers, microsphere, Au-coated tip) are described. Transmittance properties of tapered fibers during the pulling process are discussed. In the experiments, to keep high transmittance from the tapered fiber, the diameter of the tapered fiber is larger than 0.25λ. Localized surface plasmon resonance scattering spectrum of an Au-coated tip is also investigated. It was found that the wavelength of the excitation light (~780 nm) was close to the LSP resonance peak wavelength, and the efficient excitation of the LSPs at the tip apex could be expected. In addition, preparation of PIC-attached Au-coated tip using a self-assembly technique is introduced.

Chapter 4 Second harmonic generation from the top of an Au-coated tip via a tapered-fiber-coupled microsphere resonator

4.1 Introduction

In this chapter, a plasmonic-photonic hybrid system composed of an Au-coated tip and a tapered-fiber-coupled microsphere, which achieved highly focusing of light into the Au-coated tip, was proposed. In order to experimentally verify efficient LSP excitation at the metal tip, we have paid attention to second harmonic generation (SHG) from the top of an Au-coated tip via a tapered-fiber-coupled microsphere resonator. Because SHG from the metal nanostructures, which has typically been induced by a high power pulsed laser excitation [19-23], is one of the very sensitive techniques to study localized fields induced in metal nanostructures, we attempted to demonstrate SHG from the metal tip excited by a weak CW light using the plasmonic-photonic hybrid microcavity system. In the experiments, we first developed the plasmonic-photonic hybrid microcavity system that coupled an incident light with the coupling efficiency of about 63.2 % to the metal tip having the effective extinction cross section 358.2 nm^2 with the

diameter of 21.4 nm. Then using this hybrid system, we also succeeded in observing SHG from the metal tip in spite of the use of a weak CW laser excitation via a tapered fiber coupled microsphere. The result suggested the possibility that efficient LSP excitation via the tapered-fiber-coupled microsphere resonator was achieved.

4.2 Experimental setup

The detail of the experimental setup is shown in Figure 4.1. A tunable external cavity diode laser (New Focus, TLB-6312, Linewidth~300 kHz, Wavelength~780nm), whose frequency was controlled by a function generator (FG), was introduced into the tapered fiber as a probe and excitation light. For the measurements of transmission spectra, the laser frequency was scanned over the range of 5 GHz around the wavelength of ~780 nm. The pair components of half wave plates (HWP) and polarization beam splitters (PBS) controlled the power of the incident light coupled into the tapered fiber. Two quarter wave plates (QWP1, 2) and a half wave plate (HWP4) were used to adjust the polarization states of the excitation light to selectively excite transverse magnetic modes (parallel to the tip axis) in order to efficiently induce SHG from the metal tip (see section 3.2 of chapter 3). The power of the excitation light was monitored using an optical power meter (Newport, 2835-C) connected to the output of a fused fiber coupler (50:50). In order to control the coupling conditions, the separation distances between the tapered fiber and microsphere and also between the Au-coated tip and microsphere were controlled by three-dimensional piezo manipulators (PI-Polytec, P-620.ZCL). These components were placed in a plastic box, which was kept at a stable condition and filled with dry air to reduce the humidity that may cause adhesion force at the surface of microsphere decreasing the *Q*-factor [49-50]. The Transmitted light from the end of the tapered fiber was measured using a high sensitive photodiode (Thorlabs, PDA100A) and a digital oscilloscope (Tektronix, TDS5034). The transmission spectra were normalized by the transmission spectrum of the tapered fiber without the microsphere. The SHG signal emitted from the Au-coated tip was measured by a microscopy system set on the top of the sample. The SHG signal was collected by the objective lens with 0.28NA (Mitutoyo Corp.; M Plan Apo 20×), and then passed through the dichroic

mirror to eliminate the excitation light, and was incident into the multimode fiber bundle connected to the spectrometer (Princeton instruments, Acton research, PIXIS:256E, SP-2500i).

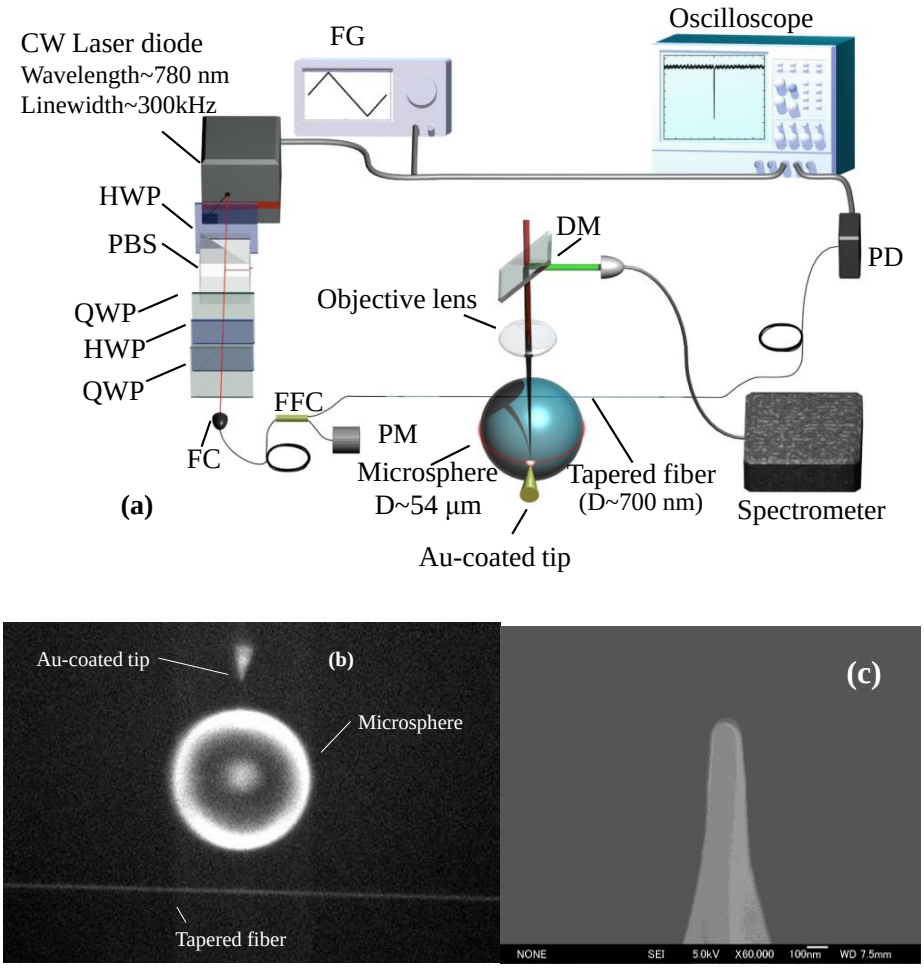

Fig. 4.1. (a) Schematic of experimental setup. FG: Function generator; LD: Laser diode; HWP: Half wave plate; PBS: Polarization beam splitter; QWP: Quarter wave plate; PD: Photodiode; DM: Dichroic mirror; Inset shows photograph of microsphere and Au-coated AFM tip and microsphere by SEM. (b) microscope image of samples.(c) SEM image of an Au-coated tip.

In chapter 3, the fabrications of a tapered fiber, a silica microsphere and an Au-coated tip have been described. In this experiment, the tapered fiber with the waist diameter of about 1 μm was used, the diameter of the microsphere used in this experiment was about 54 μm, and the curvature radius of the Au-coated tip was smaller than 100 nm. The localized surface plasmon

resonance properties have been investigated in the section 3.4 of chapter 3. From the results in chapter 3, it was found that the plasmon resonant peak was close to the excitation wavelength 780 nm of this experiment, implying the efficient LSPs excitation at the apex of the Au-coated tip.

4.3 Results and discussion

To obtain efficient SHG signal from the top of an Au-coated tip using a weak CW laser excitation via a tapered fiber coupled microsphere, it was necessary to achieve high coupling of light between the tapered-fiber-coupled microsphere resonator and the metal tip, and moreover it was acquired to build up the system that satisfied the conditions that the intrinsic cavity loss was negligibly small and the fiber-sphere coupling rate is equal to the tip-sphere coupling rate ($\kappa_{ex}=\kappa_{tip}\gg\kappa_0$). The coupling theories of fiber-microsphere and the tip-microsphere have been discussed in chapter 2.

Firstly, we analyzed the resonant properties of the tapered fiber coupled microsphere without the metal tip. Before starting the measurements, to efficiently induce SHG, TM mode in the microsphere resonator was required, through adjusting the polarization of the incident light at the tapered region by the use of the same method of Konishi et al. [97] (see section 3.2 of chapter 3). The transmittance spectra with varying the gap distance between the microsphere and tapered fiber is shown in Fig. 4.2(a). Figures 4.2(b) and 4.2(c) also show the transmittance and linewidth of the resonant dip versus the gap distances. When the tapered fiber was far away from the microsphere surface (> 940 nm), the resonant dip could not be observed and the transmittance was almost equal to 1. At the distance of 880 nm, we could observe a small resonant dip, which linewidth of this small dip was about 2.25 MHz, corresponding to the quality factor of ~2.4×10^8. At this time the fiber-sphere coupling rate κ_{ex} was very small, so the linewidth of the small dip was almost regarded as the linewidth due to the intrinsic cavity loss rate ($\kappa_0 \sim 2\pi\times2.25\times10^6$ s^{-1}). When the distance was 400nm, the dip transmittance almost became nearly zero and its linewidth was about 5.19 MHz ($\kappa_{ex}+\kappa_0 \sim 2\pi\times5.19\times10^6$ s^{-1}). As the linewidth became almost twice of κ_0, the incident light was coupled to the microsphere resonator with the 100% coupling efficiency.

Further decreasing the distance, the dip became shallower and broader. When the tapered fiber was contacted with the microsphere surface, the transmittance was nearly flat but small dip remained, whose transmittance and linewidth were about 66.5% and 26.9 MHz, respectively. Thus, these results suggested that we clearly identified different coupling regimes by changing the coupling gap distance between the tapered fiber and microsphere and achieved the condition that $\kappa_{ex} \gg \kappa_0$ was achieved, which was required for achieving the efficient light coupling to the metal tip.

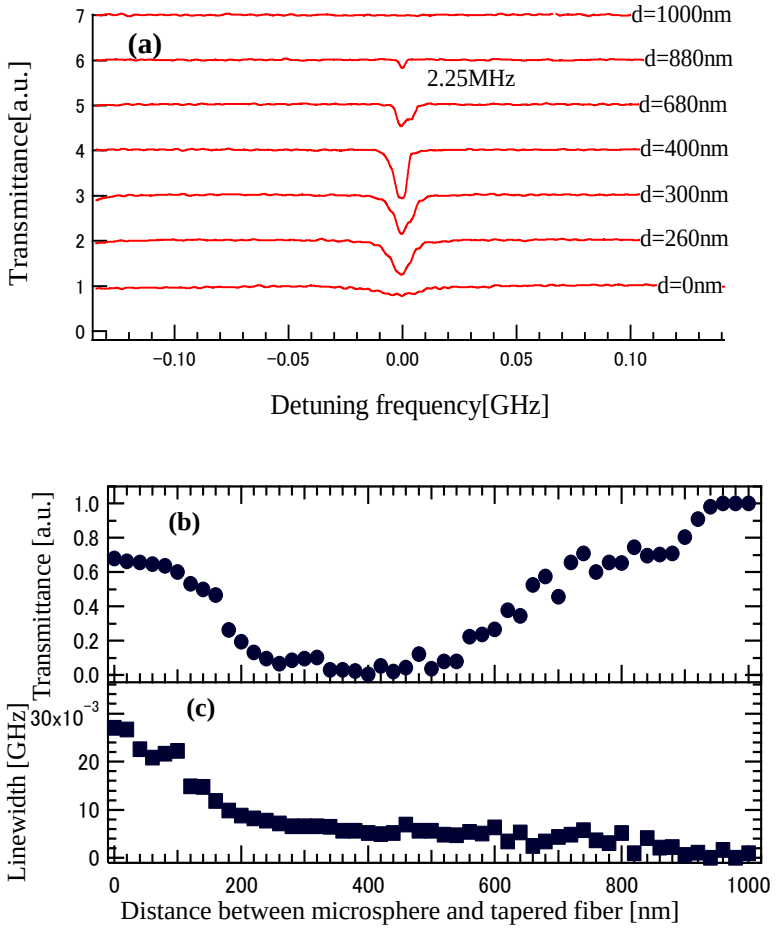

Fig. 4.2. (a)Transmittance spectrum from the end of tapered fiber; Transmittance (b) and Linewidth on resonance (c) versus distance between the tapered fiber and microsphere resonator. d is the distance between the tapered fiber and microsphere resonator in (a), and the zero point corresponds to the tapered fiber in contact with the surface of microsphere resonator.

Next, by approaching the metal tip from the opposite side of the tapered fiber to the surface of microsphere, we analyzed the light coupling between the Au-coated tip and the tapered fiber coupled microsphere. The metal tip was approached to the microsphere surface at 20-nm intervals. Figure 4.3(a) shows the transmittance spectra from the end of tapered fiber measured at different distances between the Au-coated tip and microsphere. In addition, Figures 4.3(b) and 4.3(c) plotted the transmittance and linewidth of the dip against the separation distance between the metal tip and the microsphere surface. When the Au-coated tip was far away from the microsphere surface, there was no change from the spectrum, whose dip transmittance and linewidth were asymptotically determined to be about 66.5 % (T_1) and 29.6 MHz, as shown in Fig. 4.2. Using the obtained κ_0, the fiber-sphere coupling rate κ_{ex} was estimated to 27.3 MHz. As we continued to approach the metal tip to the microsphere surface, the dip became deeper and broader, indicating the increase in the light coupling to the metal tip. At the distance of 0 nm, the dip transmittance reached to its minimum (T_2~3.3 %) and its linewidth became nearly twice (~55.7 MHz) against the initial value of 29.6 MHz. From the results, the tip-sphere coupling rate κ_{tip} was estimated to be $\sim 2\pi \times 26.1 \times 10^6$ s^{-1}. At this distance, because κ_{tip} (~ 26.1 MHz) was much larger than κ_0 (~2.25 MHz) and was approximately balanced to κ_{ex} (~27.3 MHz), these results indicated that the critical PP-LSP coupling conditions of $\kappa_{ex} = \kappa_{tip} \gg \kappa_0$ was satisfied. Moreover, the total quality factor of this system was still kept to be as high as about 6.1×10^6 even when the Au-coated tip was contacted to the microsphere surface. It was found that using the tapered-fiber-coupled microsphere resonator with high Q factor highly efficient coupling of incident light into the metal tip was achieved. According to the obtained values and Eq. (2.60) of chapter 2, the transmittance under the critical PP-LSP coupling condition was evaluated to be 0.3%, which value corresponded to the experimental data well. Note that a slight difference in the transmittance would be due to the misalignments of the tip-sphere position and polarization of the incident light at the tapered region in the experiment. In addition, from κ_{tip} and Eq. (2.62) of chapter 2, the effective extinction cross-section σ of the Au-coated tip was estimated to be 358.2 nm^2 (corresponds to the circular area with the 21.4-nm diameter). Thus, we confirmed that using this system, the strong dissipation of incident light at an Au-coated tip via a tapered fiber coupled microsphere ($\Delta T = T_1 - T_2 \approx$ 63.2%) was coupled to the Au-coated tip having the 21.4-nm diameter sized effective area.

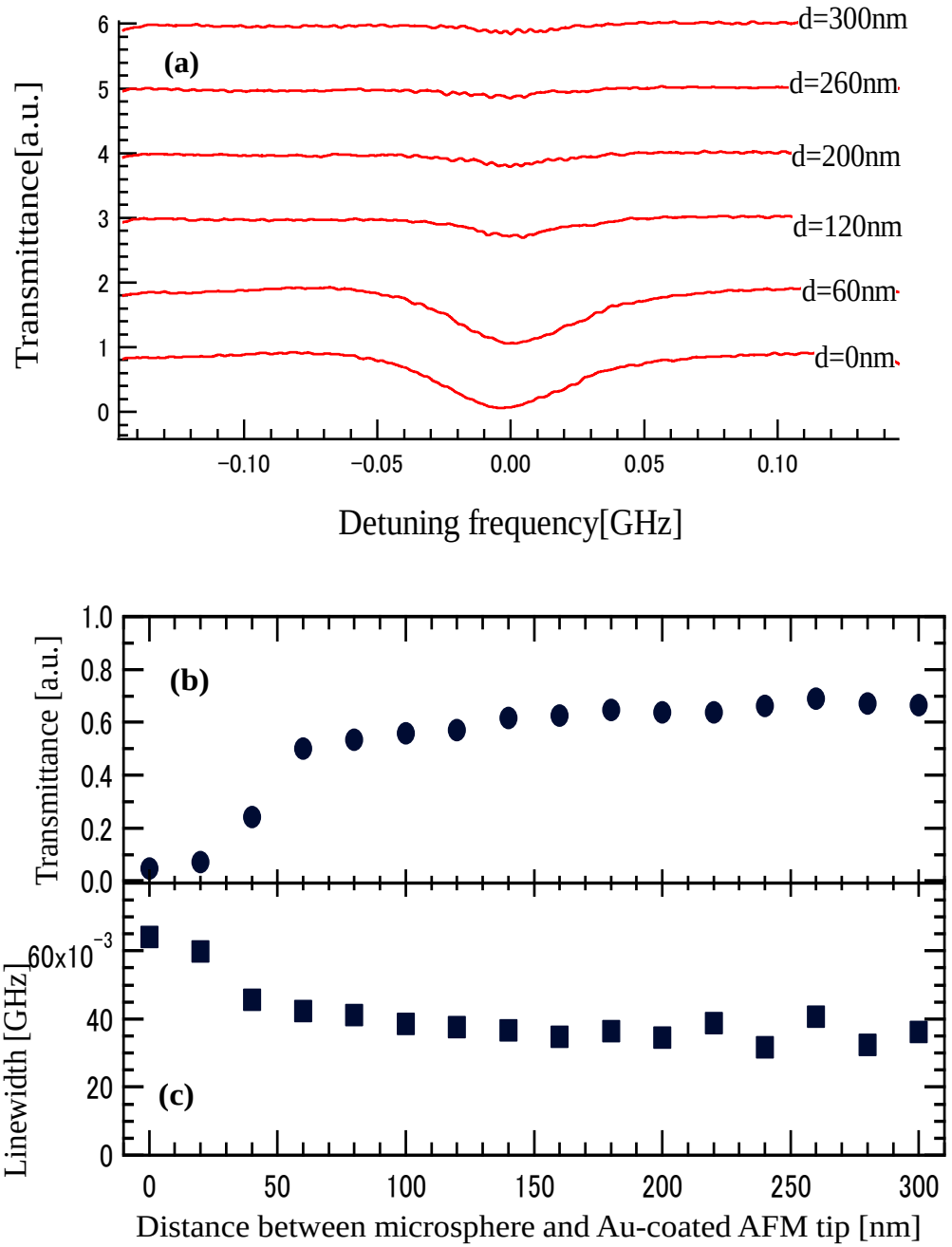

Fig. 4.3 (a)Transmittance spectra from the end of tapered fiber. Transmittance (b) and linewidth (c) of resonance dip versus distance between the Au-coated tip and microsphere resonator. d in (a) is the distance between the Au-coated tip and microsphere resonator, and the zero point corresponds to the Au-coated tip being in contact with the surface of microsphere resonator.

After building the efficient light coupling system to the Au-coated tip, then we measured SHG in order to experimentally verify the efficient plasmon excitation at the Au-coated tip. Keeping the positions of the tapered-fiber-coupled microsphere and Au-coated tip by monitoring the transmission spectra under the critical PP-LSP coupling regime, we gradually increased the power of incident CW light to about 28 μW (power density at the waist of the tapered fiber ~3.6 kW/cm^2) and measured spectra of scattered light from the Au-coated tip. In this experiment, owing to the strong confinement effect of the high-*Q* microsphere resonator and the electric field enhancement of the LSP resonance, the SHG would be expected from the Au-coated tip even using a weak CW light. Figure 4.4 shows the spectrum of SHG signal from the metal tip under the critical coupling condition, and CCD image of scattered light from an Au-coated tip via a tapered fiber coupled microsphere. From the results, a weak peak appeared around the wavelength 388.25 nm that was just half of the fundamental wavelength 776.5 nm. Moreover, we performed the same measurements after changing the polarization states of the incident light from TM modes to TE modes (perpendicular to the tip axis) by adjusting the polarization controller in order to confirm the SHG from the metal tip, because SHG from the metal tip is strongly sensitive to the polarization of the incident light. We found that when the polarization state of WGMs was set to be perpendicular to the tip axis (TE mode), no SHG signal was observed from the metal tip (Fig. 4.4(a) black line) because there would be no strong plasmonic field enhancement effect at the Au-coated tip. Therefore, these results suggested the possibility that our proposed system via the tapered fiber coupled microsphere can obtain the efficient localized plasmon excitation at the Au-coated tip, resulting in the strong light-matter interaction at the Au-coated tip.

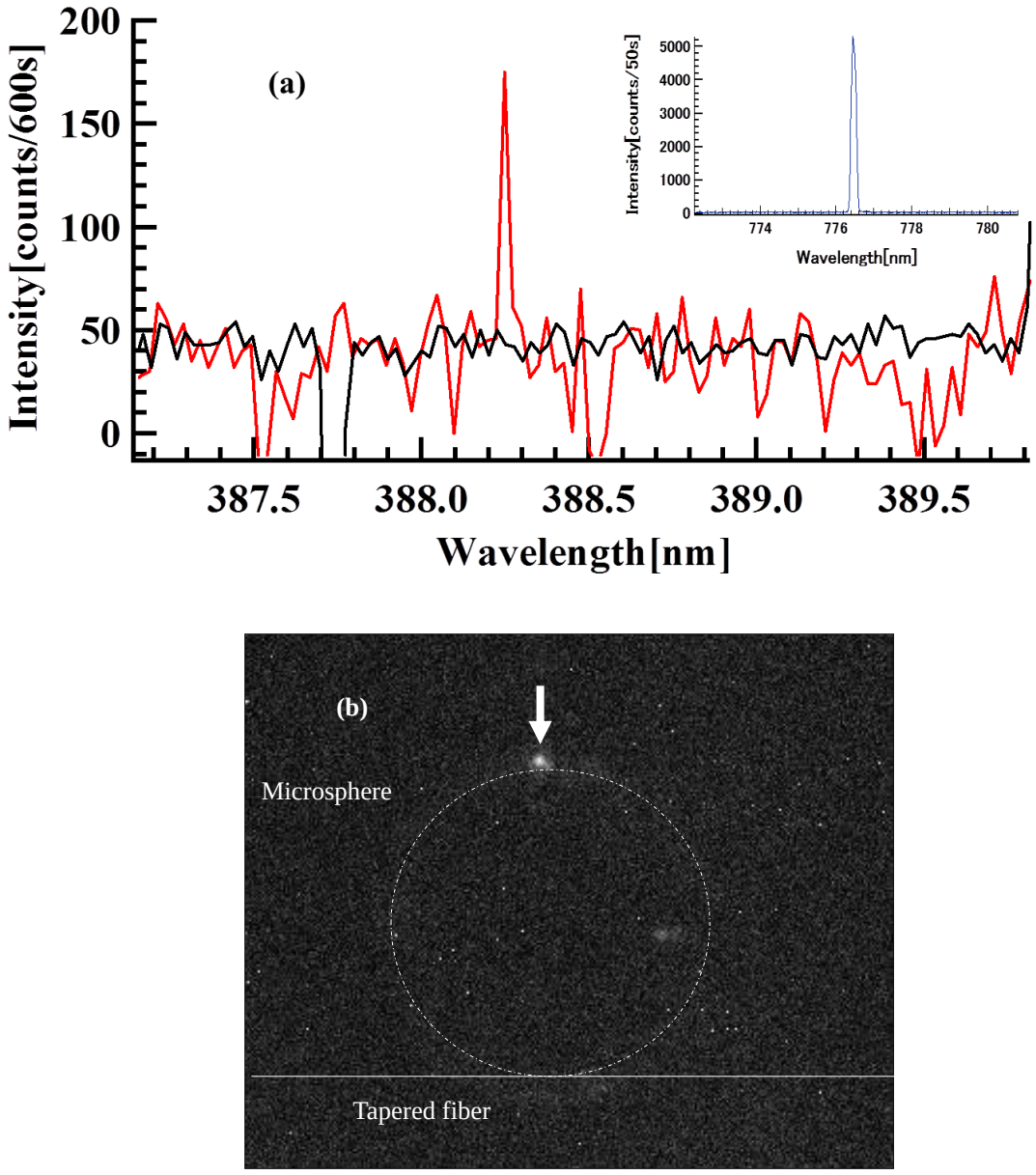

Fig. 4.4 (a): spectrum of SHG signal from the top of Au-coated tip and inset presents the spectrum of the scattered fundamental light. (b): CCD image of scattered light from an Au-coated tip via a tapered fiber coupled microsphere. White lines in the image indicate a microsphere and tapered fiber and an arrow indicate the scattered point of Au-coated tip.

4.4 Summary

Using the efficient light coupling system using a tapered-fiber-coupled microsphere resonator, we succeeded in the light focusing into a nanoscale domain (358.2 nm^2) of a metal tip with high coupling efficiency of ~63.2 % and the quality factor of ~ 6.1×10^6. In order to verify the efficient excitation of LSP at the metal tip using this system, we also succeeded to observe SHG from the metal tip in spite of the weak CW excitation (incident power ~28 μW). This result suggests that efficient light focusing and plasmon excitation at the nanoscale domain of the metal tip can be realized using plasmonic-photonic hybrid microcavity structure composed of high-*Q* microresonators and metal nanostructures. We believe that our results provide a novel viewpoint for the technological applications near single photon level, such as photovoltaic devices, single-photon nonlinear optics, photo-catalysts, and light emitting devices.

Chapter 5 Two-photon excited fluorescence from a PIC-attached Au-coated tip using a tapered-fiber-coupled microsphere resonator

5.1 Introduction

In chapter 4, we have proposed a plasmonic-photonic hybrid system with the high *Q* factor composed of an Au-coated tip and a tapered-fiber-coupled microsphere resonator, which achieved high coupling efficiency into the single metal nanostructure. Moreover, in order to verify the efficient excitation of LSPs at the Au-coated tip, we have experimentally succeeded in achieving weak SHG signal at the metal tip via a tapered-fiber-coupled microsphere under a CW excitation. In this Chapter, we demonstrated two-photon excited fluorescence (TPF) from the pseudoisocyanine (PIC) dye molecules attached on the Au-coated tip using this plasmonic-photonic hybrid system under a weak CW laser excitation.

In the experiment, we first developed a plasmonic-photonic hybrid microcavity system with the coupling efficiency of about 80.3 % to the PIC-attached Au-coated tip having the effective extinction cross section of 728.8 nm^2, and high *Q* factor ~1.9×10^6. Using this plasmonic-photonic hybrid system, we succeeded in achieving the TPF from the PIC-attached

Au-coated tip by the use of a weak CW excitation, comparing with previous reports that TPF has typically been induced by a high-power pulsed laser excitation [10-18]. The result suggests the possibility that the synergetic effect of strong optical confinement effect of tapered-fiber-coupled microsphere resonator and optical antenna effect of the Au-coated tip tremendously induce the strong light-matter interaction at the PIC-attached Au-coated tip.

5.2 Experimental setup

The experimental setup is shown in Fig. 5.1, as similar to Fig. 4.1 of chapter 4. The difference as follows: The power of the incident light was monitored using an optical power meter (Newport, 2935-C) connected to the output of a fused fiber coupler (95:5). In order to control the coupling conditions, the separation distances between the tapered fiber and microsphere and also between the PIC-attached Au-coated tip and microsphere were controlled by three-dimensional piezo manipulators (PI-Polytec, P-620.ZCL, P-621.1CD, P-621.ZCD). The Transmitted light from the end of the tapered fiber was measured using a high sensitive photodiode (Thorlabs, DET36A) and a digital oscilloscope (Tektronix, TDS5034). The emission signal was collected by an objective lens with 0.42 NA (Mitutoyo Corp.; M Plan Apo SL 50×), and then passed through a dichroic mirror and shortpass filters to eliminate the excitation light, and was incident into the multimode fiber bundle connected to a spectrometer (JASCO Corporation; iDus; Andor).

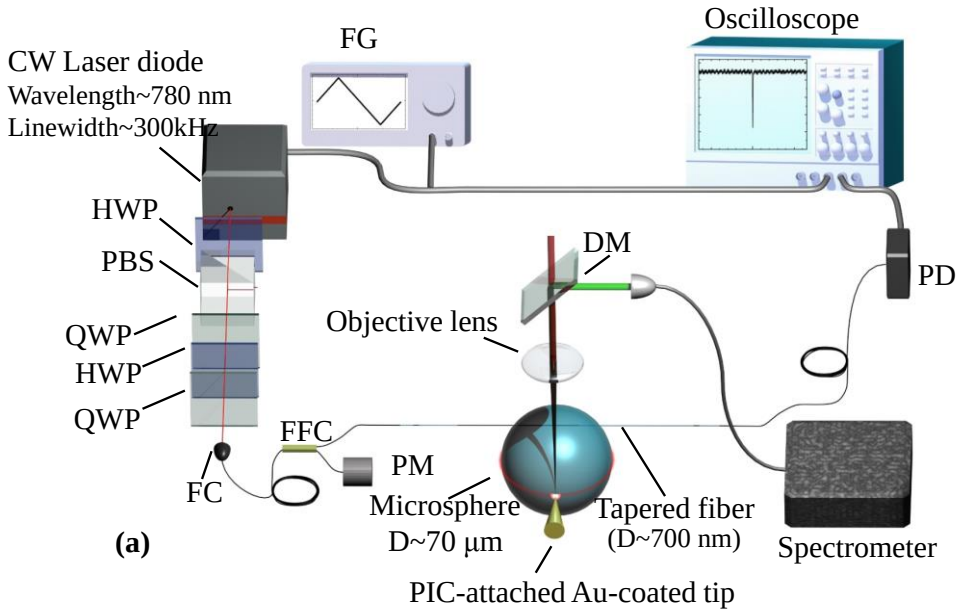

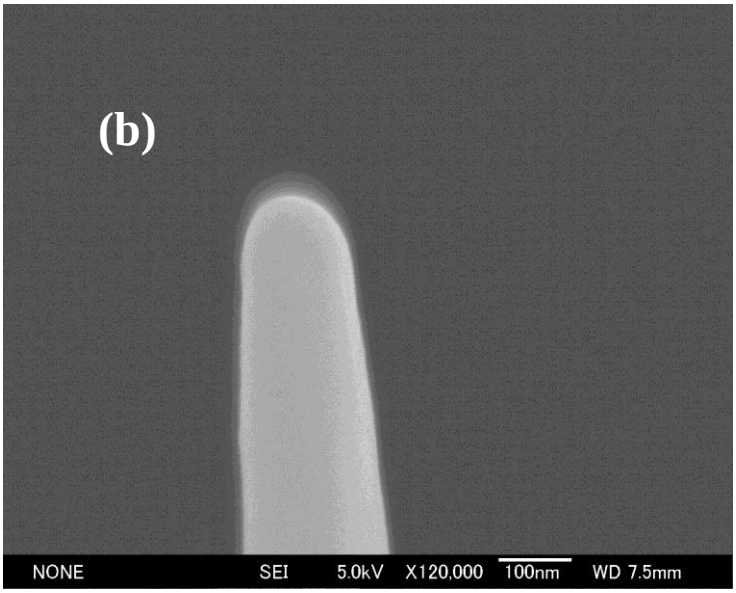

Fig. 5.1 (a) Schematic of experimental setup. FG: Function generator; LD: Laser diode; HWP: Half wave plate; PBS: Polarization beam splitter; QWP: Quarter wave plate; PD: Photodiode; DM: Dichroic mirror; (b) SEM images of a microsphere and an Au-coated tip.

Fabrications of a tapered fiber, a silica microsphere and a PIC-attached Au-coated tip are introduced in chapter 3. In the experiment, the tapered fiber with the waist diameter of about 700 nm was used; the diameter of the microsphere in this experiment was about 70 μm, which can be

controlled by the laser intensity and irradiation time; a silicon AFM tip, as a metal nanostructure, was coated by Au-coated thin film with the thickness of about 50 nm using a helicon sputter. The curvature diameter of the Au-coated tip was smaller than 100 nm. The localized surface plasmon resonance properties have been investigated in the section 3.4 of chapter 3. From the results, it was found that the plasmon resonant peak was close to the excitation wavelength 780 nm of this experiment, implying the efficient LSPs excitation at the apex of the Au-coated tip.

5.3 Results and discussion

In order to examine the LSP property of a PIC-attached Au-coated tip, the dependence of the TPF intensity from PIC dye molecules attached on an Au-coated tip on the polarization of the excitation light was investigated. Pulses from a femtosecond Ti:sapphire laser (wavelength: ~780 nm, pulse duration: ~100 fs, repetition rate: 80 MHz) for TPF excitation were focused onto the tip, as shown in Fig. 5.2(a). The excitation polarization was controlled by a half-wave plate. The TPF from the tip was collected by an objective, passed through a dichroic mirror and shortpass filters to eliminate the excitation light, and detected with a single photon counting modules (SPCM). The TPF intensity (I_{em}) from the tip was examined as a function of the angle (θ) between the polarization of the excitation light and the tip axis, as shown in Fig. 5.2(b). The TPF intensity was maximized when the polarization of excited field was parallel to the tip axis. In contrast, when the excited field was perpendicular to the axis of the tip, the TPF intensity decreased to minimum. Note that the background shown in Fig. 5.2(b) would be due to the imperfection of linear polarization state of the excitation light in the experiment. According to the reports [11], because the scattering intensity of the excitation light (I_{sca}) was proportional to $cos^2(\theta)$ owing to the existence of surface plasmon from the metallic nanostructures, the corresponding TPF intensity (I_{em}) was proportional to $(I_{sca})^2 \sim cos^4(\theta)$. Therefore, in this experiment, the TPF intensity followed $cos^4(\theta)$ dependence against the excitation polarization as expected. From the results, we found that the TPF intensity was sensitive to the incident polarization, and the incident polarized light parallel to the tip axis could efficiently excite the TPF from the tip, owing to the LSP excitation at the tip.

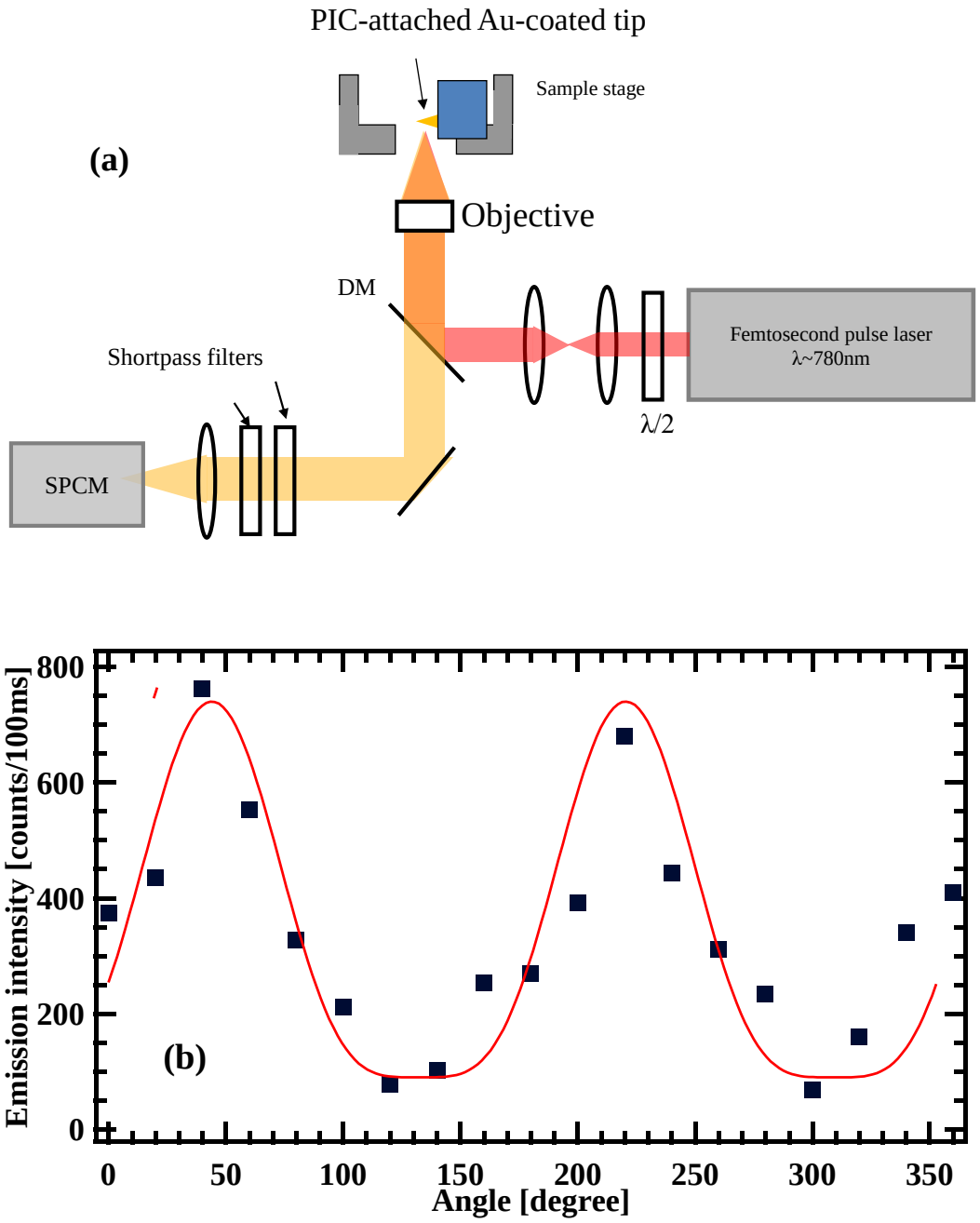

Fig. 5.2 (a) Schematic of polarization dependence measurement's experimental setup. DM: Dichroic mirror. (b) Excitation polarization dependence of TPF from the apex of a PIC-attached Au-coated tip under a femtosecond pulse laser excitation in free space. The fitting solid curve shows a $cos^4(\theta)$ function.

For the experimental realization of TPF from PIC dye molecules attached on the Au-coated tip under a weak CW excitation condition via a tapered-fiber-coupled microsphere, it is necessary to build the system that satisfied the condition ($\kappa_{ex} = \kappa_{tip} >> \kappa_0$) mentioned in section 2.5 of chapter 2 in order to achieve highly efficient coupling of the CW incident light into the tip. For this purpose, firstly, we measured the intrinsic cavity loss rate κ_0 of a microsphere without an Au-coated tip. The tapered fiber with the diameter of ~700 nm was approached to the surface of the microsphere at 20-nm interval step. Before starting the measurements, the polarization controller was adjusted to obtain a linearly polarized light in the tapered fiber, in which the polarization state of the incident light at the tapered region was determined by the use of the same method in ref. [97]. The polarization state was set to be parallel to the tip axis, which has been verified to efficiently induce TPF from the PIC dye molecules attached on the Au-coated tip. Then we scanned the laser frequency to observe the transmittance spectra.

The transmittance spectra with varying the gap distance between the microsphere and tapered fiber is shown in Fig. 5.3(a). Figures 5.3(b) and (c) also show the transmittance and linewidth of the resonant dip versus the gap distances. When the distance between the tapered fiber and the microsphere became 840 nm, we could start to observe a small resonant dip in the transmittance spectra, whose linewidth ($\Delta\upsilon_0$) of the dip was about ~13.1 MHz. Because the tapered fiber was enough far away from the surface of the microsphere indicating that the fiber-sphere coupling rate κ_{ex} was considered to be very small, the linewidth of the small dip was almost regarded as the linewidth due to the intrinsic cavity loss rate ($\kappa_0 \sim 2\pi\times13.1\times10^6$ s^{-1}), corresponding to the Q factor of $\sim3.0\times10^7$. After the measurement of κ_0, the tapered fiber was gently in contact with the surface of the microsphere equator using a three-dimensional piezo manipulator. At this time, the transmittance (T_0) and linewidth ($\Delta\upsilon_0 + \Delta\upsilon_{ex}$) were about ~89.3 % and ~107.5 MHz, and the fiber-sphere coupling rate κ_{ex} was estimated to be $\sim2\pi\times94.4\times10^6$ s^{-1}. Therefore, the over coupling condition of $\kappa_{ex} >> \kappa_0$ was achieved, which was required for achieving the efficient light coupling into the Au-coated tip.

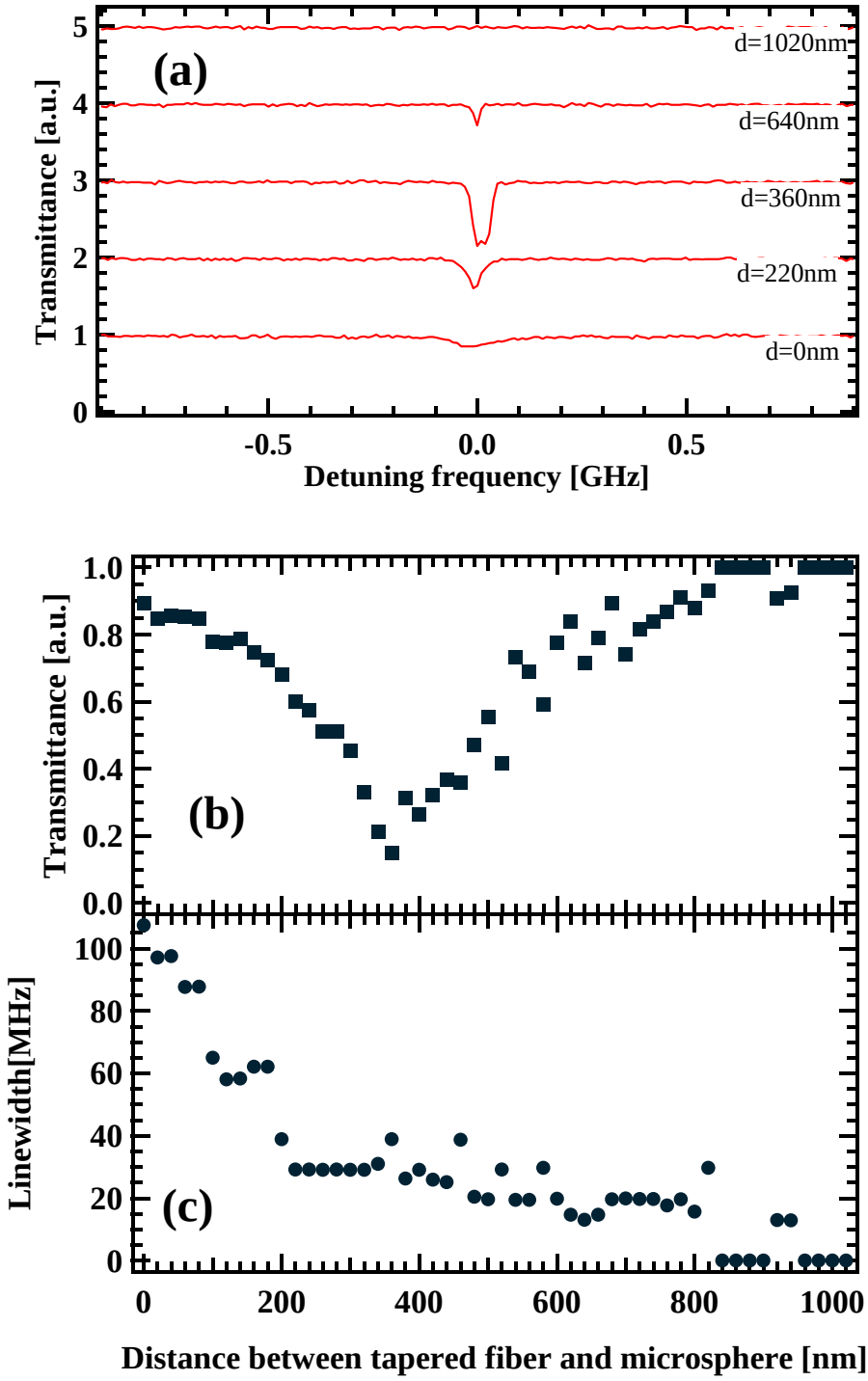

Fig. 5.3 (a)Transmittance spectrum from the end of tapered fiber; Transmittance (b) and Linewidth on resonance (c) versus distance between the tapered fiber and microsphere resonator. d is the distance between the tapered fiber and microsphere resonator in (a), and the zero point corresponds to the tapered fiber in contact with the surface of microsphere resonator.

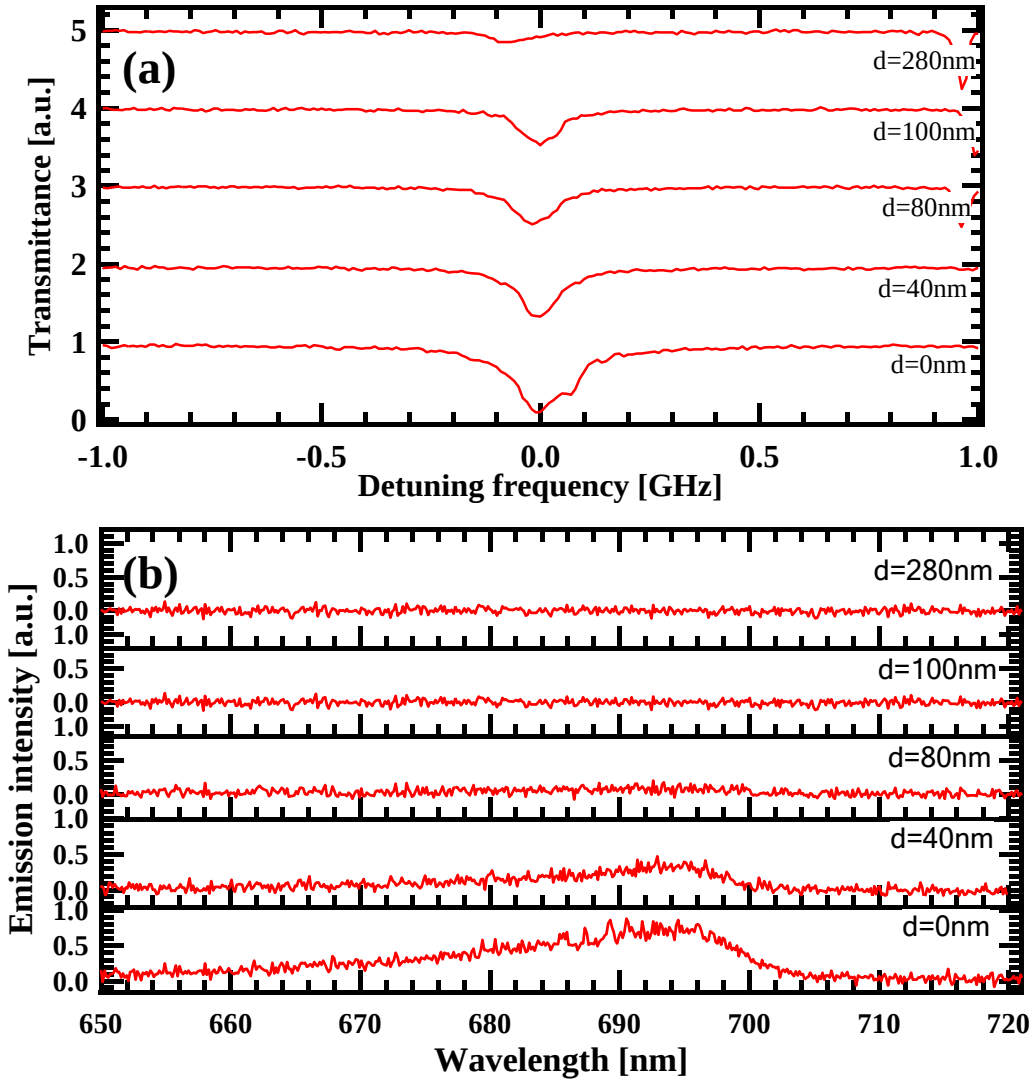

Fig. 5.4 (a) The transmittance spectra from the end of the tapered fiber and (b) Emission spectra from the apex of the PIC-attached Au-coated tip measured at different distances between the tip and the surface of microsphere. The tapered fiber was in contacted with the surface of microsphere. The transmittance in this experiment was normalized with respect to the tapered fiber enough far away from the microsphere surface.

Then, by approaching the tip from the opposite side of the tapered fiber to the surface of the microsphere equator, we realized the critical light coupling condition between the PIC-attached Au-coated tip and the tapered-fiber-coupled microsphere, and simultaneously measured the dependence of emission intensity from the tip on the distance (*d*) between the tapered-fiber-

coupled microsphere and the tip. The tip was approached to the microsphere surface at 20-nm intervals. In order to analyze the coupling condition between the tapered-fiber-coupled microsphere and the tip, the frequency of the incident light was also continuously scanned during the measurements of transmittance and emission spectra. Figures 5.4(a) and (b) represent the transmittance spectra from the end of the tapered fiber and emission spectra from the apex of the tip measured at different distances between the tip and microsphere. We found that the resonant dip became deeper and broader and accordingly the emission intensity increased, when gradually approaching the tip to the microsphere surface. Note that the spectral shapes of emission light at the longer wavelength regions (> 700 nm, in Fig. 5.4(b)) were strongly modified due to the shortpass filters to eliminate the incident light.

In accordance with Figs. 5.4(a) and (b), we plotted the transmittance and linewidth of the resonant dip and emission intensity at the tip against the distance between the PIC-attached Au-coated tip and the microsphere surface, as shown in Figs. 5.5(a-c). When the tip was enough far away from the microsphere surface, there was no change from the spectrum shown in the top of Fig. 5.4(a), whose dip transmittance (T_0) and linewidth ($\Delta\upsilon_0 + \Delta\upsilon_{ex}$) were asymptotically determined to be about 89.3 % and 107.5 MHz from the Figs. 5.5(a) and (b), and no emission light form the apex of the tip was observed (Fig. 5.5(c)). As we continued to approach the tip to the microsphere surface, the transmission dip became deeper and broader, indicating the increase in the light coupling to the tip, and the intensity of emission light increased. At the distance of 0 nm, the transmittance of the resonant dip reached to its minimum (T_{min} ~ 9.0 %), whose linewidth became almost twice (~210.0 MHz) against the initial value of ~107.5 MHz, and the emission intensity reached to the maximum. From the values of κ_{ex} and κ_0, the tip-sphere coupling rate κ_{tip} was estimated to be $\sim 2\pi\times 102.5\times 10^6$ s^{-1}. At this distance, because κ_{tip} ($\sim 2\pi\times 102.5\times 10^6$ s^{-1}) was much larger than κ_0 ($\sim 2\pi\times 13.1\times 10^6$ s^{-1}) and was approximately equal to κ_{ex} ($\sim 2\pi\times 94.4\times 10^6$ s^{-1}), these results indicated that the critical PP-LSP coupling condition of $\kappa_{ex} \approx \kappa_{tip} >> \kappa_0$ was satisfied, indicating efficient coupling of the incident light into the tip. Furthermore, the total Q factor of this system was still kept to be as high as about 1.9×10^6 even when the PIC-attached Au-coated tip was contacted to the microsphere surface. According to the obtained values and Eq. (2.60) of chapter 2, the transmittance under the critical PP-LSP coupling condition was evaluated to be 1.0 %, whose value was approximately corresponded to the

experimental data (T_{min}). A slight difference in the transmittance would be due to the misalignments of the tip-sphere position and polarization of the incident light at the tapered region in the experiment. In addition, from κ_{tip} and Eq. (2.62), the effective extinction cross-section σ_{ext} of the tip was estimated to be ~728.8 nm^2 (D_{ext} ~ 30 nm). Thus, we confirmed that using this system, about 80.3 % of the incident light (T_0 - T_{min}) via the tapered-fiber-coupled microsphere resonator was coupled to the PIC-attached Au-coated tip, resulting in maximizing the emission intensity from the apex of the tip as shown in Fig. 5.5(c).

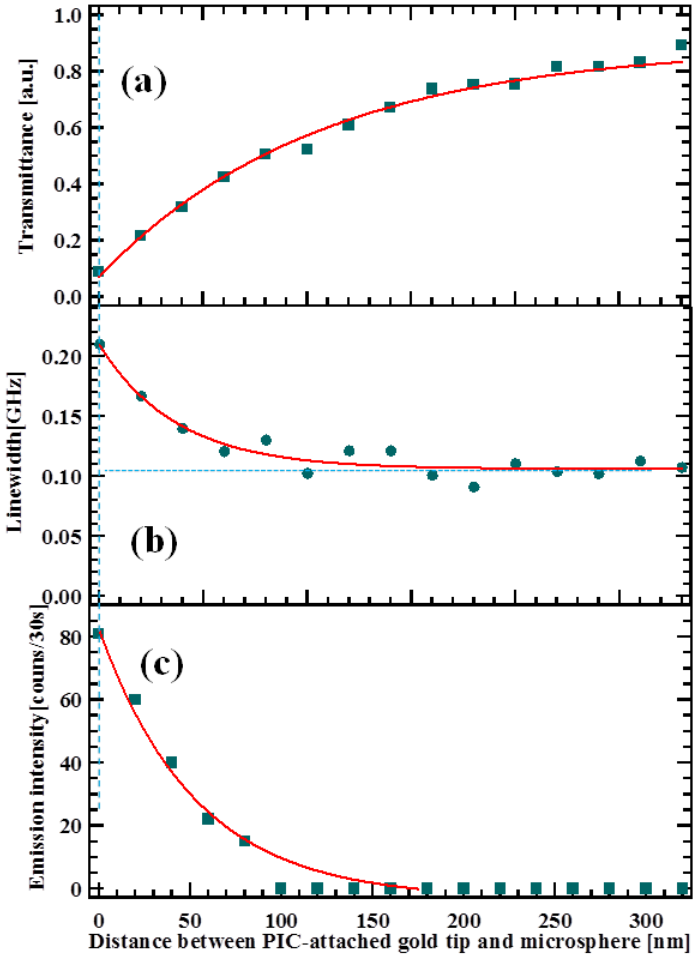

Fig. 5.5 (a) Transmittance, (b) linewidth of the resonant dip and (c) emission intensity at the apex of the PIC-attached Au-coated tip against the distance between the PIC-attached Au-coated tip and the microsphere surface.

From the Fig. 5.5(a), because the dissipation by the PIC-attached Au-coated tip would depend on the spatial profile of the evanescent field around the microsphere, the transmittance has T(d) ~ T_0(1-exp(-αd)), where T_0 and α are the initial transmittance and coefficient of exponential function, respectively. Using the obtained experimental data (T_0 ~ 89.3 %), the transmittance was fitted by the exponential function (red line in Fig. 5.5(a)) and the coefficient α was determined to be ~0.009 nm^{-1}. Because the coupling efficiency and the intensity of the incident light (I_{in}) coupled into the tip would be proportional to $\eta \sim T_0 - T(d)$, the TPF intensity would be expressed as $I_{em} \sim (I_{in})^2 \sim (\eta)^2 \sim \exp(-2\alpha d)$. By fitting the data (red line in Fig. 5.5(c)), we confirmed that the coefficient of exponential function was ~0.018 nm^{-1}, which was just twice of α ~ 0.009 nm^{-1}, suggesting the quadratic dependence on the incident power. Thus, because the efficient interaction between light and the PIC-attached Au-coated tip owing to the synergetic effect of strong optical confinement effect of the tapered-fiber-coupled microsphere resonator and optical antenna effect of the Au-coated tip would cause the enhancement of two-photon excitation process, the TPF from the PIC-attached Au-coated tip could be observed.

Furthermore, after building the efficient light coupling system, we also verified the TPF from the PIC-attached Au-coated tip by measuring the dependence of the TPF intensity on the power of incident light. As we kept the position of the tapered-fiber-coupled microsphere and the tip by monitoring the transmission spectra, we gradually increased the power of incident CW light, and the emission spectra from the tip were measured by a spectrometer. Figure 5.6 shows the dependence of the TPF intensity on the power of the incident light with the slope value of ~2.04, indicating that the two-photon excitation process was occurred. In order to compare with the previous reports [10-18], in which TPF has typically been induced by a high-power pulsed laser excitation (typical peak power density: several MW/cm^2), we estimated the effective power density at the tapered region by taking into account of the influence of the frequency scan. Because the incident light coupled into WGM modes was only contributed to induce TPF at the tip, the effective incident power was compensated by the ratio of the linewidth of resonant dip and the total frequency scanning range, and then the effective power density at the tapered region was estimated to be several kW/cm^2 (~ 3 μW), which value was much smaller than those excited by a high-power pulsed laser excitation [10-18]. Thus, these results suggest the possibility that using the hybrid system via the tapered-fiber-coupled microsphere under a weak CW excitation

condition, the highly efficient LSP excitation can be achieved, resulting in the strong light-matter interaction at the tip.

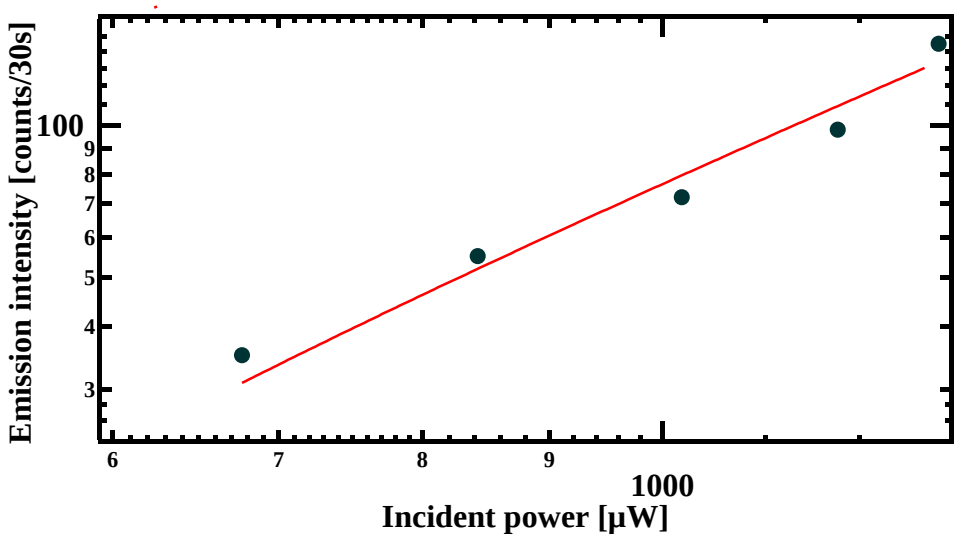

Fig. 5.6 Log-log plot of dependence of the TPF intensity on the power of the incident light. The slope value is ~2.04 (red solid line), indicating TPF from the PIC-attached Au-coated tip via a tapered-fiber-coupled microsphere resonator. The tip was contacted to the surface of microsphere.

5.4 Summary

We proposed a plasmonic-photonic hybrid system in which a tapered-fiber-coupled microsphere resonator was employed to efficiently couple light into a PIC-attached Au-coated tip, and achieved the light localized into a nanoscale domain (~728.8 nm^2) of the tip apex with high coupling efficiency of ~80.3 % and the *Q* factor of ~1.9×10^6. In order to experimentally verify the strong interaction between light and matter at the apex of the Au-coated tip owing to efficient LSP excitation, we succeeded in observing the TPF from PIC dye molecules attached on the Au-coated tip under a weak CW excitation condition using this plasmonic-photonic hybrid system. These results suggested the possibility that, using our proposed system, the synergetic effect of

strong optical confinement effect of tapered-fiber-coupled microsphere resonator and optical antenna effect of the Au-coated tip tremendously results in the strong light-matter interaction at the PIC-attached Au-coated tip.

Chapter 6 Two-photon excited fluorescence from a PIC-attached Au-coated tip via a thin tapered fiber

6.1 Introduction

In chapter 4 and 5, a plasmonic-photonic hybrid system with high *Q* factor, composed of an Au-coated tip and a tapered-fiber-coupled microsphere resonator, have been proposed. The tapered-fiber-coupled microsphere resonator could efficiently and controllably focus light into the single metal nanostrucuture. Using this hybrid system, nonlinear phenomena (SHG and TPF) were observed under a weak CW excitation condition, owing to efficient LSPs at the metal tip and optical confinement of microsphere resonator. Whereas the photonic microsphere resonator with the ultra-high *Q* factor facilitates the efficient focusing of light from the tapered fiber to the single plasmonic nanostructure, this hybrid system is complicated which result in difficult alignment in the experiment. Hence, a simple tapered fiber based photonic-plasmonic hybrid nanostructure consisted of an Au-coated tip and a thin tapered fiber in this chapter. Using this

simple tapered fiber based photonic-plasmonic hybrid nanostructure combining the merits of both plasmonic and photonic elements, we also succeeded in observing two-photon excited fluorescence (TPF) from the PIC dye molecules attached on the Au-coated tip even under a weak CW excitation condition.

Especially we note that Sanchez et al. [13] have also demonstrated that TPF from PIC dye molecules dispersed on a substrate was enhanced by an Au tip, where the incident pulsed laser light was focused on the tip by an objective lens and the emission from PIC dye molecules were collected by the same objective. Although in their papers, the plasmonic enhancement at the tip apex would also play an important role for improving the excitation and emission efficiencies for observing TPF, the coupling of incident light into the Au tip would be low due to the scale mismatch of the focused spot and the apex of the tip, resulting in the use of a high intense pulsed laser excitation.

The simple tapered fiber based photonic-plasmonic hybrid nanostructure studied here was composed of an optical thin tapered fiber and a PIC-attached Au-coated tip. The tip-fiber distance dependence and excitation polarization dependence were measured. It was found that by the use of a thin tapered fiber and an Au-coated tip, efficient coupling of the incident light (~ 95 %) and LSP excitation at the Au-coated tip could be realized and this effect makes it possible to induce two-photon excited fluorescence from the PIC dye molecules attached on the Au-coated tip with a weak CW excitation. We consider that this simple photonic-plasmonic hybrid system is one of the promising tools for single photon sources, highly efficient plasmonic sensors, and integrated nonlinear plasmonic devices.

6.2 Experimental setup

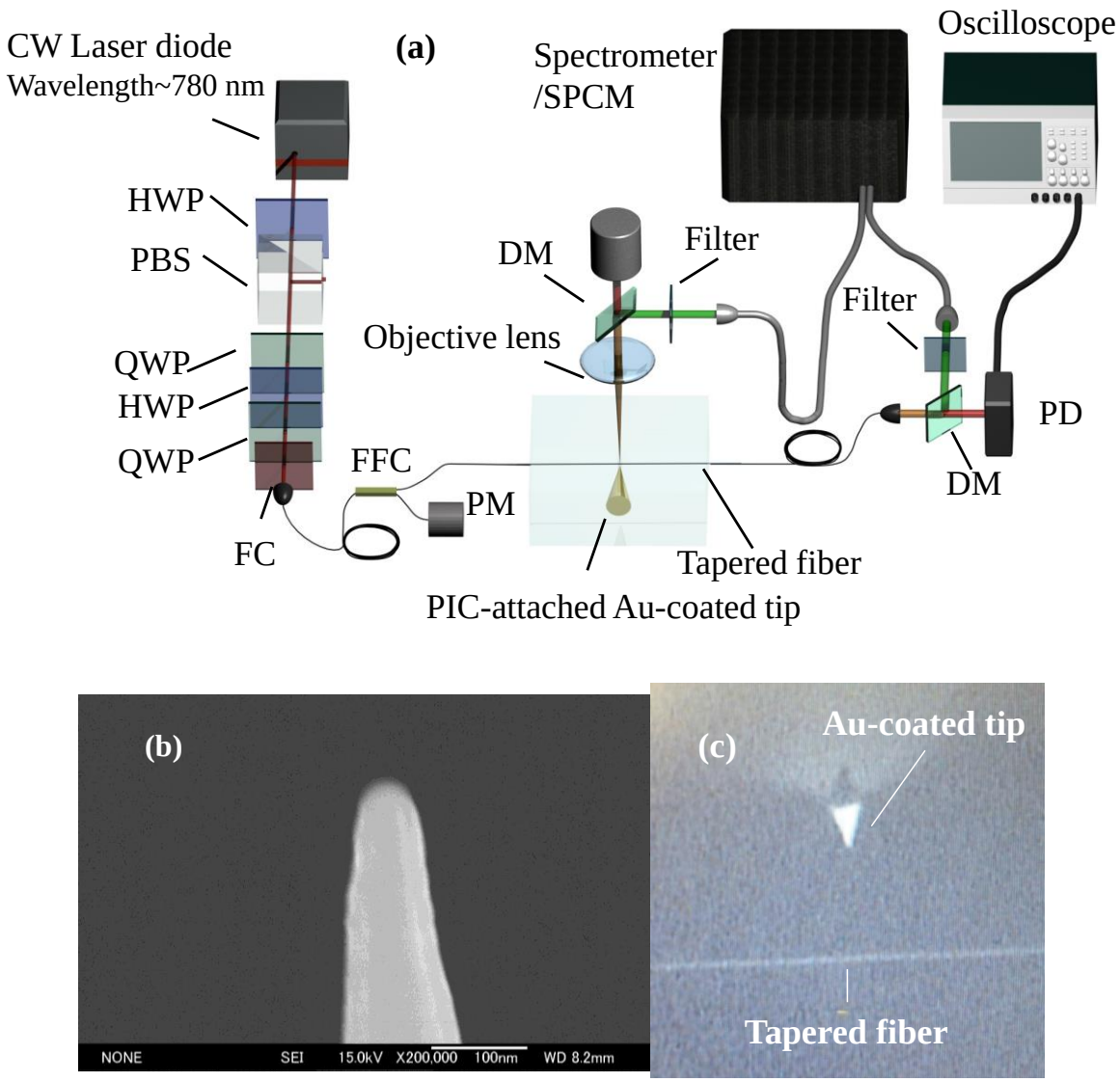

Fig. 6.1 (a) Schematic of experimental setup. LD: Laser diode; HWP: Half wave plate; PBS: Polarization beam splitter; QWP: Quarter wave plate; PD: Photodiode; DM: Dichroic mirror; FC: fiber coupler. (b) SEM image of an Au-coated tip by FE-SEM. (c) CCD image of samples.

The experimental setup is shown in Fig. 6.1, similar to Fig. 5.1 of chapter 5. A diode laser (New Focus, TLB-6312, Wavelength ~ 780 nm) without frequency scan was introduced into a tapered fiber as a probe and excitation light. In order to control the coupling conditions, the separation distance between the tapered fiber and the PIC-attached Au-coated tip was controlled by piezo manipulators (PI-Polytec, P-621.1CD, P-621.ZCD). The origin of the

distance between the tapered fiber and the tip was determined as the position where the tip was contacted to the surface of the tapered fiber. The emission light from the PIC-attached Au-coated tip was collected by two ways. One way was that the emission light was collected using a microscopy system set on the top of the sample (free-space collection), as the same to emission collection method of chapters 4 and 5. The other way was that the emission light was collected by the tapered fiber (tapered-fiber collection) and was measured at the end of the tapered fiber by the same spectrometer after using shortpass filters to block the excitation light.

Fabrication of a tapered fiber has been introduced in the section 3.3 of chapter 3. In this experiment, diameters of the tapered fibers were from 200 nm to 1000 nm. We monitored the transmittance in the tapered fibers at wavelength about 780 nm during the fabrication process (see section 3.2 of chapter 3). The transmittances of the tapered fibers in the experiment were over 0.90. The fabrication of an Au-coated tip was reported in the section 3.4 of chapter 3. The localized surface plasmon resonance properties have been investigated in the section 3.4 of chapter 3. From the results, it was found that the plasmon resonant peak was close to the excitation wavelength 780 nm, expecting the efficient LSPs excitation at the apex of the Au-coated tip. PIC molecules were attached on the surface of the Au-coated tip using a self-assembly technique (see section 3.5 of chapter 3).

6.3 Results and discussion

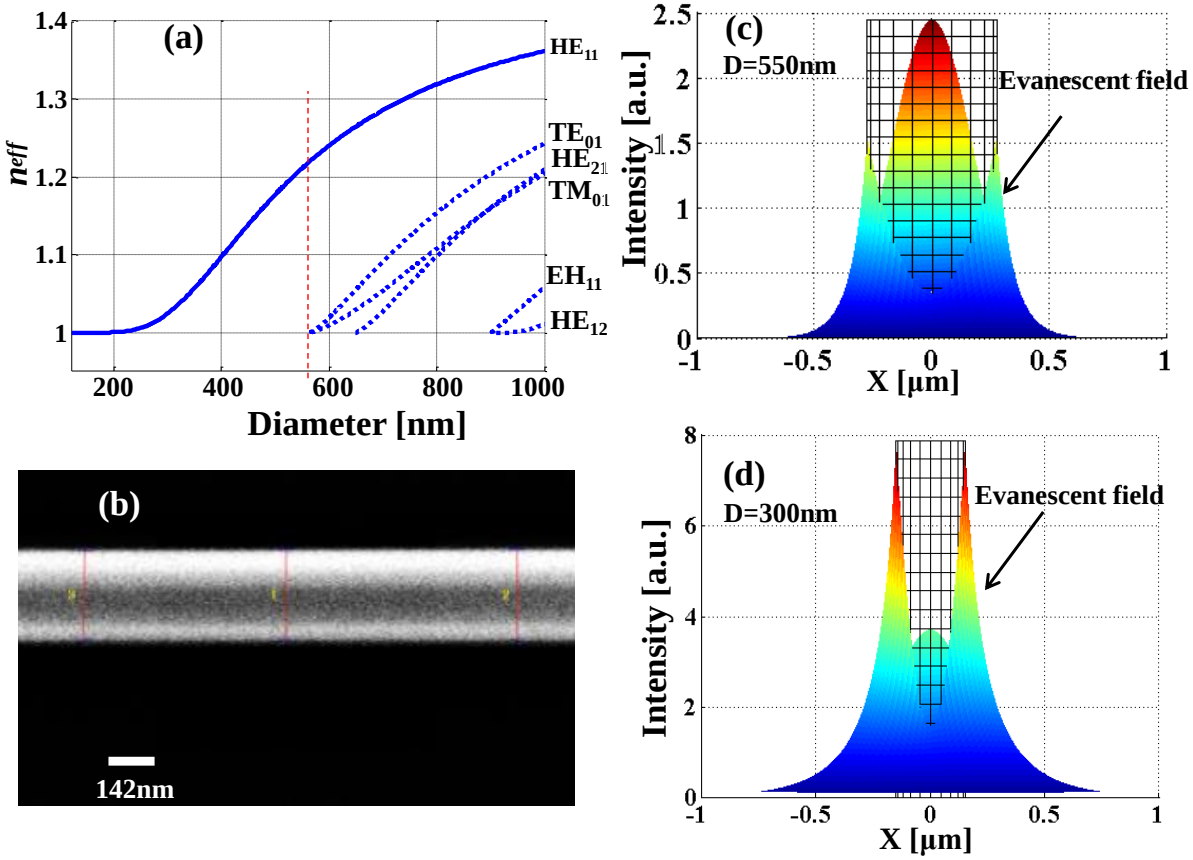

Fig. 6.2 (a) Numerical diameter dependence of effective refractive index n_{eff} of the guided mode at 780-nm wavelength. Solid line: fundamental mode. Dot lines: higher order modes; (b) Scanning electron micrograph of a tapered fiber by SEM. Diameter (D): 274 nm; Calculated cross-section profile of the total field intensity distribution of the electric field in the fundamental mode HE_{11} for tapered fibers with diameter of 550 nm (c) and 300 nm (d) at 780-nm wavelength. Cylindrical mesh indicates the tapered fiber as a reference.

First, we numerically analyzed the propagation mode properties of a thin tapered fiber, which has been discussed in the section 2.2 of chapter 2. According to the exact solutions of Maxwell's equations and eigenvalue equations for waveguide modes [61-64], the diameter (D) dependence of effective refractive index of the guided mode (n_{eff}) was obtained numerically, as shown in Fig. 6.2(a) where refractive index of tapered region (n_1), that of surrounding medium (n_2), and the incident light wavelength (λ) were assumed to be 1.45, 1.0, 780 nm. It was found

that, when the diameter of the tapered fiber (D) was reduced to 565 nm (red dashed line in Fig. 6.2(a)), the tapered fiber only supported the fundamental mode HE_{11} with quasi-linear polarization. Then we numerically calculated the fundamental mode distributions of a thin tapered fiber with the diameters of 300 nm and 550 nm, as shown in Figs. 6.2(c) and 6.2(d). From the results, the thick tapered fiber with the diameter of 550 nm confined major power inside the tapered fiber, while a large amount of light as an evanescent field was in the outside of the thin tapered fiber with the 300-nm diameter. These results corresponded to the previous reports [61-64] that an intense evanescent field was generated in the vicinity of a thin tapered fiber, indicating the possibility of the efficient interaction of the propagating photons in the tapered fiber with the Au-coated tip.

To experimentally confirm this, we measured the dependence of transmittance from the end of tapered fiber on the tapered-fiber diameter (Fig. 6.3). In the absence of the PIC-attached Au-coated tip (squares in Fig. 6.3), almost no change of the transmittance (T_1) dependent on the tapered-fiber diameter was observed, and T_1 was almost equal to 1, when the diameter was changed from 1000 to 200 nm. As the same results were reported in refs. [99][106], they suggested that when the diameter of the tapered fiber was larger than ~ 0.25 λ (λ: light wavelength), the transmittance of a tapered fiber could keep high transmittance. In the two ends of untapered region, only the fundamental mode HE_{11} of the standard single-mode fiber was existed in the fiber core. When the shape of a fiber was adiabatically changed, the light was guided by the silica-air interface as the hybrid fundamental mode or higher order modes with strong evanescent field around the tapered region. Thus, when the diameter of the tapered fibers was larger than ~200 nm in our experiments, hybrid propagation modes of a thin tapered fiber maintained the high transmittance as shown in Fig. 6.3. However, when the tip was contacted to the surface of the tapered fiber (circles in Fig. 6.3), the transmittance (T_0) was decreased with decreasing the diameter of the tapered fiber, and T_0 almost reached to 0 as the diameter decreased to 300 nm. We note that the circles with error bars in Fig. 6.3 present the standard deviation of experimental measurements. These results suggested that the dissipation ($\eta_c = T_1 - T_0$) of the incident light at the tip increased when the tapered-fiber diameter decreased owing to the increase in the amount of the evanescent field. As the tapered-fiber diameter was decreased to ~ 300 nm where the dissipation (η_c ~ 93.0 %) reached to maximum, the efficient LSP excitation at

the Au-coated tip would be expected. Therefore, taking into account these results and the technical reason that thinner fibers were easily broken, the diameter of the tapered fiber was chosen to be ~ 300 nm in the experiments.

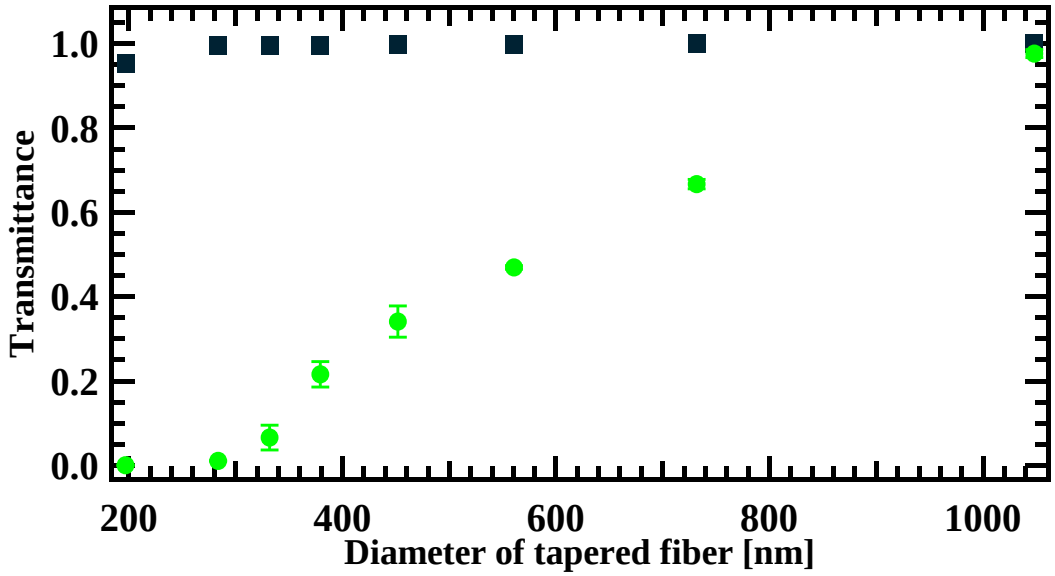

Fig. 6.3 The tapered-fiber diameter dependence of transmittance from the end of the tapered fiber with the PIC-attached Au-coated tip contacted to the surface of the tapered fibers (circles) and without the PIC-attached Au-coated tip (squares).

Then, we also experimentally analyzed the dependences of transmittance from the end of tapered fiber and emission intensity from the PIC-attached Au-coated tip on the distance (d) between the tapered fiber and the tip. The diameter of the tapered fiber in the experiment was ~ 300 nm. The tip was approached to the surface of the tapered fiber at 20-nm interval step. Figure 6.4 (circles) represents the distance dependences of the transmittance from the end of the tapered fiber and the emission intensity from the tip through tapered-fiber collection. When the tip was far away from the surface of the tapered fiber, there was no change in the transmittance (T_2 ~ 1) and no emission from the tip. As we continued to approach the tip to the tapered-fiber surface, the transmittance decreased, and emission intensity increased. At the distance (d) of 0 nm, the transmittance reached to the minimum ~ 0.05 (T_{min}), and emission intensity reached to the

maximum. Thus, at this distance, about 95 % of the incident light via the thin tapered fiber was coupled into the tip ($\eta_c = T_2 - T_{min}$), resulting in maximizing the emission intensity from the tip (circles in Fig. 6.4(b)). The cross section σ_{ext} of the Au-coated tip could be estimated to be 8×10^4 nm^2 with the diameter D_{ext} of ~ 320 nm owing to the highly efficient coupling of light into the Au-coated tip (~ 100 %, also see Fig. 6.3) at the ~ 300-nm diameter of the tapered fiber. Here, the diameter of cross section was defined as the distance from the tapered center to where the intensity became half of the total intensity.

Because the dissipation by the tip would depend on the spatial profile of the evanescent field around the tapered fiber, the transmittance has $T(d) \sim 1\text{-}exp(-\alpha d)$, where α is coefficient of an exponential function. When the transmittance was fitted by the exponential function (red solid line in Fig. 6.4(a)), the coefficient α was determined to be ~ 0.008 nm^{-1}. Assuming that the intensity of the incident light coupled into the tip followed $I_{in} \sim \eta_c \sim 1\text{-}T(d) \sim exp(-\alpha d)$, the TPF emission intensity would be expressed as $I_{em} \sim (I_{in})^2 \sim exp(-2\alpha d)$. By fitting the data (red solid line of Fig. 6.4(b)), we confirmed that the coefficient of the exponential function was ~ 0.016 nm^{-1} which was just a twice of α ~ 0.008 nm^{-1} and suggested the quadratic dependence on the incident power. Thus, because the efficient interaction between the tapered fiber and the Au-coated tip would cause the enhancement of two-photon excitation process, the TPF from the PIC-attached Au-coated tip could be observed. Note that in order to confirm the reproducibility, we also measured the data using different Au-coated tips fabricated under the same conditions. When the tip was contacted to the surface, we confirmed that the deviation of the transmittance was evaluated to be ± 0.01 and the emission intensity was 130 ± 20 counts/30s at the incident intensity of ~ 200 μW, as shown in Fig. 6.5.

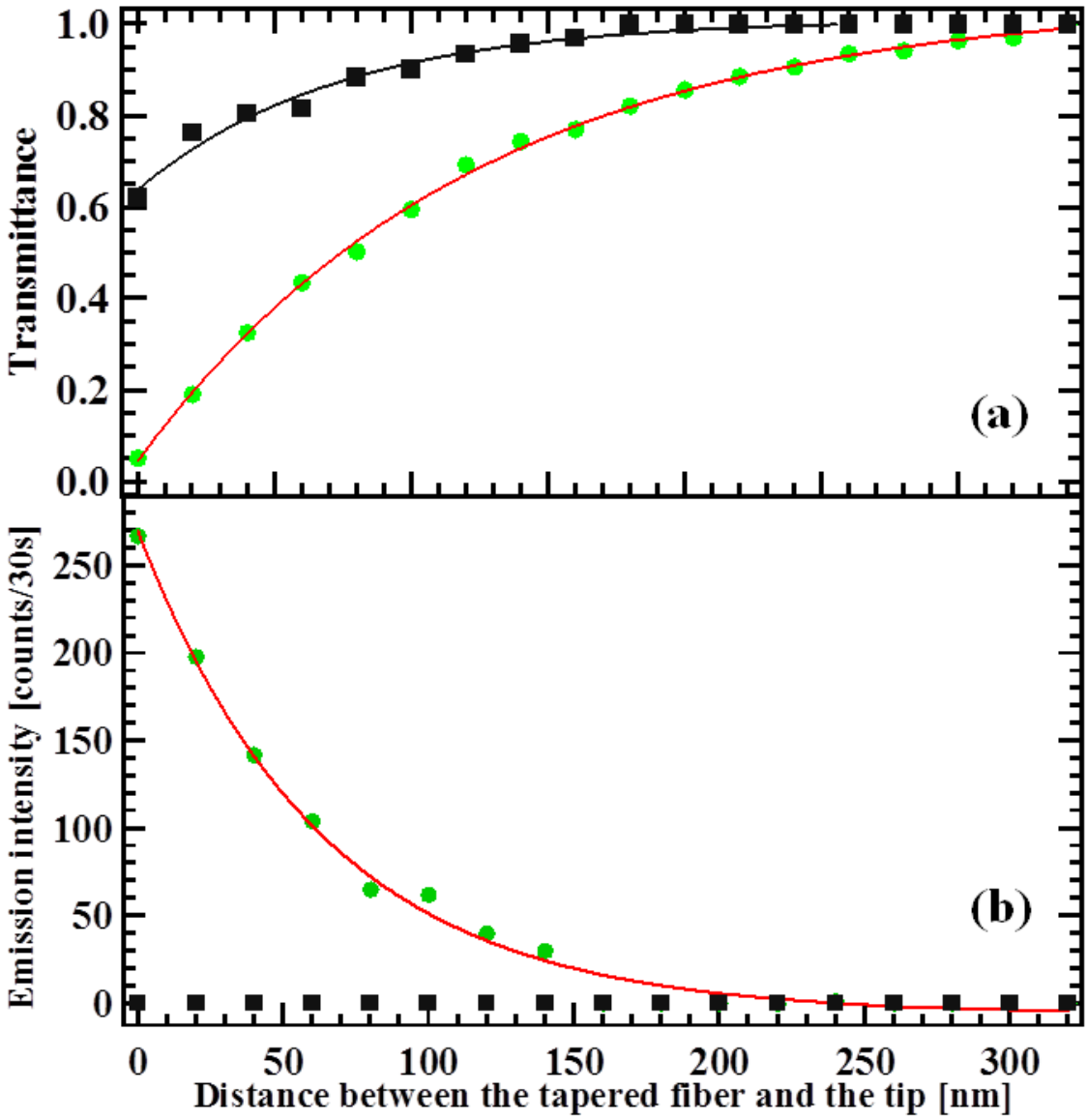

Fig. 6.4 (a) The transmittance from the end of tapered fiber dependent on various distance between the tapered fiber and the PIC-attached tip with (circles) and without (squares) Au coating. (b) The distance dependence of TPF intensity emitted from the PIC-attached tip with (circles) and without (squares) Au coating. The solid curves are exponential fit to the data.

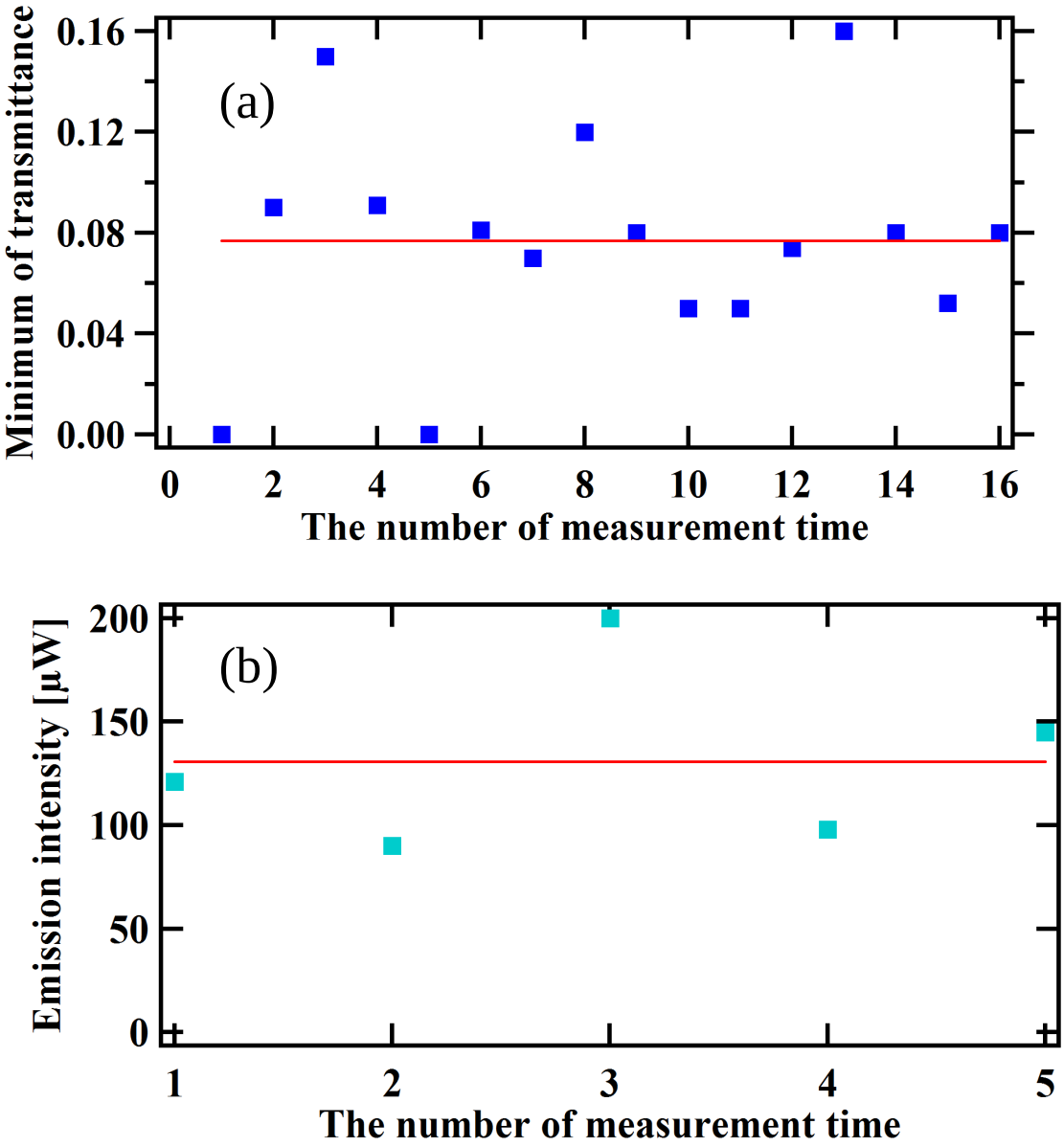

Fig. 6.5 Error analysis of transmittance (a) and emission intensity (b) when the tip was contacted to the surface of the tapered fiber. Fittings by mean are drawn by red curves. Transmittance: ~ 0.08±0.01; Emission intensity at the incident intensity of ~ 200 μW : 130± 20μW.

In order to further prove the importance of the Au coating on the tip, similar distance dependences of the transmittance and TPF intensity from a PIC-attached silicon tip without Au coating were also measured. The silicon tip having curvature diameter of ~ 100 nm, which was

almost the same as the apex size of Au-coated tip, was used in the experiment. In order to attach PIC dye molecules on the silicon tip, we used the same method as for the Au-coated tip mentioned in section 3.5 of chapter 3. We compare the photon count rates from PIC-attached Au-coated tip and silicon tip excited by a CW Ar^+ laser (wavelength: ~ 488 nm). Form the results, we found that the ratio of the averaged photon count rates was evaluated to be ~ 1.1, implying almost the same number of PIC dye molecules attached on the Au-coated tip and non-coated tip. When gradually approaching the tip to the surface of a tapered fiber with the diameter of ~ 300 nm, the transmittance (squares in Fig. 6.4(a)) was decreased to the minimum (~ 0.62). However, although about ~ 38 % of the incident light via the tapered fiber was coupled into the tip without Au coating, no emission light (squares in Fig. 6.4(b)) from the tip was observed even when the tip was contacted to the tapered-fiber surface. Comparing the results with and without Au coating, we considered that the enhancement caused by LSPs at the Au-coated tip would improve the evanescent coupling of incident light to the tip and also the excitation efficiency of PIC dye molecules. These results suggested that the combination of LSPs of an Au-coated tip and a thin tapered fiber could make it possible to induce nonlinear phenomena even under a weak CW laser excitation.

We also verified TPF from the PIC dye molecules attached on the Au-coated tip by measuring the excitation intensity dependence of the emission intensity. Figure 6.6(a) and (b) indicate emission spectra and the excitation intensity dependences of the emission intensities measured by the free-space (squares) and tapered-fiber (circles) collections, when the tip was in contact with the surface of the thin tapered fiber. We clearly found a quadratic dependence with the slope values of ~ 2.15 through the tapered-fiber collection and ~ 2.04 through the free-space collection. Thus, these results indicate that the two-photon excited emission from PIC dye molecules attached on the Au-coated tip was observed. From the effective radius of the field distribution at the tapered region in Fig. 6.2(d), the excitation power density at the tapered region was roughly evaluated to be about 61 kW/cm^2 (incident power at the tapered-fiber input: ~ 120 μW). According to the distance dependence of the transmittance shown in Fig. 6.4(a), the difference in the transmittances when the tip was far away and contacted to the surface of tapered fiber suggested about 100% coupling of incident light into the Au-coated tip. Thus, the power excited at the tip apex could be estimated to be the same power of the incident light through the

tapered fiber (~ 120 μW). Comparing with results of Tanaka et al. [102] where TPF from PIC dye molecules without metal nanostructures was induced by a strong CW excitation light in free space (incident power: ~ 350 mW), the excitation intensity enhancement of TPF from the PIC-attached Au-coated tip in our simple hybrid system via the thin tapered fiber was estimated to be about three orders of magnitude larger. This enhancement was originated from LSPs of the Au-coated tip and the thin tapered fiber. Therefore, these results suggest the possibility that using this simple system via the thin tapered fiber under a weak CW excitation condition, the highly efficient LSP excitation can be achieved, resulting in the strong light-matter interaction at the Au-coated tip.

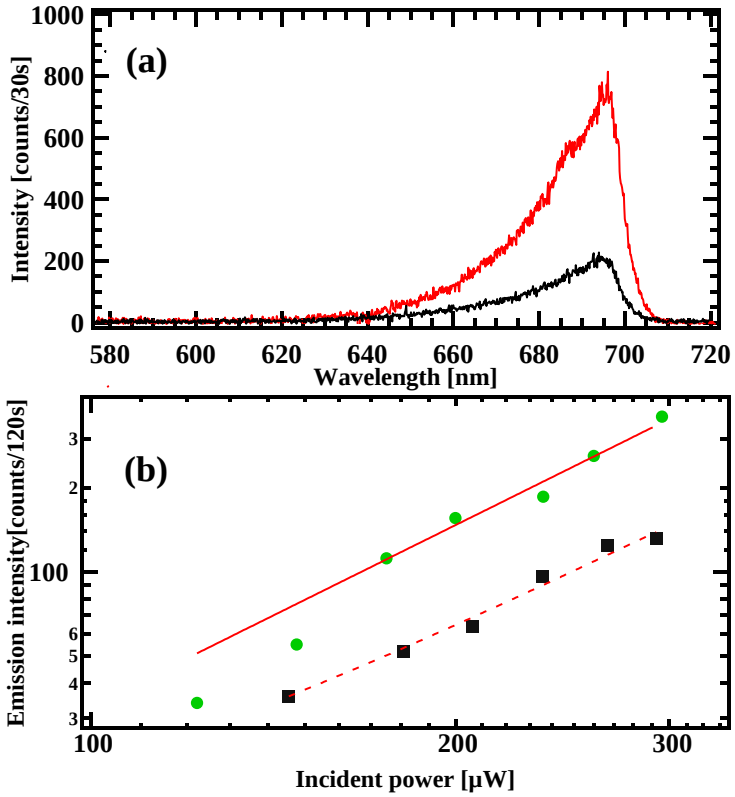

Fig. 6.6. (a) TPF spectra from the PIC-attached Au-coated tip collected by an objective (black curve) and the tapered fiber (red curve). (b) Log-log plot of dependence of the TPF intensity on the incident power through tapered-fiber collection (circles) and free-space collection (squares). The slope value is ~ 2.15 (solid line) in tapered-fiber collection (~ 2.04 (dashed line) in free-space collection).

Furthermore, to clarify the LSP excitation at the apex of the PIC-attached Au-coated tip, we simultaneously measured the excitation polarization dependences of the transmitted intensity of the incident light from the end of the tapered fiber and the TPF intensity emitted from the PIC dye molecules attached on the Au-coated tip, when the tip was contacted to the surface of the thin tapered fiber. Before starting the measurements, the polarization controller was adjusted to obtain a linearly polarized light in the tapered fiber, in which the polarization state at the tapered region was determined by the use of the same method of Konishi et al. [97] (see section 3.2 of chapter 2). Then, using the polarization controller, the angle (θ) between the polarization direction of the incident light and the tip axis was controlled, and the polarization of the incident light in the tapered region was first set to be parallel to the axis of the tip ($\theta \sim 0$ deg.). Figure 6.7 shows the excitation polarization dependences of the transmitted intensity and TPF intensity. The transmitted intensity of the incident light and TPF emission intensity was expected to be modified as a function of the angle (θ) between the polarization of the incident light and the tip axis. The transmitted intensity from the end of the tapered fiber would show a $sin^2(\theta)$ intensity dependence [11] because the intensity of the scattering light at the tip depended strongly on the polarization of the incident light owing to the LSP excitation at the tip. As a result, because the scattered light intensity at the tip apex (I_{sca}) would be proportional to 1 - $sin^2(\theta)$, the TPF intensity (I_{em}) would follow a $cos^4(\theta)$ dependence on the excitation polarization, $I_{em} \sim cos^4(\theta) \sim (1\text{-}sin^2(\theta))^2 \sim (I_{sca})^2$. From solid lines in Figs. 6.7(a) and 6.7(b), we found that these results are well fitted by the functions of $sin^2(\theta)$ and $cos^4(\theta)$, and in good agreement with previous theoretical and experimental results [11][16]. From Fig. 6.7(b), the TPF intensity (I_{em}) was maximized when the polarization of excited field was set along the tip axis (θ = 10 and 190 deg.), while the TPF intensity decreased when the excited field was perpendicular to the tip axis (θ = 100 deg.), which well followed a $cos^4(\theta)$ dependence. Note that due to the imperfection of linear polarization state of the incident light at the tapered region, the transmitted and the emission light were partially polarized in Figs. 6.7(a) and 6.7(b). Thus, we concluded that owing to the LSP enhancement, the two-photon excited process could be induced at the PIC-attached Au-coated tip even under the weak CW excitation.

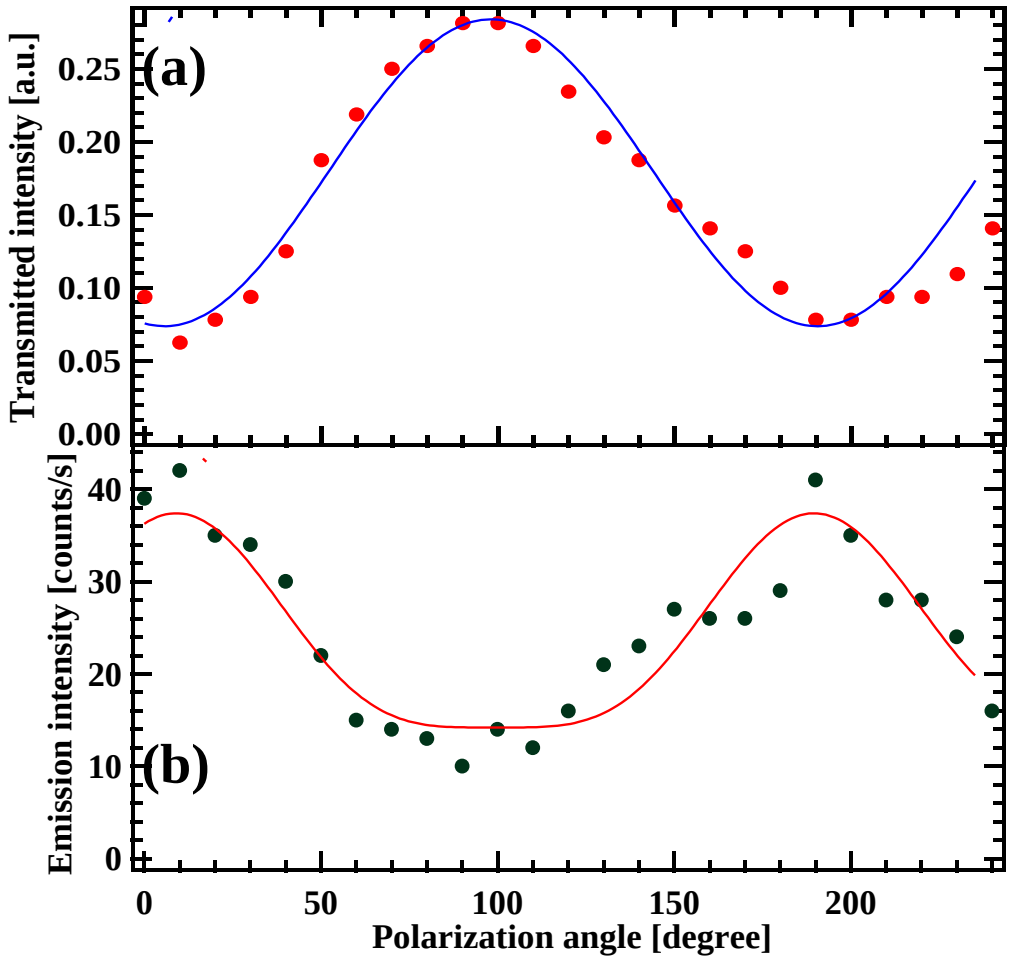

Fig. 6.7. (a) Transmitted intensity of the incident light from the end of the tapered fiber against the polarization of the incident light. The fitting curve in (a) shows a $sin^2(\theta)$ function. (b) Incident light polarization dependence of the TPF intensity from the PIC-attached Au-coated tip. The fitting solid curve in (b) shows a $cos^4(\theta)$ function. The tip was in contact with the surface of the tapered fiber.

In this chapter, we have realized the TPF from the PIC-attached Au-coated tip via a thin tapered fiber without microsphere resonator, in order to verify efficient LSP excitation at the apex of the tip. When the incident power of CW laser was ~ 120 μW, the TPF was observed using this plasmonic-photonic hybrid system. Comparing with the other plasmonic-photonic hybrid cavity system which was discussed in chapter 4 and 5, this hybrid system was simple and easy to alignment in the experiment. However, serious absorption and scattering loss of metal tip

resulted in the very low Q factor (<10). Although using this simple hybrid system, high coupling efficiency have succeeded to be achieved, the diameter of cross section (D_{ext} ~ 320 nm) at the Au-coated tip was large, resulting in low photon density at the nanoscale area. For the other plasmonic-photonic hybrid cavity system in chapter 4 and 5, a tapered-fiber-coupled microsphere was also used to couple light into single Au-coated tip efficiently, high Q factor (~ 10^6) and small cross section with the diameter D_{ext} of ~ 21 nm at the Au-coated tip in chapter 5 have been achieved. Because of the strong confinement effect of the high-Q microsphere resonator and the field enhancement of the LSP resonance at the metal tip, this hybrid cavity system can strongly enhance light-matter interaction at the nanoscale area. TPF would be expected from the PIC-attached Au-coated tip at a weak CW excitation light of ~ 3 μW weaker several ten times than that of the simple hybrid system.

6.4 Summary

We proposed a simple tapered fiber based plasmonic-photonic hybrid nanostructure composed of a thin tapered fiber (diameter: ~ 300 nm) and a PIC-attached Au-coated tip, and succeeded in observing two-photon excited fluorescence from the PIC dye molecules attached on the Au-coated tip even under a weak CW excitation condition (several tens kW/cm^2). From the results of the tip-fiber distance dependence and excitation polarization dependence, we found that by the use of a thin tapered fiber and an Au-coated tip, the efficient coupling of the incident light (~ 95 %) and LSP excitation at the Au-coated tip could be realized, and this effect makes it possible to induce two-photon excited fluorescence from the PIC dye molecules attached on the Au-coated tip with a weak CW excitation. We consider that this simple photonic-plasmonic hybrid system is one of the promising tools for single photon sources, highly efficient plasmonic sensors, and integrated nonlinear plasmonic devices.

Chapter 7 Conclusions

In this thesis, two plasmonic-photonic hybrid systems, which resulted in highly efficient coupling of incident light into the metal tip, were proposed. One hybrid system was composed of an Au-coated tip and a tapered-fiber-coupled microsphere resonator. The other one consisted of an Au-coated tip and a very thin tapered fiber. In order to experimentally verify the efficient excitation of LSPs at the Au-coated tip, nonlinear phenomena within these plasmonic-photonic hybrid systems under a CW laser excitation condition were demonstrated.

In chapter 2, propagation modes of tapered fibers, optical properties of microresonators, general properties of localized surface plasmon resonance were theoretically described. The optical properties of microresonators include optical modes, mode volume, *Q* factor, mode spacing. Regarding general properties of localized surface plasmon resonance, we presented absorption cross section, scattering cross section and field enhancement. Then, coupling theory among tapered fibers, microspheres, and Au-coated tips were briefly discussed.

In chapter 3, the basic setup for experiments and fabrication of experimental samples (tapered fibers, microsphere, Au-coated tip) were described. Transmittance properties of tapered fibers during the pulling process were discussed. Localized surface plasmon resonance scattering spectrum of an Au-coated tip was also investigated. In addition, preparation of PIC-attached Au-coated tip using a self-assembly technique was introduced.

In chapter 4, we have investigated the efficient coupling of light from a tapered-fiber-coupled microsphere resonator to localized surface plasmon modes of Au-coated tip. To verify efficient localized surface plasmon excitation at the metal tip via a tapered-fiber-coupled

microsphere resonator, we measured SHG from the top of Au-coated tip. From the results, in spite of a weak CW excitation (~ 28 μW), we succeeded in repeatedly observing SHG from the top of the Au-coated tip via a tapered fiber coupled microsphere resonator system, which could focus the light with the coupling efficiency of about 63.2 % into the nanoscale domain of the metal tip with the effective cross section (σ_{ext}) of 358.2 nm^2 (D_{ext} ~ 21 nm).

In chapter 5, we have reported a plasmonic-photonic hybrid system composed of a tapered-fiber-coupled microsphere resonator and a PIC-attached Au-coated tip to focus the incident light into a nanoscale domain (σ_{ext} ~728.8 nm^2; D_{ext} ~ 30 nm) with high coupling efficiency of ~80.3 % and the Q factor of ~1.9×10^6. In order to experimentally verify the strong interaction between light and matter owing to efficient excitation of localized surface plasmon at the Au-coated tip, we demonstrated to observe TPF from PIC dye molecules attached on the Au-coated tip even under a weak CW excitation condition (~ 3 μW) via a tapered-fiber-coupled microsphere resonator.

In chapter 6, a simple tapered fiber based photonic-plasmonic hybrid nanostructure composed of a thin tapered fiber and a PIC-attached Au-coated tip has been demonstrated. We succeeded in observing TPF from the PIC dye molecules under a weak continuous wave excitation condition (~ 120 μW) using this simple hybrid nanostructure, which could focus the light with the coupling efficiency of about 95 % into the nanoscale domain of the metal tip with the effective cross section (σ_{ext}) of 8×10^4 nm^2 (D_{ext} ~ 320 nm). From the results of the tip-fiber distance dependence and excitation polarization dependence, we found that using a thin tapered fiber and an Au-coated tip realized efficient coupling of the incident light and LSP excitation at the Au-coated tip, suggesting the possibility of efficiently inducing two-photon excited fluorescence from the PIC dye molecules attached on the Au-coated tip.

Comparing with the related reports about nonlinear phenomens induced by surface plasmon, e.g. Sanchez et al. [13] have demonstrated that TPF from PIC dye molecules dispersed on a substrate was enhanced by an Au tip, where the incident pulsed laser light (peak power: ~ 2 W) was focused on the tip by an objective lens, and Grycaynski et al. [15] also have reported that TPF from rhodamine derivatives near silver islands formed quartz microscope slides was enhanced by the silver islands using the same excitation method (Peak power: ~ 70 kW). In this study, we proposed two highly efficient plasmonic-photonic hybrid systems. One was composed

of a tapered-fiber-coupled microsphere resonator and an Au-coated tip. The other one consisted of a thin tapered fiber and an Au-coated tip. They largely improved the coupling of light onto single metal nanostructure (~ 100%), and succeeded to observe SHG and TPF under a weak CW excitation (~ μW).

In summary, taking merits of both plasmonic and photonic elements, the two types of plasmonic-photonic hybrid systems were proposed to improve the efficient coupling of light into the nanoscale domain of single metal nanostructure, which tremendously result in the strong light-matter interaction at the nanoscale. Moreover, nonlinear phenomena within these hybrid systems under a weak CW excitation condition (~ kW/cm^2) were investigated. These hybrid systems are the promising tools for single photon sources, highly efficient plasmonic sensors, and integrated nonlinear plasmonic devices

References

[1] M. Barth, S. Schietinger, S. Fischer, J. Becker, N. Nusse, T. Aichele, Lochel, B., C. Sonnichsen, and O. Benson, "Nanoassembled plasmonic-photonic hybrid cavity for tailored light-matter coupling", Nano Lett., 10, 891-895 (2010).

[2] C.-L. Zou, Y.-F. Xiao, Z.-F. Han, C.-H. Dong, X.-D. Chen, J.-M. Cui, G.-C. Guo, and F.-W. Sun, "High-Q nanoring surface plasmon microresonator", J. Opt. Soc. Am. B, 27(12), 2495-2498 (2010).

[3] H. J. Kimble, "The quantum internet", Nature 453, 1023-1030 (2008).

[4] L. Barnes, A. Dereux, T. Ebbesen, "Surface Pasmon subwavelength optics," Nature, 424, 824-830 (2003).

[5] J. A. H. Nieuwstadt, M. Sandtke, R. H. Harmsen, F. B. Segerink, J. C. Prangsma, S. Enoch, and L. Kuipers, "Strong modification of the nonlinear optical response of metallic subwavelength hole arrays", Phys. Rev. Lett. 97, 146102 (2006).

[6] J. Homola, "Surface plasmon resonance sensors for detection of chemical and biological species", Chem.Rev. 108, 462-493 (2008).

[7] G. Raschke, S. Kowarik, T. Franzl, C. Sonnichsen, T. Klar, J. Feldmann, A. Nichtl, and K. Kurzinger, "Biomolecular recognition based on single gold nanoparticle light scattering", Nano Letters 3, 935-938 (2003).

[8] F. J. Bezares, J. D. Caldwell, O. Glembocki, R. W. Rendell, "The role of propagating and localized surface plasmons for SERS enhancement in periodic nanostructures", Plasmonics 7,143-150 (2012).

[9] K. Kneipp, Y. Wang, H. Kneipp, L. T. Perelman, I. Itzkan, R. R. Dasari, and M.S. Feld, "Single molecule detection using surface-enhanced Raman scattering(SERS)," Phys. Rev. Lett., 78(9), pp. 1667-1670 (1997).

[10] W. Wenseleers, F. Stellacci, T. M.- Friedrichsen, T. Mangel, C. A. Bauer, S. J. K. Pond, S. R. Marder, and J. W. Perry, "Five orders-of-magnitude enhancement of two-photon absorption for dyes on silver nanoparticle fractal clusters", J. Phys. Chem. B, 106, 6853-6863 (2002).

[11] H. Wang, T. B. Huff, D. A. Zweifel, W. He, P. S. Low, A. Wei and J.-X. Cheng, "In vitro and in two-photon luminescence imaging of single gold nanorods", PNAS, 102(44), 15752-15756 (2005).

[12] N. J. Durr, T. Larson, D. K. Smith, B. A. Korgel, K. Sokolov, and A. B.- Yakar, "Tunable two-photon luminescence in single gold nanowires fabricated by lithographically patterned nanowire electrodeposition", J. Phys. Chem. C, 112, 12721-12727 (2008).

[13] E. J. Sanchez, L. Novotny, and X. S. Xie, "Near-field fluorescence microscopy based on two-photon excitation with metal tips", Phys. Rev. Lett., 82(20), 4014-4017 (1999).

[14] M. Iosin, P. Baldeck, and S. Astilean, "Plasmon-enhanced fluoscence of dye molecules", Nuclear Instrumens and Methods in Physics Reseach B, 267, 403-405 (2009).

[15] I. Gryczynski, J. Malicka, Y. Shen, Z. Gryczyski, and J. R. Lakowicz, "Multiphoton excitation of fluorescence near metallic particles: enhanced and localized excitation", J. Phys. Chem. B, 103, 2191-2195 (2002).

[16] H. Kano, and S. Kawata, "Two-photon-excited fluorescence enhanced by a surface plasmon", Optics Letters, 21(22), 1848-1850 (1996).

[17] K. Imura, T. Nagahara, and H. Okamoto, "Near-field two-photon-induced photonluminescence from single gold nanorods and imaging of plasmon modes", J. Phys. Chem. B, 109, 13214-13220 (2005).

[18] D.-S. Wang, F.-Y. Hsu, and C.-W. Lin, "Surface plasmon effects on two photon luminescence of gold nanorods", Optics Express, 17(14), 11350-00359 (2009).

[19] S. Takahashi and A. V. Zayats, "Near-field second harmonic generation at a metal tip apex", Appl. Phys. Lett., 80(19), 3479-3481 (2002).

[20] A. Bouhelier, M. Beversluis, A. Hartschuh, and L. Novotny, "Near-field second-harmonic generation induced by local field enhancement", Phys. Rev. Lett. 90(1), 013903 (2003) .

[21] C. C. Neacsu, G. A. Reider, and M. B. Raschke, "Second-harmonic generation form nanoscopic metal tips: Symmetry selection rules for single asymmetric nanostructures", Phys. Rev. B 71, 201402(R) (2005).

[22] S. S. Pal, S. K. Mondal, P. P. Bajpai, and P. Kapur, "Optical fiber tip for field-enhanced second harmonic generation", Optics Letters, 37(19), 4017-4019(2012).

[23] A. Slablab, L. L. Xuan, M. Zielinski, Y. d. Wilde, V. Jacques, D. Chauvat, and J. –F. Roch, "Second-harmonic generation from coupled plasmon modes in a single dimer of gold nanospheres", Optics Express, 20(1), pp. 220-227 (2012).

[24] http://en.wikipedia.org/wiki/Surface_plasmon.

[25] C. Ropers, C. C. Neacsu, T. Elsaesser, M. Albrecht, M. B. Raschke, and C. Lienau, "Grating-coupling of surface plasmons onto metallic tips: A nanoconfined light source", Nano Lett. 7(9), 2784-2788 (2007).

[26] S. T. Koev, A. Agrawal, H. J. Lezee, and V. A. Aksyuk, "An efficient large-area grating copler for surface plasmon polaritons", Plasmonics 7, 269-277(2012).

[27] U. Schroter and D. Heitmann, "Grating couplers for surface plasmons excited on thin metal films in the Kretschmann-Raether configuration", Physical Review B, 60(7), 4992-4999 (1999).

[28] M. Fevrier, P. Gogol, A. Aassime, R. Megy, C. Delacour, A. Chelnokov, A. Apuzzo, S. Blaize, J. Lourtioz, and B. Dagens, "Giant coupling effect between metal nanoparticle chain and optical waveguide," Nano Lett. 12, 1032-1037 (2012).

[29] S. A. Maier, M. D. Friedman, P. E. Barclay, and O. Painter, "Experimental demonstration of fiber-accessible metal nanoparticle plasmon waveguides for planar energy guiding and sensing," Appl. Phys. Lett. 86, 071103 (2005).

[30] P. Wang, L. Zhang, Y. Xia, L. Tong, X. Xu, and Y. Ying, "Polymer nanofibers embedded with aligned gold nanorods: a new platform for plasmonic studies and optical sensing," Nano Lett. 12, 3145-3150(2012).

[31] P. K. Tien and R. Ulrich, "Theory of prism-film coupler and thin-film light guides", JOSA. 60, 1325-1337 (1970).

[32] E. Hutter and J. H. Fendler, "Exploitation of localized surface plasmon resonance", Adv. Mater. 16, 1685-1706 (2004).

[33] H. Ditlbacher, J. R. Krenn, A. Hohenau, A. Leitner, and F. R. Aussenegg, "Efficiency of local light plasmon coupling", Appl. Phys. Lett., 83(18), 3665-3667 (2003).

[34] A. –L. Baudrion, F. Leon-Perez, O. Mahboub, A. Hohenau, H. Ditlbacher, F. J. Garcia-Vidal, J. Dintinger, T. W. Ebbesen, L. Martin-Moreno, and J. R. Krenn, "Coupling efficiency of light to surface plasmon polariton for single subwavelength holes in a gold film", Opt. Express, 16(5), 3420-3429 (2008).

[35] C. Chao, and L. J. Guo, "Polymer microring resonators fabricated by nanoimprint technique", J. Vac. Sci. B 20, 2862 (2002).

[36] A. L. Martin, D. K. Armani, L. Yang, and K. J. Vahala, "Replica-molded high-Q polymer microresonators", Optics Letters, 29(6), 533-535 (2004).

[37] T. Grossmann, S. Schleede, M. Hauser, T. Beck, M. Thiel, G. Freymann, T. Mappes, and H. Kalt, "Direct laser writing for active and passive high-Q polymer microdisks on silicon", Optics Express, 19(12), 11451-11456 (2011).

[38] H. Cao, J. Y. Xu, W. H. Xiang, Y. Ma, S. –H. Chang, S. T. Ho, and G. S. Solomon, "Optically pumped InAs quantum dot disk lasers", Appl. Phys. Lett. 76, 3519 (2000).

[39] P. Michler, A. Kiraz, L. Zhang, C. Becher, E. Hu, and A. Imamoglu, "Laser emission from quantum dots in microdisk structures", Appl. Phys. Lett. 77, 184 (2000).

[40] T. Baba, and D. Sano, "Low-threshold lasing and Purcell effect in microdisk lasers at room temperature", IEEE journal of Selected Topics in Quantum Electronics, 9(5), 1340-1346 (2003).

[41] J. Campenhout, P. Rojo-Romeo, P. Regreny, C. Seassal, D. Van Thourhout, S. Verstuyft, L. Di Cioccio,J. –M. Fedeli, C. Lagahe, and R. Baets, "Electrically pumped InP-based microdisk lasers integrated with a nanophotonic silicon-on-insulator waveguide circuit", Optics Express, 15(11), 6744-6749 (2007).

[42] V. B. Braginsky, M. L. Gorodetsky, V. S. Ilchenko, "Quality-factor and nonlinear properties of optical whispering-gallery modes", Physics Letters A, 137(7-8), 393-397 (1989).

[43] M. L. Gorodetsky, A. A. Savchenkov, and V. S. Ilchenko, "Ultimate Q of optical microsphere resonators", Optics Letters, 21(7), 453-455 (1996).

[44] D. W. V ernooy , V. S. Ilchenko, H. Mabuchi, E. W. Streed, and H. J. Kimble," High-Q measurements of fused-silica microspheres in the near infrared", Optics Letters, 23(4), 247-249 (1998).

[45] S. M. Spillane, T. J. Kippenberg, K. J. Vahala, K. W. Goh, E. Wilcut, and H. J. Kimble, "Ultrahigh-Q toroidal microresonators for cavity quantum electrodynamics", Phys. Rev. A 71, 013817 (2005).

[46] L. Yang, D. K. Armani, and K. J. Vahala, "Fiber-coupled erbium microlaser on a chip", Appl. Phys. Lett. 83, 825 (2003).

[47] D. K. Armani, T. J. Kippenberg, S. M. Spillane, and K. J. Vahala, "Ultra-high-Q toroid microcavity on a chip", Nature 421, 925-928 (2003).

[48] V. Sandoghdar, F. T reussart, J. Hare, V. Lefevre-Seguin, J. M. Raimond, and S. Haroche, "Very low threshold whispering-gallery-mode microsphere laser", Phys. Rev.A 54(3), 1777-1780 (1996).

[49] H. Fujiwara and K. Sasaki, "Microspherical lasing of en Erbium-Ion-Doped glass particle", Jpn. J. Appl. Phys. 41, L46-L48 (2002).

[50] H. Takashima, H. Fujiwara, S. Takeuchi, and K. Sasaki, "Fiber-microsphere laser with a submicrometer sol-gel silica glass layer codoped with erbium, aluminum, and phosphorus", Applied Physics Letters 90, 101103 (2007).

[51] B. Min, T. J. Kippenberg, and K. J. Vahala, "Compact, fiber-compatible, cascaded Raman laser", Optics Letters, 28(17), 1507-1509 (2003).

[52] B. Min, L. Yang, and K. J. Vahala, "Controlled transition between parametric and Raman oscillations in ultrahigh-Q silica toroidal microcavities", Applied Physics Letters 87, 181109 (2005).

[53] D. J. Alton, N. P. Stern, Takao Aoki, H. Lee, E. Ostby, K. J. Vahala and H. J. Kimble, "Strong interactions of single atoms and photons near a dielectric boundary", Nature Physics, 7, 159-165(2011).

[54] R. Miller, T. E. Northup, K. M. Birnbaum, A. Boca, A. D. Boozer and H. J. Kimble, " Trapped atoms in cavity QED: coupling quantized light and matter", J. Phys. B: At. Mol. Opt. Phys. 38, S551-S565(2005).

[55] S. Nubmann, K. Murr, M. Hijkema, B. Weber, A. Kuhn and G. Rempe, "Vacuum-stimulated cooling of single atoms in three dimensions", Nature Physics, 1, 122-126(2005).

[56] B. Min, E. Ostby, V. Sorger, U. Erick, L. Yang, X. Zhang, K. Vahala, "High-Q surface-plasmon-polariton whispering-gallery microcavity," Nature, 457, 455-459 (2009).

[57] I. White, H. Oveys, and X. Fan, "Increasing the enhancement of SERS with dielectric microsphere resonators", Spectroscopy Mag. 21, 1-5 (2006).

[58] F. D. Angelis, M. Patrini, G. Das, I. Maksymov, M. Galli, L. Businaro, L. Claudio, and E. D. Fabrizio, "A hybrid plasmonic-photonic nanodevice for label-free detection of a few molecules", Nano Letters, 8(8), 2321-2327 (2008).

[59] M. Chamanzar and A. Adibi, "Hybrid nanoplasmonic-photonic resonators for efficient coupling of light to single plasmonic nanoresonators," Opt. Express, 19, 22292-22304 (2011).

[60] Y.-F. Xiao, Y.-C. Liu, B.-B. Li, Y.-L. Chen, Y. Li, and Q. Gong, "Strongly enhanced light-matter interaction in a hybrid photonic-plasmonic resonator", Physical Review A 85, 031805(R) (2012).

[61] F. L. Kien, J. Q. Liang, K. Hakuta, and V. I. Balykin, "Field intensity distribution and polarization orientations in a vacuum-clad subwavelength-diameter optical fiber," Opt. Commun. 242, 445-455 (2004).

[62] L. Tong, J. Lou, and E. Mazur, "Single-mode guiding properties of subwavelength-diameter silica and silicon wire waveguides," Opt. Express 12, 1025-1035 (2004).

[63] L. Tong, R. R. Gattass, J. B. Ashcom, S. He, J. Lou, M. Shen, I. Maxwell, and E. Mazui, "Subwavelength-diameter silica wires for low-loss optical wave guiding," Nature 426, 816-819 (2003).

[64] R. Yalla, F. L. Kien, M. Morinaga, and K. Hakuta, "Efficient channeling of fluorescence photons from single quantum dots into guided modes of optical nanofiber," Phys. Rev. Lett. 109, 063602 (2012).

[65] M. Fujiwara, K. Toubaru, T. Noda, H.-Q. Zhao, and S. Takeuchi, "Highly efficient coupling of photons from nanoemitters into single-mode optical fibers," Nano Lett. 11, 4362-4365 (2011).

[66] T. Schroder, M. Fujiwara, T. Noda, H.-Q. Zhao, O. Benson, and S. Takeuchi, "A nanodiamond-tapered fiber system with high single-mode coupling efficiency," Opt. Express 20, 10490-10497 (2012).

[67] F. L. Kien, V. I. Balykin, and K. Hakuta, "Atom trap and waveguide using a two-color evanescent light field around a subwavelength-diameter optical fiber," Phys. Rev. A 70, 063403 (2004).

[68] F. L. Kien, V. I. Balykin, and K. Hakuta, "Scattering of an evanescent light field by a single cesium atom near a nanofiber," Phys. Rev. A 73, 013819 (2006).

[69] F. L. Kien, S. D. Gupta, V. I. Balykin, and K. Hakuta, "Spontaneous emission of a cesium atom near a nanofiber: Efficient coupling of light to guided modes," Phys. Rev. A 72, 032509 (2005).

[70] E. E. M. Khaled, S. Hill, P. Barber, and D. Chowdhury, "Near-resonance excitation of dielectric spheres with plane waves and off-axis Gaussian beams", Appl. Opt. 31, 1166-1169(1992).

[71] A. Mazzei, S. Gotzinger, L. Menezes, V. Sandoghdar, and O. Benson, "Optimization of prism coupling to high-Q modes in a microsphere resonator using a near-field probe", Optics Communications, 250, 428-433 (2005).

[72] V. Ilchenko, S. Yao, and L. Maleki, "Pigtail the high-Q microsphere cavity: a simple fiber coupler for optical whispering-gallery modes", Optics Letters, 24, 723-725 (1999).

[73] J. P. Laine, B. E. Little, D. R. Lim, H. C. Tapalian, L. C. Kimerling and H. A. Haus, "Microsphere resonator mode characterization by pedestal anti-resonant reflecting waveguide coupler," IEEE Photon. Technol. Lett. 12, 1004-1006 (2000).

[74] J. C. Knight, G. Cheung, F. Jacques, and T. A. Birks, "Phase-matched excitation of whispering-gallery-mode resonances by a fiber taper," Opt. Lett. 22, 1129-1131 (1997).

[75] G. Griffel, S. Arnold, D. Taskent, A. Serpenguzel, J. Connolly, and N. Morris, "Morphology-dependent resonances of a microsphere-optical fiber system", Optics Letters, 21, 695-697 (1996).

[76] A. sperpenguzel, S. Arnold, and G. Griffel, "Excitation of resonances of microspheres on an optical fiber", Optics Letters, 20, 654-656 (1995).

[77] M. Fevrier, P. Gogol, A. Aassime, R. Megy, C. Delacour, A. Chelnokov, A. Apuzzo, S. Blaize, J. Lourtioz, and B. Dagens, "Giant coupling effect between metal nanoparticle chain and optical waveguide," Nano Lett. 12, 1032-1037 (2012).

[78] S. A. Maier, M. D. Friedman, P. E. Barclay, and O. Painter, "Experimental demonstration of fiber-accessible metal nanoparticle plasmon waveguides for planar energy guiding and sensing," Appl. Phys. Lett. 86, 071103 (2005).

[79] P. Wang, L. Zhang, Y. Xia, L. Tong, X. Xu, and Y. Ying, "Polymer nanofibers embedded with aligned gold nanorods: a new platform for plasmonic studies and optical sensing," Nano Lett. 12, 3145-3150(2012).

[80] J. D. Love, W. M. Henry, W. J. Stewart, R. J. Black, S. Lacroix, and F. Gonthier, "Tapered single-mode fibres and devices Part 1: Adiabaticity criteria", IEE Proceedings-J, 138(5), 343-354 (1991).

[81] M. J. Levene, J. Korlach, S. W. Turner, M. Foquet, H. G. Craighead, and W. W. Webb, "Zero-mode waveguides for single-molecule analysis at high concentrations," Science 299, 682-686 (2003).

[82] A. B. Marsko and V. S. Ilchenko, "Optical resonators with whispering-gallery modes-Part Ⅰ: Basics", IEEE J. Sel. Top. Quantum Electron. 12, 3-14 (2006).

[83] J. Ward and O. Benson, "WGM microresonators: sensing, lasing and fundamental optics with microspheres", Laser Photonics Rev., 1-18 (2011)

[84] A. N. Oraevsky, "Whispering-gallery waves", Quantum Electronics, 32(5), 377-400 (2002).

[85] B. E. Little, J. –P. Laine, and H. A. Haus, "Analytic theory of coupling from tapered fibers and half-blocks into microsphere resonators", Journal of Lightwave Technology, 17(4), 704-715 (1999).

[86] A. B. Matsko, A. A. Savchenkov, D. Strekalow, V. S. Ilchenko, and L. Maleki, "Review of applications of whispering-gallery mode resonators in photonics and nonlinear optics", IPN Progress Report 42-162, 1-27 (2005).

[87] L. He, S. K. Ozdemir, and L. Yang, "Whispering gallery microcavity lasers", Laser Photonics Rev., 1-23 (2012).

[88] S. Mehrabani and A. M. Armani, "Blue upconversion laser based on thulium-doped silica microcavity", Optics Letters, 38(21), 4346-4349 (2013).

[89] W. L. Barnes, A. Dereux, and T. S. Ebbesen, "Surface plasmon subwavelength optics", Nature 424, 824-830 (2003).

[90] K. A. Willets and R. P. Duyne, "Localized surface plasmon resonance spectroscopy and sensing", Annu. Rev. Phys. Chem. 58, 267-297 (2007).

[91] F. Wang and Y. R. Shen, "General properities of local plasmons in metal nanostructures", Physical Review Letters 97, 206806 (2006).

[92] E. Grades, "Excitation, interaction, and scattering of localized and propagating surface polaritons", Technische Universtat Dresden, 2006.

[93] H. A. Haus, "Waves and fields in optoelectronics", Massachusetts Institute of Technology, Prentice-Hall series in solid state physical electronics, 197-228 (1984).

[94] T. J. A. Kippenberg, "Nonliear optics in ultra-high-Q whispering-gallery optical microcavities", California Institute of Technology Pasadena, California, 2004.

[95] S. M. Spillane, T. J. Kippenberg, O. J. Painter, and K. J. Vahala, "Ideality in a fiber-tapered-coupled microresonator system for application to cavity quantum electrodynamics", Physical Review Letters, 81(4), 043902 (2003).

[96] F. Ren, K. Kitajima, H. Takashima, H. Fujiwara, and K. Sasaki, "Second harmonic generation from the top of an Au-coated tip via a tapered fiber coupled microsphere resonator", Proc. SPIE 8463, 846305 (2012).

[97] H. Konishi, H. Fujiwara, S. Takeuchi, and K. Sasaki, "Polarization-discriminated spectra of a fiber-microsphere system," Appl. Phys. Lett. 89, 121107 (2006).

[98] F. Ren, H. Takashima, Y. Tanaka, H, Fujiwara, and K. Sasaki, "Nonlinear phenomena from a PIC-attached gold tip using a plasmonic-whispering gallery mode hybrid system", Proc. SPIE 8816 (2013).

[99] A. Harung, S. Brueckner, and H. Bartelt, "Limits of light guidance in optical nanofibers", Optics Express, 18, 3754-3761 (2010).

[100] F. Ren, H. Takashima, Y. Tanaka, H. Fujiwara, and K. Sasaki, "Two-photon excited fluorescence from a pseudoisocyanine-attached gold-coated tip via a thin tapered fiber under a weak continuous wave excitation", Optics Express, 21(23), pp. 27759-27769 (2013).

[101] K.-C. Fan, H.-Y. Hsu, P.-Y. Hung, and W. Wang, "Experimental study of fabricating a microball tip on an optical fiber," J. Opt. A, Pure Appl. Opt. 8(9), 782–787 (2006).

[102] Y. Tanaka, H. Yoshikawa, and H. Masuhara, "Two-photon fluorescence spectroscopy of individually trapped pseudoisocyanine J-aggregates in aqueous solution," J. Phys. Chem. 110, 17906-17911 (2006).

[103] D. A. V. Bout , J. Kerimo, D. A. Higgins, and P. F. Barbara, " Near-field optical studies of thin-film mesostructured organic meterials", Acc. Chem. Res. 30, 204-212 (1997).

[104] K. D. Belfield, M. B. Bondar, F. Hernandez, O. Przhonska, and S. Yao, "Two-photon absorption of a supramolecular pseudoisocyanine J-aggregate assembly", Chem. Phys. 320, 118-124 (2006).

[105] A. Touzov and C. B. Gorman, "Tip-induced structural rearrangements of Alkanethiolated self-assembled monolayers on gold," J. Phys. Chem. B 101, 5263-5276 (1997).

[106] M. Fujiwara, K. Toubaru, and S. Takeuchi, "Optical transmittance degradation in tapered fibers," Opt. Express, 19, 8596-8601 (2011).

Publication lists

I. Journal paper

(1) **Fang Ren**, Hideaki Takashima, Yoshito Tanaka, Hideki Fujiwara, and Keiji Sasaki, ”Two-photon excited fluorescence from a pseudoisocyanine-attached gold-coated tip via a thin tapered fiber under a weak continuous wave excitation”, Optics Express, Vol. 21, Issue 23, pp. 27759-27769 (2013). (IF=3.546)
(Selected for virtual journal for biomedical optics, Vol. 9, Iss. 1, Jan. 14, 2014.)

II. Proceedings

(1) **Fang Ren**, Hideaki Takashima, Yoshito Tanaka, Hideki Fujiwara, and Keiji Sasaki, "Nonlinear phenomena from a PIC-attached gold tip using a plasmonic-whispering gallery mode hybrid system", Proc. SPIE 8816, Nanoengineering: Fabrication, Properties, Optics, and Devices X, 881612 (2013).

(2) **Fang Ren**, Kazutaka Kitajima, Hideaki Takashima, Hideki Fujiwara, and Keiji Sasaki,"Second harmonic generation from the top of an Au-coated tip via a tapered fiber coupled microsphere resonator", Proc. SPIE 8463, Nanoengineering: Fabrication, Properties, Optics, and Devices IX, 846305 (2012).

III. Academic conferences

(1) **Fang Ren**, Hideaki Takashima, Hideki Fujiwara, and Keiji Sasaki, “Two-photon excited fluorescence from a PIC-attached Au-coated tip via a thin tapered fiber under a weak CW excitation”, The 14th RIES-Hokudai International Symposium “網 [mou]”, Sapporo, Japan (2013/12/11-12/12). (poster presentation)

(2) **Fang Ren**, Hideaki Takashima, Yoshito Tanaka, Hideki Fujiwara, and Keiji Sasaki,"Nonlinear phenomena from the top of a PIC attached gold tip using a plasmonic-photonic hybrid system", SPIE Optics+Photonics, San Diego, USA (2013/8/25-8/29). (oral presentation)

(3) 高島秀聡, **任芳**, 田中嘉人, 藤原英樹, 竹内繁樹, 笹木敬司, "ファイバ-微小球共振器に結合した金属ナノ構造体からの二光子発光",第 28 回量子情報技術研究会 (QIT28), 北海道大学（2013/5/27～28). (poster presentation)

(4) 高島秀聡, **任芳**，田中嘉人, 藤原英樹, 笹木敬司, "ファイバ-微小球共振器に結合した金属ナノ構造体からの非線形発光",第 60 回応用物理学会春季学術講演会、神奈川工科大学(2013/3/27-30). (oral presentation)

(5) **Fang Ren**, Hideaki Takashima, Hideki Fujiwara, and Keiji Sasaki, "Second harmonic generation by an efficient localized plasmon excitation via a tapered fiber-coupled microresonator", The 13th RIES-Hokudai International Symposium "律"[ritsu], Sapporo, Japan (2012/12/13-12/14). (poster presentation)

(6) **Fang Ren**, Hideaki Takashima, Kazutaka Kitajima, Hideki Fujiwara, and Keiji Sasaki, "Second harmonic generation from the top of an Au-coated tip via a tapered fiber coupled microsphere resonator", SPIE Optics+Photonics, San Diego, USA (2012/8/12-8/16). (oral presentation)

(7) **Fang Ren**，Kazutaka Kitajima，Hideaki Takashima，Hideki Fujiwara，and Keiji Sasaki, "Second harmonic generation by an efficient localized plasmon excitation using a tapered fiber-coupled microsphere", The 59th JSAP (the Japan Society of Applied Physics) Spring meeting, 2012, Waseda University, Tokyo, Japan (2012/3/15~18). (poster presentation)

Acknowledgements

Time flies, three and half years abroad life ended in a twinkling of an eye. The time I have spent at Hokkaido University was enjoyable and fruitful. There are many people who I thank for their support and encouragement. First, I would like to thank my advisor Professor Keiji Sasaki, who has supported me throughout my research with his intelligence, understanding and knowledge. I feel very grateful that he allowed me to be a member of the Photo-system physics laboratory.

I would like to express my sincere appreciation to Associated Professor Hideki Fujiwara. He expertly guided me to research and I have benefited from his patience, creativity, and rigorous approach to science. Our numerous discussions have shown me how to recognized and focus on the truly novel aspects of research.

I have learned much from the many members of the Sasaki Lab. that I had the opportunity to interact with Sakai-sensei, Ishida-sensei, Takashima-san, Tanaka-san, Kaneda-san, Kitajima-san, Kondo-san, and Sugai-san. Specially, I would like to thank Dr. Hideaki Takashima for insightful discussions and useful suggestions on my research.

I want to thank Yamada-san for her kind help in setting various registration procedures during my study.

I also thank my family—my parents, my husband, Yulai Xie, without their continuous encouragement and support, I could not have finished my PhD research.

Lastly, I wish my regards and blessings to all of those who helped me in any respect during the completion of this thesis.

REN Fang

December, 2013

Sapporo, Hokkaido, Japan